ABSTRACT

Title of Dissertation:	DYNAMIC COCULTURE OF A PREVASCULARIZED ENGINEERED BONE CONSTRUCT
	Bao-Ngoc B. Nguyen, Doctor of Philosophy in Bioengineering, 2016
Dissertation Directed By:	Fischell Family Distinguished Professor & Department Chair, John P. Fisher, Fischell Department of Bioengineering

The generation of functional, vascularized tissues is a key challenge for the field of tissue engineering. Before clinical implantations of tissue engineered bone constructs can succeed, *in vitro* fabrication needs to address limitations in large-scale tissue development, including controlled osteogenesis and an inadequate vasculature network to prevent necrosis of large constructs. The tubular perfusion system (TPS) bioreactor is an effective culturing method to augment osteogenic differentiation and maintain viability of human mesenchymal stem cell (hMSC)-seeded scaffolds while they are developed *in vitro*. To further enhance this process, we developed a novel osteogenic growth factors delivery system for dynamically cultured hMSCs using microparticles encapsulated in three-dimensional alginate scaffolds.

In light of this increased differentiation, we characterized the endogenous cytokine distribution throughout the TPS bioreactor. An advantageous effect in the

'outlet' portion of the uniaxial growth chamber was discovered due to the system's downstream circulation and the unique modular aspect of the scaffolds. This unique trait allowed us to carefully tune the differentiation behavior of specific cell populations.

We applied the knowledge gained from the growth profile of the TPS bioreactor to culture a high-volume bone composite in a 3D-printed femur mold. This resulted in a tissue engineered bone construct with a volume of $200cm^3$, a 20-fold increase over previously reported sizes. We demonstrated high viability of the cultured cells throughout the culture period as well as early signs of osteogenic differentiation. Taking one step closer toward a viable implant and minimize tissue necrosis after implantation, we designed a composite construct by coculturing endothelial cells (ECs) and differentiating hMSCs, encouraging prevascularization and anastomosis of the graft with the host vasculature. We discovered the necessity of cell to cell proximity between the two cell types as well as preference for the natural cell binding capabilities of hydrogels like collagen. Notably, the results suggested increased osteogenic and angiogenic potential of the encapsulated cells when dynamically cultured in the TPS bioreactor, suggesting a synergistic effect between coculture and applied shear stress. This work highlights the feasibility of fabricating a high-volume, prevascularized tissue engineered bone construct for the regeneration of a critical size defect.

DYNAMIC COCULTURE OF A PREVASCULARIZED
ENGINEERED BONE CONSTRUCT

by

Bao-Ngoc Bich Nguyen

Dissertation submitted to the Faculty of the Graduate School of the
University of Maryland, College Park, in partial fulfillment
of the requirements for the degree of
Doctor of Philosophy
2016

Advisory Committee:
Professor John P. Fisher, Chair
Professor Yu Chen
Professor Kimberly M. Stroka
Professor Zhihong Nie
Professor Isabel K. Lloyd

Dedication

This work is dedicated to my parents,
whose sacrifices enabled me to pursue my dreams.

Acknowledgements

Table of Contents

List of Figures

in the highest expression of all four markers by day 7. The symbol '*'
indicates statistical significance within groups at a timepoint (p<0.05). F)
Immunofluorescence staining of hMSCs, HUVECs, and coculture in static
and dynamic. hMSCs were stained for BMP-2 (pink/red), counterstained
with DAPI (blue). HUVECs were stained for CD31 (green), VEGF (red),
and counterstained with DAPI (blue). Cocultured samples were stained for
BMP-2 (pink/red), CD31 (green), and counterstained with DAPI (blue).
Images were taken at 40x with an additional 2x zoom (right panel). …141

List of Tables

Chapter 1: Introduction

Over 1.5 million Americans suffer from critically-sized bone defects each year, yet treatment remains a major clinical challenge due to the complications associated with autologous grafts as well as long recovery periods[1]. While engineering efforts to regenerate tissues have advanced, they continue to be hindered by inadequate vasculature throughout large constructs, leading to cell death once implanted into the defect site[2,3]. Therapies for critical-sized bone defects, which are injuries that are unable to regenerate themselves, require high-volume tissue engineered constructs with an existing network of nutrient and oxygen delivery to maintain cell viability and encourage integration with the host. Therefore, an *in vitro* method to develop prevascularized tissue engineered bone grafts holds tremendous therapeutic potential towards providing a viable regeneration solution.

To address this issue, we first demonstrate the ability to tune dynamic culture conditions in the TPS bioreactor for osteogenic differentiation of 3D encapsulated mesenchymal stem cells (MSCs). The roles of applied shear stress and release of growth factors were investigated, and the results indicated that these endogenous signals help regulate differentiation within a cell population.

Next, to provide an endothelial network for subsequent vascularization of bone, we utilize the inherent link between osteogenesis and angiogenesis to coculture endothelial cells (ECs) and osteogenic differentiating MSCs. A variety of *in vitro* coculture methods have been attempted, but few have succeeded as viable long-term *in vivo* options[4–6]. Dynamic *in vitro* culture environments such as the TPS bioreactor mimic *in vivo* environments by providing mechanical stimulation and

sufficient nutrient and oxygen transport. Therefore, to emulate their native environments during bone ossification and angiogenesis, the cocultured cells can be seeded onto three-dimensional hydrogel scaffolds, creating a prevascularized tissue-engineered bone construct for *in vivo* applications. These constructs will allow a vascular network that can integrate and anastomose to the host vasculature after implantation.

In this work, we leverage the benefits of dynamic culture in the TPS bioreactor to provide shear stress to the two encapsulated cell population for the application of fabricating a high-volume, patient specific tissue engineered bone construct. Four primary objectives of this work include:

1. Delivery of osteogenic growth factors via PLGA microparticles to hMSC-encapsulating alginate beads to promote osteogenic differentiation under static and dynamic culture.

2. Characterization of the growth chamber environment of the tubular perfusion system (TPS) bioreactor to evaluate the effects of shear and direction of flow on the enhancement of osteogenic differentiation of hMSCs.

3. Fabrication of a high-volume bone tissue engineering construct using the TPS bioreactor for the regeneration of critical-sized defects.

4. Determination of coculture parameters for HUVECs and hMSCs in alginate and collagen scaffolds to promote angiogenesis and osteogenesis, respectively.

Chapter 2: In vivo techniques and strategies for enhanced vascularization of engineered bone[1]

2.1 Introduction

Tissue engineering expanded rapidly throughout the 1990s based on the promise to create new organs and tissue constructs to replace diseased or damaged organs [7]. However, two decades later, few products have successful passed the Food and Drug Administration (FDA) clinical trials [8]; a feasible transplantable organ is still unattainable. More importantly, an organ shortage continues to persist because a consistent technique of providing vasculature and integration of tissue-engineered constructs into the host has not yet been realized [9].

Most tissues in the body rely on oxygen and nutrients supplied from blood vessels. It has been shown that new blood vessel formation is required once tissue has grown beyond 100-200 microns from a nearby vasculature due to oxygen diffusion limitations [10]. If implanted engineered tissues cannot obtain the appropriate amount of nutrients, the tissue experiences decreased function, nutrient deficiencies, or hypoxia, especially at the core of the construct [11]. Therefore, three-dimensional constructs depend on rapid development of new blood vessels and vascular networks to provide nutrients.

The development of mature vasculature is one of the major hurdles in the field of tissue engineering research, preventing a successful transition from lab bench to relevant clinical applications. Without a sufficient supply of oxygen, engineered tissue scalability, survival, and integration with the host tissue is extremely limited

---

[1] BNB Nguyen, JP Fisher, "In Vivo Techniques and Strategies for Enhanced Vascularization of Engineered Bone." Vascularization: Regenerative Medicine and Tissue Engineering (2013). CRC Press, Boca Raton, FL.

[9]. It is the hope that with advances in vascularization technology, many of the tissue-engineered constructs currently only viable in vitro will be able to become a reality. Tissue engineering aims to not only build artificial tissues in the lab, but also ultimately enhance or restore function of diseased and damaged tissues. Therefore, vascularization of engineered-tissues is a vital next step in moving the field towards successful regenerative medicine.

While a tremendous amount of research is conducted using in vitro methods of vascularization of engineered tissues, fewer advances have been made within the field of in vivo techniques due to the complex microenvironment, cost, and poorly understood synergy between host and implanted cells. This chapter assesses the current state of the field by outlining fundamental approaches taken towards developing prevascularized bone tissues in vivo, as well as highlighting their advantages and disadvantages.

2.1.1 Bone tissue engineering

Tissue loss as a result of injury or disease leads to reduced quality of life, especially with an increasing aging population. However, strategies that encourage bone formation by significantly increasing bone density have yet to become available. It is a major clinical requirement that has stimulated increasing interest in the tissue-engineering field to develop new therapies that involve bone regeneration. While significant advances have been made combining biomaterials and cells for *in* vitro culture, the field is has seen relatively fewer developments towards clinical trials.

The gold standard to prevent or treat a fractured non-union is autologous bone grafting or delivering bone chips from a secondary donor site into the defect site,

where they can then promote and attract other cells responsible for the bone-forming process [12]. However, significant donor morbidity such as chronic pain, hypersensitivity, infection, and paraesthesia occur in up to a third of the patients [13]. In addition, the limited supply and relatively unpredictability of the autologous bone grafts have led to the use of alternatives, including allograft. Those can be used for larger defects but are limited by the possibility of immune rejection, disease transmission, and relatively lower incorporation rate compared to autografts [14]. In addition, allografts associated with the reduced cellularity and vascularization compared to autologous grafts, leading to poorer bone healing. Xenografts, tissue derived from another species, are used less frequently because they have many of the same drawbacks in addition to their dissimilarity to human tissue structure and function [15]. This in turn led to the development and fabrication of synthetic scaffolds, which can be molded into different shapes and sizes to fit the defect site [16]. The goal is to engineer constructs with similar properties as natural bone, including mechanical strength and structure. However, like many of the other tissue-engineered organs, bone constructs have been hampered by their inability to remain viable *in vivo*. Unlike other tissues, such as muscle bundles, bone tissue lacks an abundant preexisting vascular network, able to rapidly penetrate the scaffold and avoid tissue necrosis at the center of the graft. Current methods of graft implantation *in vivo* show slow integration of the host's vasculature and sufficient nutrient and oxygen concentrations only at the host tissue-construct interface.

2.2 Scaffold material

The three-dimensional architecture and design of scaffolds has been shown to have a profound effect on the rate of vascularization once implanted *in vivo*. For example, bone scaffolds are typically made out of porous, degradable materials that are able to provide the proper mechanical strength during repair and regeneration of damaged or disease bone. Some of the design and material property requirements for an ideal graft include biocompatibility, adequate pore size, and bioresorbability [6]. Biocompatibility describes the scaffold's ability to support normal cellular activity, including molecular signaling, without exhibiting any toxic effect to the host tissue [17,18]. For a bone scaffold, this means it must be conducive to cell recruitment and subsequent bone formation. It has been shown that pores need to be at least 100 microns in diameter to allow for diffusion of essential nutrients and oxygen [19]. Porosity also plays an important role in cell migration and physical communication between cells. Unfortunately, increased porosity reduces the mechanical strength of the scaffold, affecting the compressive as well as the degradation properties. Therefore, finding a delicate balance between architectural and mechanical properties is critical during bone scaffold fabrication. Finally, bioresorbability is another important factor because the scaffold has to exhibit similar properties as the surrounding host tissue, yet degrade at a desired rate to accommodate neovasculature and bone formation.

In the event that the construct is prevascularized in a well-supplied region of the body prior to implantation in the defect site, the scaffolding material is expected to remain intact for a significantly longer period of time than if implanted directly

into the defect site. A variety of biomaterials have been utilized for this purpose, ranging from fibrin [20,21], to poly(lactic-co-glycolic) acid (PLGA) [13,22,23], to processed bovine cancellous bone (PBCB) [21]. Many of these scaffolds have been evaluated for long-term cytotoxic effects and have shown to have slow degradation rates.

Several different kinds of hydrogels have been found to facilitate osteogenesis. Of those, a few have shown to also promote formation of vascular sprouts. Matrigel^{TM} is one of the more popular scaffolds used as a vascularization platform [24–26]. It is a decellularized matrix derived from mouse sarcoma cells and contains many important proteins such as laminin, entactin, and collagen. Cells encounter these structural components in their natural environment, which promote cell adhesion and spreading. In addition, Matrigel^{TM} contains certain growth factors that can promote differentiation and proliferation for a variety of cells lines [27,28]. However, due to source variance, the actual composition of Matrigel^{TM} can fluctuate from lot to lot and results are inconsistent, making Matrigel^{TM} non-ideal for tissue engineering techniques [25]. In addition, its xenogenic origin results in unfavorable immune responses and could hinder blood vessel formation *in vivo*. For the purpose of bone tissue engineering, growth factor-enriched Matrigel^{TM} has been used as an additive to standard scaffolds, such as PLGA, to enhance vascularization [29]. Laschke *et al.* demonstrated that Matrigel^{TM} did not have any effect on the biocompatibility of the PLGA scaffold with the seeded cells, but instead improved the *in vivo* ingrowth of new blood vessels from the surrounding tissue.

More complicated, lab-generated scaffolds include modified polyethylene glycol diacrylate (PEGDA) hydrogels containing adhesive ligands and encapsulated growth factors [30], or protease-sensitive PEG gels with functionalized integrin binding sites [31]. Porous scaffolds can be advantageous for vascularization of bone tissue, including electrospun scaffolds made out of degradable poly(e-caprolactone) (PCL) [32] or silk fibroin [33]. Scaffolds fabricated with a more random porous architecture can lead to only partially connected pathways, impeding the formation of a dense vascular system. Therefore, scaffolds with well-defined, interconnected pores may result in better vessel formation. Such grafts can be best produced with the use of rapid-prototyping techniques, which utilizes computer-aided design (CAD) templates to print the scaffold layer by layer out of a desired biomaterial [34].

2.3 Stem and progenitor cells

A variety of cell types are involved in creating vascularized bone tissue, the most obvious being osteoprogenitor and endothelial cells. Recently, mural cells have also started to gain more attention as an important component of vascular network formation within bone tissue. This section describes different aspects of each cell type and their importance to bone vascularization.

2.3.1 Stem cells

Stem cells have become the forerunner in the field of tissue engineering due to their capability to differentiate into a variety of cell types. Mesenchymal stem cells especially have been used more frequently in bone tissue engineering applications. Human mesenchymal stem cells (hMSCs) are often used as a source for

osteoprogenitor cells because these multipotent cells are isolated from the bone marrow and have the ability to differentiate into a variety of lineages to become adipocytes, chondrocytes, or osteocytes. In addition, because they reside in the bone marrow, they can be obtained fairly easily from an adult patient by way of a bone marrow biopsy [35]. For the purpose of bone tissue engineering, the cells can be guided towards osteogenesis with the use of mechanical stimulation or growth factors, such as bone-morphogenic protein-2 or dexamethasone [36]. In terms of immune response, hMSCs are non-immunogenic *in vitro*, as well as allogenic *in vivo*, making them an ideal candidate for bone regeneration [37].

2.3.2 Endothelial cells and source

Endothelial cells are a thin layer of cells that make up the interior of blood vessels. They have shown to accelerate neovascular formation in many tissue-engineering constructs by creating blood vessels networks [18,38,39]. In addition to their ability to improve vascularization and bone graft survival, endothelial cells are able to support osteogenesis, by mediating cell-cell communication via soluble factors [40–42] and gap junction proteins [20]. Unfortunately, some of the drawbacks of endothelial cells include their limited proliferation ability and the necessity for inhibition of the apoptotic response [43].

The source of endothelial cells can have an important effect on the success of a tissue-engineering construct. There is considerable phenotypic variation among cells depending on their source. For example, human umbilical vein endothelial cells (HUVECs) are easily obtained from discarded umbilical cords, can be easily expanded, and have been shown to be ideal for *in vitro* applications. However, they

have resulted in immature and leaky vessels once implanted in *vivo* [44] On the other hand, embryonic stem cells have resulted in some promising outcomes when implanted *in vivo*, including formation of stable microvessels and integration with host endothelial cells [27,45]. However, due to the ethical concerns associated with them as well as their ability to differentiate into almost every cell type if not tightly controlled, their clinical use has been limited. Promising results have recently been seen with the use of endothelial progenitor cells (EPCs) [Lin 2000]. EPCs are a small population of circulating mononuclear cells that have shown to differentiate into and able to keep their endothelial cell characteristic *in vitro* [46].

2.3.3 Mural cells

Mural cells are a generally used to refer to vascular smooth cells and pericytes, which are both involved in the process of blood vessel formation [47]. They have been shown to migrate toward sprouting endothelial cells in response to vascular endothelial growth factor (VEGF) and are able to help provide a stabilizing environment for the cells [47]. They allow for cell-to-cell communication, secrete angiogenic factors and extracellular matrix components, and promote endothelial blood vessel maturation. The latter involves a series of steps that involve important spatial and temporal coordination of the endothelial cells and their signaling pathways, such as altering endothelial cell proliferation rate and changing their morphology [48]. Several groups have shown the involvement of mural cells in angiogenesis [22,23,44], concluding that the recruitment of mural cells greatly affects endothelial behavior when cocultured with endothelial cells. Fluorescent microscopy shows integration of mural cells into the blood vessel network, which is especially

enhanced with the addition of VEGF as a growth factor *in vitro* [47]. The resulting architectural layout of the neovasculature has also been shown to be more mature and dense when endothelial cells have been cultured with mural cells.

Based on these results, it shows that formation of neovasculature is an orchestrated effort of several cell types. Therefore, future experiments may have more success if tissue-engineered constructs are implanted *in vivo* surrounded by a source of mural cells to better enable mature blood vessel formation.

2.4 Cocultures

While singular endothelial-derived cell types have been able to demonstrate formation of vascular networks, the ultimate goal of generating prevascularized tissues may require the coculture of endothelial cells and the target tissue cell population. Coculture methods allow for concurrent creation of a vascular network as well as the target tissue. The use of the technique has also been shown that osteoprogenitor cells show a higher expression of alkaline phosphatase (ALP), an early osteogenic differentiation marker, when cocultured with endothelial cells. An vast amount of research has been published on coculture techniques for bone tissue engineering, ranging from preculture of endothelial cells *in vitro* followed by the addition of the osteoprogenitor cells to the scaffold but prior to *in vivo* implantation[20] (Figure 2.1), preculture of both cell types *in vitro* and eventual implantation into an animal model [32,49–51] (Figure 2.2), to a direct coculture *in vivo* [21,37,52]. However, despite these efforts, there has been limited success with complete integration of the implanted scaffold with the functional perfusion of the host tissue's vascular system.
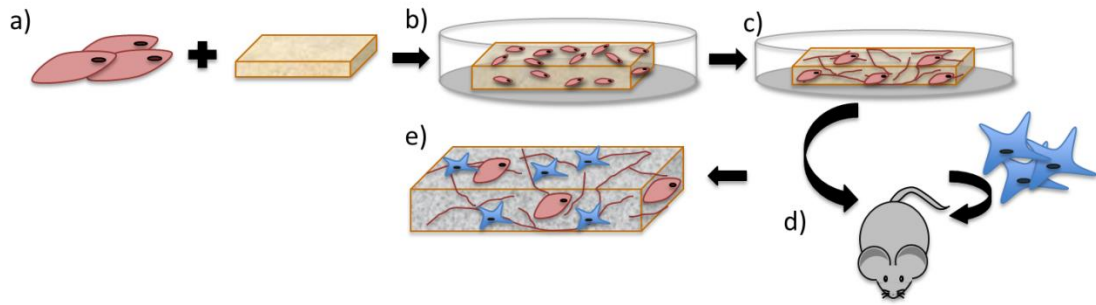
Figure 2.1 In vitro prevascularization using endothelial cells followed by *in vivo* coculture. Scaffolds can be prevascularized *in vitro* when seeded with endothelial cells prior to *in vivo* coculture with osteoprogenitor cells. a) Endothelial cells seeded on scaffold and cultured *in vitro*. b) Endothelial sprouting and tube formation indicate a prevascularized network. c) Prevascularized scaffold is co-seeded with osteoprogenitor cells and then implanted *in vivo*. d) Resulting scaffold shows mature blood vessel formation and bone tissue development.
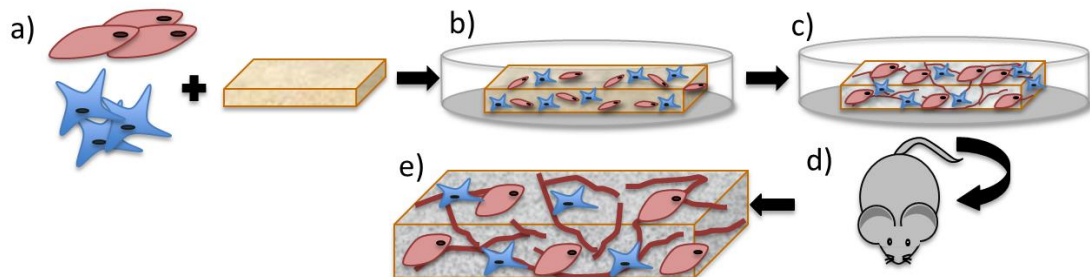
Figure 2.2. *In vitro* prevascularization via coculture of endothelial and osteoprogenitor cells. An *in vitro* coculture of endothelial cells and osteoprogenitor cells can prevascularized a scaffold prior to implantation *in vivo*. a) Seeding and coculture of endothelial cells (red) and osteoprogenitor cells (blue) onto scaffold. b) *In vitro* culturing of construct will result in c) neovascular tube and bone tissue formation. d) Once implanted *in vivo*, the scaffold will become further vascularized while extracellular bone matrix is formed.

There are some general considerations to bear in mind when it comes to cocultures. In addition to the cell type, the choice of culture media, seeding density, culturing environment, and scaffold architecture are less apparent. For example, as described previously, the source and type of endothelial cells and stem cells can have a lasting effect on the engineered bone, with promising results emerging with the use of EPCs and hMSCs. Likewise, the ratio of endothelial to osteogenic culturing media as well as proportion of endothelial to osteoprogenitor cells will affect vascular formation and osteogenic differentiation [20,53]. Ma *et al*. determined that a 1:1 ratio of the two cell populations, cocultured in osteogenic media only, resulted in the most mineralization and angiogenic development *in vitro*.

The combination of endothelial and osteoprogenitor cells has been especially common in bone tissue engineering cocultures. Both cells types are known to secrete specific growth factors that are beneficial for growth and differentiation for each other. For example, osteoprogenitor cells secrete VEGF that can be used for proliferation and angiogenic processes by endothelial cells [54]. Likewise, endothelial cells are known to secrete growth factors such as insulin growth factor-1 [55], endothelin-1, and bone-morphogenic protein-2, promoting osteogenic growth and differentiation [56]. In addition, it has been shown that the cell-to-cell communication between endothelial cells and osteoprogenitor cells can increase the production of the early osteogenic marker alkaline phosphatase [38,39].

Lastly, evidence from literature shows that mechanotransduction plays a synergistic role in the coculture of cells on scaffolds for bone tissue engineering. The phenomenon converts a mechanical stimulus into chemical activity, such as a

signaling pathway. It is hypothesized that the fluid flow experienced by the cells imposed by loading regimes can influence cell proliferation and differentiation downstream [57]. However it is still far from being completely understood. Therefore, further research should investigate the effect of mechanical stimulation on signaling pathways within and between endothelial cells and osteoprogenitor cells that lead to enhanced angiogenic and osteogenic effects. Preliminary studies have shown that the mechanical stimulation of coupled gap junction proteins between the two cell lines can drive osteoblastic differentiation, emphasizing the importance of cell-to-cell communication [58].

2.5 Growth factors

While scaffold properties such as porosity and degradation rates have shown to affect angiogenesis both *in vitro* and *in vivo*, a variety of different growth factors have been used to in the modification of scaffolds to further promote the formation of vascular networks. Promising results have been published about combination therapies of cell and angiogenic growth factor deliveries to tissue defect sites [59]. These additions to the cell culture mimic *in* vivo conditions, stabilizing the cells and protecting them from proteolytic digestion. It has been shown that successful vascular network formation requires coordination of not only the right cell type, but also the appropriate signaling factors, such as VEGF, delivered at the proper concentration and exposure times [9]. Approaches so far have focused on pre-seeding scaffolds with growth factors prior to implantation or the incorporation of a slow-release of soluble pro-angiogenic factors within the scaffolds.

14

VEGF is one of the most used pro-angiogenic factors and plays multifunctional roles in vascular permeability, repair, and remodeling processes. In addition, it maintains vascular structure and function. It has been used extensively in a variety of different scaffolds, at different concentrations, and at different time points during culture of endothelial cells for the purpose of bone tissue engineering [31,59–61]. Studies have confirmed that VEGF plays an essential role in the neovascularization of tissue and modulates endothelial growth, proliferation, migration, and tube formation, therefore making it an important factor in inducing angiogenesis. Bone morphogenetic protein (BMP) is another family of growth factors identified to support the use of cells for bone-tissue engineering. They promote bone formation by inducing MSCs towards osteoblastic differentiation. The combination of BMP-2 and BMP-7 as osteogenic promoters has shown to be the most effective inducer of bone morphogenesis [62]. Yilgor *et al*. also showed that the incorporation of both growth factors lead to more effective differentiation than when added individually.

Although the relationship and interaction between VEGF and BMP has been thoroughly examined, angiogenesis' direct effect on osteogenesis is not yet fully understood. It is hypothesized that VEGF is able to elicit two stages (considered early and late phases) of angiogenesis while BMP promotes osteogenesis [63]. In turn, while undergoing osteogenic differentiation, MSCs secrete more BMP and VEGF than when cultured alone, enhancing both processes [37].

However, even though the delivery of these growth factors is known to enhance vascularization and osteogenesis in constructs after implantation, their

15

dosage and timing must be tightly controlled. Ozawa *et al.* determined that a sufficiently high local VEGF concentration of around $70ng/10^6$ endothelial cells/day had a more positive impact on angiogenesis than the same concentration sustained over a 28 days [64]. In addition, the group discovered that above $100ng/10^6$ endothelial cells/day, the resulting unstable blood vessel formation. Excessive amounts of VEGF have also shown to lead to severe vascular leakage, tumor growth, and retinopathies in neighboring tissues [40]. Geuze *et al*. explored the effect of controlled release BMP-2 and VEGF on bone formation in a large-animal model when encapsulated in PLGA microparticles and implanted in critical sized ulnar defects in dogs [65]. The group determined that ectopic bone formation was highly dependent on the dosage and speed of BMP-2 release, but independent of VEGF release.

2.6 Experimental Setups/Techniques

2.6.1 In vitro prevascularization

When cultured with angiogenic growth factors such as VEGF *in vitro,* endothelial cells are able to form prevascular structures before the construct is implanted *in vivo*. For this method, endothelial cells are usually added to the target tissue cell population, such that they are cocultured to create a prevascularized network within the tissue. After implantation, the network can then spontaneously anastomose with the host's tissue vascular system and allow for complete perfusion of the graft [66]. This method is advantageous because it does not rely on the slow integration of the surrounding blood vessel network, which often leads to tissue necrosis at the center of the graft. Instead, the pre-established endothelial system can

directly connect to the surrounding network, allowing for faster blood perfusion. On the other hand, complete *in vivo* vascularization of the construct can still take days or even weeks because the construct's vascular system is not microsurgically connected to the surrounding network following implantation. The effectiveness of *in vitro* vascularization could be improved if micro-surgical methods were used to help with the graft anastomosis.

Although prevascularization of endothelial cells has shown great promise for the formation of blood vessels, has Ghanaati *et al.* demonstrated that the *in vitro* preculture period of osteoblast cells seeded on scaffolds may not play as prominent a role in vascularization as previously thought. The group cultured primary human osteoblasts (hOBs) on fibrin scaffolds for 24 hours as well as 14 days before implanting the constructs subcutaneously in an immunodeficient mouse model. After 14 days *in vivo*, both groups showed significant scaffold vascularization. The 14-day preculture group resulted in significantly better penetration of the hOBs throughout the scaffold [33], possibly leading to better neo-bone formation and dramatic enhancement of the host-derived vasculature. This phenomenon may be explained by the hOBs ability to create sufficient extracellular matrix and signaling factors during the preculture period, providing a strong pro-angiogenic stimulus once implanted *in vivo*.

   2.6.2 *In vivo* prevascularization

Even though a variety of the body's complex physiological conditions may be mimicked *in vitro*, it does not provide a complete picture of a scaffold's potential and effect within a defect site. A successful *in vivo* implantation of a construct will be

more revealing of the bone tissue-engineered capability to be translated into a relevant clinical application. The location and length of implantation can have a significant effect on the resulting growth and maturation of seeded cells. *In vivo* prevascularization can be completed using a variety of different techniques and the concept should be applicable to many engineered tissue types. In almost all cases, the purpose is to implant an endothelial cell- and target cell-seeded graft into a highly vascularized tissue, such as muscle. There, the graft will become naturally become vascularized over a period of time, after which it can be harvested and implanted into the defect site.

2.6.2.1 Cell sheet layering

Another recently developed *in vivo* vascularization technique is cell sheet engineering. It utilized the thermo-responsive properties of poly(N-isopropylacrylamide) (PIPAAm), which is a well-known temperature-activated polymer, to induce detachment of intact cell sheets [67]. Cell sheet engineering was originally used for corneal surface reconstruction, blood vessel grafts, and myocardial tissue engineering [11]. Since then, the technique has also been utilized in some bone tissue engineering applications [68]. A variety of different cells that secrete their own extracellular matrix (ECM) can be cultured in monolayer and then recovered within their own ECM without the use of a proteolytic enzyme, lifting as an entire sheet. Cell sheet-based tissue engineering has been applied for regenerative medicine for several different tissues, including myocardial, corneal epithelial, lung, and liver tissue [69–72]. Seeding the sheets on scaffolds allows for a three-dimensional environment. To determine cellular behavior and study biomaterial immune response

in vivo, the construct is implanted subcutaneously into animal models. The cell-sheet

tissue engineering technique is depicted in Figure 2.3. Pirraco *et al.* cocultured rat

bone marrow stromal cells and HUVECs into a cell sheet using thermal-responsive

culture dishes [51] and then implanted them subcutaneously into the dorsal flap of

nude mice, demonstrating new bone formation as well as neovascularization by day 7.

Others have used cell sheet layers to cover scaffolds before *in vivo* implantation. A

range of scaffold materials have been used, including coral scaffolds [73],

hydroxyapatite ceramic scaffolds [74], and polycaprolactone-calcium phosphate

scaffolds [37]. Layering of cell sheets has also shown improved overall

vascularization because one cell sheet is added at a time, with 1-3 days of

subcutaneous vascularization culturing in between. Even though time-consuming, this

resulted in completely vascularized tissues after several weeks of *in vivo* culturing

[68].

Even though this technique has been extensively utilized in myocardial tissue

reconstruction [69], more research should be done to apply the technique to bone

tissue vascularization where is evident that it can provide efficient blood vessel

formation within the bone tissue construct. However, further optimization of the

coculture methods for repair of a bone defect would be necessary. For example, while

both endothelial cells and osteoprogenitor cells have been shown to form cell sheets

independently from each other, their behavior and function when cocultured together

in such form has not yet been investigated. Similarly, the dense and intertwined cells

within the sheet may inhibit vascularization and bone formation by the respective cell

types. However, alternating cell type layers could be a possible solution for creating

larger vascularized cell constructs. Lastly, a dynamic *in vitro* culture of layered cell

sheets could further enhance the endothelial network formation as well as promote

bone formation prior to implantation into an animal model.
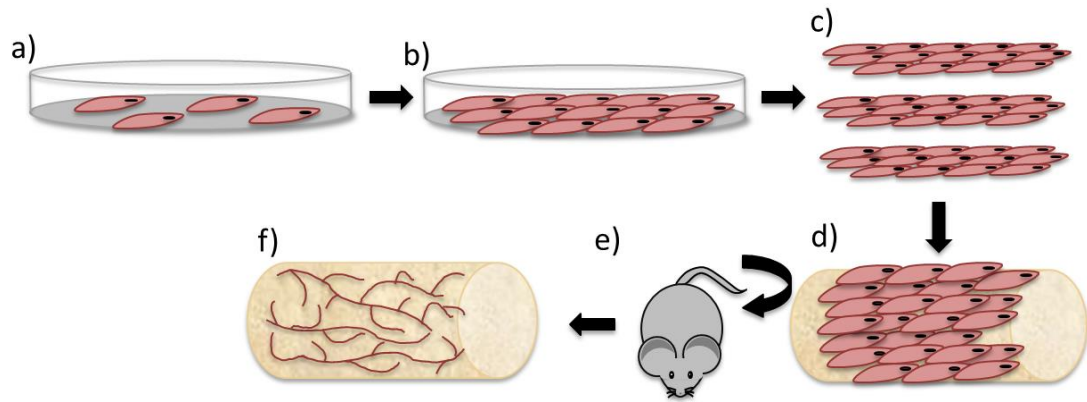
Figure 2.3 Cell sheet layering used for *in vivo* vascularization of tissue-engineered scaffold. Endothelial cells can be cultured into confluent cell sheets and used to cover tissue-engineered scaffolds to create a prevascularized network. a) Endothelial cell can be cultured on special thermo-responsive tissue-culture plates. b) When confluent, the cells will have attached to each other via their extracellular matrix forming a cell sheet. c) Several of such sheets can be combined and d) seeded onto a scaffold. e) The endothelial cell-sheet- covered scaffold can be implanted subcutaneously *in vivo*, resulting in f) a prevascularized graft.

2.6.2.2 Dorsal skinfold chamber

Implant observation chambers have been used for decades to monitor living tissues. They are frame structures surgically attached to an animal, which allow for continuous monitoring of through a glass slide window. Since its invention, the dorsal skinfold chamber's use has been adapted to different animals and applications. Most advantageously, observation chambers allow for intravital microscopy of the microcirculation of tissue [75].

To create the dorsal skinfold chamber, a small incision is made in the dorsal region of the animal to remove the cutis skin layer, around 15mm in mice. The remaining layers, consisting of the epidermis, subcutaneous tissue, and a thin layer of striated skin muscle are then covered with a coverslip and incorporated into a metal frame, usually composed of titanium or aluminum. The frame sandwiches the thin layers and keeps them in place using steel nuts as spacers, thus preventing compression of the nutritional blood vessels. Within these layers, pieces of biomaterial scaffold can be implanted to study their vascularization while cultured in the dorsal skinfold chamber. The cover-slipped window allows for intravital microscopy of the area and observation of the developing vascular network. Several groups have shown that the animal shows no sign of discomfort, including changes in feeding or sleeping habits after chamber implantation.

This experimental setup has been used to investigate a wide range of scaffold and cell combinations to optimize the vascularization of a tissue. For example, sphingosine 1-phosphate (S1P) is a bioactive phospholipid, which affects migration, proliferation, and survival of endothelial cells and osteoprogenitor cells [44] and has

been tested using the dorsal skinfold chamber. The study evaluated its direct impact

on the structural remodeling response of the vascularization and subsequent healing

of a bone defect site and found that sustained release of S1P resulted in enhanced

luminal diameter of formed vasculatures as well as increased bone formation after 2

and 6 weeks [44].

In order to image the blood vessels more effectively, a contrast agent is often

injected, such as fluorescein isotheiocyanate-labeled dextran [75], which labels

plasma. In addition, leukocytes can be traced after intravenous injection of

fluorescent markers such as acridine orange [75], to better understand the immune

response to the implanted scaffold.

One of the major advantages of the dorsal skinfold chamber method is that it

allows for repeated microscopic analysis over a long period of time, often lasting for

several weeks, without causing any noticeable harm or discomfort to the animal. The

subcutaneous location and finely striated tissue provides the ideal environment for the

purpose of studying the development of a vascular network within a foreign

biomaterial *in vivo*.

 However, some limitations of the dorsal skinfold chamber method do exist.

For example, due to the size limitations of the animal and the corresponding size of

the surgical incision, the implanted engineered construct cannot exceed 5mm in

diameter in order to properly fit in the 15mm-sized chamber [76]. In addition, the

height, or thickness, of the construct cannot surpass 1mm, so that it does not interfere

with the closure of the chamber tissue by the coverslip. Such limitations may prevent

the use of this *in* vivo technique for large-scale bone tissue applications. A thicker

biomaterial will require a thicker layer of tissue within the chamber, inhibiting image quality. Laschke *et al*. [28] utilized the dorsal skin chamber to evaluate the angiogenic response of their nano-sized hydroxyapatite particles mixed with and without poly(ester-urethane) and found that capillary sprouts were forming at the border of the scaffold, coming from the surrounding tissue, in both groups with no significant difference. Druecke *et al.* also utilized the dorsal skinfold method to test the neovascularization within a poly(ether ester) block-copolymer scaffold. Intravital fluorescent microscopy and quantitative data analysis of data showed that after 20 days of implantation, the microcirculation at the border of the construct resembled that of the surrounding tissue. However, the center of the graft showed significant leakage of plasma, indicating that the newly formed endothelial network was not yet mature [77].

Several issues would have to be addressed if used for bone tissue-engineering applications. For example, the beyond the size limitations, the dorsal skinfold chamber does not provide the same bone growth and signaling factors, nor does it provide any of the mechanical loading normally applied in a bone defect site. Therefore, this technique could be used as prevascularization scaffold, but osteoprogenitor cells would be require additional stimulation for bone formation.

2.6.2.3 Arteriovenous (AV) loops

An arteriovenous loop is another common *in vivo* method used to prevascularize scaffold prior to the injection or seeding of the target cells. This method utilizes the native blood vessel system by forming a shunt loop between an artery and a vein using a synthetic graft. This is then enclosed within a chamber that

is either empty or houses a tissue-engineered scaffold, which will be vascularized over time [Dong 2012]. Within bone tissue-engineering, several people have taken advantage of this efficient *in vivo* method to create a mature endothelial network within a scaffold [73,78]. When a processed bovine cancellous bone (PBCB) matrix was implanted into an animal model using the AV loop as a vascular carrier, adequate vascular density and kinetics demonstrated that capillary sprouting was occurring in all parts of the graft even the center. After 8 weeks of *in vivo* culturing, the group was able to demonstrate the first successful vascularization of a solid porous matrix using the AV loop technique, followed by bone formation throughout once implanted into a bone defect. Dong *et al.* evaluated vascularization of a natural coral block using the AV loop method in a rabbit model. Results showed that natural coral blocks, a biocompatible and osteoconductive scaffold, can be vascularized using the AVL method and be used for future bone substitute following osteoblast seeding.

One of the disadvantages of the AVL technique, however, is that control the ingrowth pattern of fibrovascular cells is difficult. Therefore, the vascular network may dominate the scaffold structure, especially on the border, minimizing the space for target cell seeding. In addition, similar to the dorsal skinfold chamber method, following implantation and vascularization in the AV loop, the bone tissue-engineered scaffold will have to be removed for further culturing and transplantation into the actual bone defect potentially resulting in donor site morbidity.

2.6.2.4 Chick embryo chorioallantoic membrane (CAM)

One of the innovative techniques used to accomplish prevascularization of a scaffold involves the use of the chorioallantoic membrane of a chick egg (Figure 2.4).

To obtain this thin membrane, which surrounds the inside of the shell, a fertilized and developing egg is incubated at physiological conditions for three days. The egg contains a special extraembrionic membrane that supports respiratory capillaries, ion exchange, and embryonic vasculature while the chick is developing. After a brief incubation, a circular window is made into the shell and is resealed with tape and cultured for an additional 7 days. Then, the tissue-construct is carefully implanted by placing it onto the surface of the CAM and then resealing it with cellotape and incubating for an additional 8 days, at which point the scaffold is removed for analysis. This relative brief culturing period, compared to week to month long periods required by other methods, is possible because the CAM undergoes significant capillary formation until day 20 of chick embryo development [79].

Steffens *et al.* performed a chick embryo chorioallantoic membrane assay to evaluate the angiogenic potential of cell-seeded processed bovine cancellous bone and found that vessel formation was visible after 8 days of implantation [21]. Similarly, Buschmann et al. used the CAM method to show rapid and homogenous vascularization of human adipose-derived stem cells on PLGA/calcium phosphate nanoparticles scaffold [80].

However, one of the major disadvantages of the CAM method is that there may be a nonspecific inflammatory response to the implanted biomaterial, altering the seeded cell response and behavior. This hurdle may be overcome if the implantation is made very early in the development of the CAM, when its immune system is still relatively immature. In addition, the CAM method is not ideal for long-term monitoring of angiogenesis because the egg will continue to mature and prevent

removal of the scaffold [79]. The method of using chick chorioallantoic membranes from embryos could also be ethically controversial, although less so than the use of human embryonic stem cells. In addition, the combination of human cells with animal cells could also lead to disease transmission and rejection after the scaffold is explanted from the CAM system and implanted into a bone defect.

On the other hand, the CAM method could be advantageous, because it provides the growth factors and microenvironment necessary to promote neovascularization, a process still poorly understood. The rapid vascularization of the system provides a simple, inexpensive, and effective method of evaluating the response of seeded scaffolds. With a few improvements to the current validation strategies used to evaluate the constructs while still implanted, CAM can be a great tool to study the biological response to biomaterials and cultured cells before moving on to large animal *in vivo* studies. In addition, it is a relatively easy assay and inexpensive to perform, requiring only minimally invasive techniques to obtain a prevascularized tissue-engineered construct.
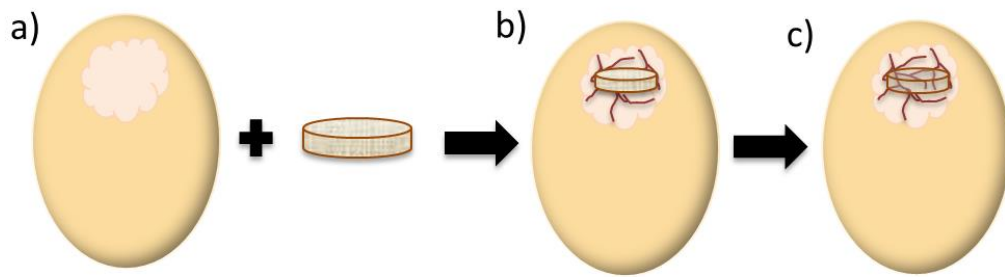
Figure 2.4 Scaffold prevascularization using the Chick Embryo Chorioallantoic Membrane (CAM) Technique. Scaffolds can be prevascularized without the use of endothelial cells by implanting them into fertilized chick embryo eggs. a) A small portion of the eggshell is removed, exposing the embryo's chorioallantoic membrane. b) A scaffold is then placed on top of the membrane and the shell is taped up. c) After 8 days of culture, the scaffold will become vascularized as the chick embryo develops its own vascular network.

2.6 Methods of Validation

After *in vivo* transplantation of cell and scaffold constructs, the development and functionality of microvascularization need to be evaluated. The most common methods of evaluation include histological analysis, imaging techniques, or a combination of assays, imaging, and quantitative analysis.

2.6.1 Histological Analysis

Histology has become one of the most common methods of validation for all types of tissue engineering applications. For the purpose of tracking and evaluating vascularization of bone tissue constructs, this method has been especially invaluable. It allows for clear visual validation of the blood vessel formation at the borders and the center of the graft. With protein-specific labeling, the implanted endothelial cells can be differentiated from those of the host tissue, further indicating the extent of neovascularization and integration into the surrounding tissue. Histologically processed tissues are most commonly fixed, embedded, and then sliced into micron-thick sections, after which they can be stained for proteins of interest using primary antibodies. Immunofluorescence has also become a popular technique as it allows for simultaneous staining and visualization of proteins within the tissue.

The bone formation progress can be tracked and visualized with the help of histological protein markers. Early osteogenic differentiation proteins include ALP and osteoprotegerin (OPN) [74,81], while late markers, such as osteocalcin, osteopontin, and collagen type I are expressed during the latter phase of osteogenic differentiation [23,37]. In addition, mineralization of the scaffold can be visualized using von Kossa or alizarin red stains, which is indicative of calcium deposition and

early bone formation [20,23,37]. The development of vascularization can also be easily followed by staining for specific angiogenic markers, such as CD31, CD34, and von Willebrand factor (vWF) [82]. Certain adhesive proteins are located at endothelial cell junctions, including VE-cadherin, connexins, and claudins, and are indicative of the tight cell-cell junctions formed between endothelial cells [83] and increase in density as angiogenesis progresses.

The advantage of a histological analysis is that tissues can be easily visualized under bright-field or fluorescence microscopy and it can provide a three-dimensional representation based on different sections within the construct. One of the disadvantages of performing histology on *in vivo* cultured constructs, however, is that it is a terminal procedure. Therefore, the animal is usually sacrificed in order to remove the implanted scaffold after a certain period of time.

Histomorphometry is a subsection of histology where the specific change in morphology of a structure is especially important, allow for a more macro-scale analysis of the entire construct. Computer-aided software is able to quantify the formation of new bone on the surface, as well as within the porous structure of the graft. More specifically, histomorphometric sections have also been used to quantify vessel diameter and vessel density in the scaffold [84]. Images are taken at up to 200x magnification to see structures such as formed vessel cross-sections, bone interface contact, and bone volume densities. This type of information can be used to evaluate bone growth, scaffold integration, and vascular formation. However, similarly to the basic histology technique, this method is terminal and does not provide live and functional information.

2.6.2 Imaging Techniques

The combination of *in vivo* fluorescence microscopy and the dorsal skinfold chamber technique has proven to be invaluable to monitoring the inflammatory and angiogenic response of the body to a biomaterial. It also provides for a quantitative method to assess the formation of vasculature.

After capture, images can be analyzed quantitatively offline using a variety of software packages. For example, leukocyte-endothelial interaction can be observed within the scaffold, indicating the acute inflammatory response to the implanted construct, by classifying them into either adherent, rolling, or free flowing cells [28]. In the case of nanosized hydroxyapatite particles/poly(ester-urethane) scaffolds, the number of adherent leukocytes was comparable to the control poly(ester-urethane) scaffold, demonstrating that the body had an insignificant immune response to the implant.

Traditionally, immunostaining has been used to quantify and visualize induced vascularization *in vivo*. However, one drawback to this method is that it is a terminal procedure for the animal. Therefore, more advanced and techniques have been developed that allow for functional measurement of the architecture and perfusion of the newly created vasculature.

Three-dimensional scaffolds have been scanned with resolutions of up to 10 microns using microCT, giving enough detail to determine density, branching, and connectivity of the networks [85]. Blood flow has also been studied using laser Doppler diffusion imaging [30] as well as the use of transfected cells labeled with GFP that can be tracked using a fluorescence microscope [86].

Offline analysis software has been used extensively to quantify microscopy images. Wernike *et al*. determined the functional capillary density of the scaffold post-implantation, defined as the length of perfused capillaries per area [52]. The group also looked at bone formation properties such as volume of bone pores, bone density, and the areas of interaction between bone and vessels. In addition, vascular leakage has become an established parameter used to evaluate the success of vascularization because it indicates the maturity level of the neovasculature.

2.7 Limitations in Current Coculture Techniques

Overall, *in vivo* techniques have shown that integration of a bone tissue-engineered construct with the host vasculature can lead to successful anastomosis. Full or partial perfusion of the graft has been demonstrated, with endothelial sprouting and vessel formation shown after implantation.

However, the field of tissue engineering still faces some major challenges that need to be addressed before these approaches can be used for clinical applications. The importance of the cell source cannot be overlooked, especially due the risk of infection and disease transmission. The method of prevascularization must also be carefully considered; *in vitro* pre-seeding of endothelial and osteoprogenitor cells onto scaffolds may lead to a basic layout for a vascular network of endothelial cells prior to *in vivo* implantation. On the other hand, an *in vivo* prevascularization technique may result in a denser vascular network, yet it requires an additional invasive surgical step. It is also important to note that if implanted for prevascularization for too long, scaffolds often degrade and become too highly integrated into the host tissue to remove.

Even though most of these bone-engineering techniques are performed *in vivo* to determine the effect of the unique microenvironment provided by the body, few actually study the direct effect of implantations into bone defects. While subcutaneous implantations into muscle pockets are valuable in terms of determining the immune- and cytotoxic effect of the constructs, they do not properly mimic the structural and dynamic environment of the bone. Experiments that transplant the tissue-engineered constructs into highly vascularized tissues such as the muscle, falsely provide high blood flow and the presence of a variety of different types that fail to mimic the environment of a bone defect. While successful neo-bone and vascular network formations have been demonstrated in these experimental setups, an additional transplantation into the actual bone defect site might lead to site morbidity and increased risk of infection. These *in vivo* techniques also result in a longer culturing time. Before cells can be seeded onto the scaffolds, they are cultured and conditioned *in vitro* first. Once implanted, it can take weeks to months for the entire scaffold to be completely vascularized.

Some of the advantages of *in vivo* vascularization techniques include a more accurate microenvironment to evaluate the scaffold and cell construct interactions with the surrounding tissue environment compared to current *in vitro* methods. Even though they have significantly improved the culturing environment to closely resemble that found *in vivo*, there are still many factors that are poorly understood. Small-scale *in vivo* studies, such as the CAM assay, can provide preliminary, yet critical data on bone tissue-engineering constructs prior to larger *in vivo* experiments.

While the field of bone tissue-engineering has made tremendous strides towards bringing bench top applications towards clinical use via the use of *in vivo* experiments, there is much left to do until a fully vascularized bone construct can successfully heal a bone defect in a patient.

2.8 Overcoming Current Restraints

The compilations of studies described in this work address some of the above described obstacles in coculture systems. First, the use of primary human cells, such as human mesenchymal stem cells (hMSCs) and human umbilical vein endothelial cells (HUVECS), provide an essential basis for a bone tissue engineering platform. These cells will prevent adverse immune response to non-native cells as well as decrease the chance for disease transfer if cells are harvested directly from the patient. Second, the *in vitro* prevascularization of the bone construct will expedite the integration of the implant with the host tissue after surgery without adding an addition step such as *in vivo* vascularization with a secondary surgery. The anastomosis of organized endothelial cells in vascular networks with existing blood vessel structures will provide critical nutrients and oxygen to the bone graft, therefore preventing necrosis of the implanted cells.. Additionally, the pre-culture of the graft in dynamic culture using a perfusion bioreactor supports the cell function of both cell types during coculture, closely mimicking the *in vivo* environment in regards to providing shear and nutrient supplies. Combined, these steps result in major improvements over current bone tissue engineering techniques

Chapter 3: Mesenchymal Stem Cells: Roles and Relationships in Vascularization[2]

3.1 Introduction

Complete vascularization of engineered tissues is currently a major hurdle in the field of tissue engineering, inhibiting successful post-implantation viability. Several strategies have been investigated to overcome this problem, often involving overexpression of angiogenic and vasculogenic factors such as vascular endothelial growth factor (VEGF)[41,58] or combining bioactive scaffolds with encapsulated cells [52][40,42] In addition to molecular signals, several other environmental factors have been considered to play an important role in promoting vascularization in the presence of MSCs. These include environmental effects and interactions with various cell populations. Still, complete vascularization of tissue engineered constructs and subsequent host integration for clinical applications has yet to be fully realized. To overcome these challenges, research has focused on optimizing culturing conditions *in vitro* in preparation for clinical applications. Mesenchymal stem cells (MSCs) have become a standard cell population to be cultured with vascular cell types due to their ability to act as support cells and accelerate vascularization and angiogenesis. The availability and differentiation potential of MSCs makes them a popular choice in many developing technologies designed for clinical applications.

To further illustrate the importance of the role of MSCs in vascularization, a survey was conducted by querying leaders in the field of tissue engineering to

---

[2] BNB Nguyen*, AJ Melchiorri*, and JP Fisher. "Mesenchymal Stem Cells: Roles and Relationships in Vascularization." Tissue Engineering Part B: Reviews. 20: 1-11 (2014).

compile and rank strategies for achieving the clinical development of tissue

engineering technologies [87]. The analysis of the survey results identified key

strategic concepts in the future development of the field. The two most important

strategies were found to be angiogenic control and stem cell science. Thus, in the

spirit of these findings, we present current concepts and strategies focusing on the

interactions of MSCs and vascularization. The interactions between MSCs and the

process of tissue vascularization are intimately related, revealing interdependent roles

in the goal of developing functional tissue constructs with MSCs. This review will

evaluate current strategies used to improve vascularization of engineered constructs

using MSCs and a variety of vascular cell types. The individual roles of these various

cells in vascularization have been extensively characterized and reviewed, as

illustrated by Table 1, and we present how environmental conditions and these cell

types influence vascularization.

Cell Type	Function	Common Markers	Relevant Reviews
MSC	• Non-hematopoietic stromal cells • Can differentiate into bone, cartilage, fat, or muscle lineages • Homing ability for tissue regeneration	CD34-, CD106, CD166, CD 146, SH2, Stro-1	[88–91]
EC	• Innermost layer of blood vessels • Performs crucial regulatory roles • Enables nutrient and waste transfer	CD31, VE-Cadherin, VEGFR-1, VEGFR-2, vWF	[92–94]
EPC	• Express VEGF • Support new vessel formation • May differentiate into ECs	Early EPCs: CD14, CD31, CD34, CD45, VEGFR-2, VE-cadherin, vWF Late EPCs: CD31, CD133, VEGFR-2, VE-cadherin, vWF	[95–97]
Pericyte	• Wrap around EC layer • Initiate vessel maturation • Regulate microvessel integrity, structure, and function	α-SMA, PDGFR-β, NG2-proteoglycan, annexin A5 (Markers dependent on resident tissue)	[98–100]

Table 3.1 MSCs and Other Relevant Cell Types Involved in Vascularization of Tissues

3.2 Vascularization interactions with MSCs

3.2.1 Hypoxia

The optimal culturing conditions for MSCs have long been studied, with oxygen tension being one major characteristic[101]. It has been determined that developing embryos have much lower oxygen tension than most normal adult tissue, while tissues known to contain stem cells are often in an even lower oxygen concentrated environment[102]. This low oxygen tension has been shown to maintain the undifferentiated state of mesenchymal stem cells as well as prolong their lifespan and proliferation capabilities[103]. However, differentiation into adipocytes and osteocytes was hindered at such low oxygen levels and required subsequent stimulation at higher oxygen concentrations. This discovery highlights the importance of oxygen levels as a critical influence on MSC growth and differentiation. Therefore, these culturing conditions have been widely investigated in order to optimize vascularization in engineered tissues[104–106].

The molecular mechanism of hypoxia has been widely studied, for the purpose of neovascularization as well as angiogenesis for cancer metastasis. It has been found that hypoxia-inducing factor 1 (HIF-1) is one of the major regulators that orchestrates the cellular response to hypoxia[104]. As a transcription factor, it is able to modulate vascularization through activation of endothelial growth factors and transcription factors. Under hypoxic conditions, HIF-1's alpha subunit is upregulated exponentially, triggering a series of downstream transcription cascades that result increased expression of vascular proteins such as VEGF [106].

4

MSCs have been found in close association with blood vessels in a wide variety of tissues.[107,108] Even though MSCs are located very closely to vascular structures, they are often still found in a relatively low oxygen environment, which indicates that a hypoxic surrounding may be necessary in order to maintain the cells' undifferentiated state[101]. Hypoxia leads to decreased adipogenic and osteogenic differentiation,[109,110] triggering the release of angiogenesis factors as well as promoting the expression of vasculogenic characteristics and functions in MSCs [111,112].

With physiological conditions in mind, there are proliferation benefits for cells cultured in low oxygen environments. The effects on MSCs' behavior include better survival, proliferation, and differentiation. More specifically, hypoxia can stimulate proangiogenic factors in MSCs. For example, VEGF and Interleukin-6 (IL6) show increased expression after hypoxic stimulation. In addition, MSCs that were cultured under physiologically relevant hypoxia (2% oxygen) in a 3D environment saw longer proliferation periods as well as expression of increase in MSC gene expression than those cultured at normoxic (20%) conditions. [102] The level of hypoxia, as well as the time of application, has also shown to be important for *in vivo* vascularization applications. Preculturing of MSCs in hypoxic conditions have demonstrated improved angiogenic function once transferred into an *in vivo* environment.[113–115] MSCs were shown to have enhanced migration rates and a number of upregulated growth factors and corresponding receptors, such as hepatocyte growth factor (HGF), which is responsible for MSC recruitment to damaged and ischemic tissues.[113] These results demonstrate the sensitivity of

MSCs to their culturing conditions and the potential to fine-tune their environment to enhance vascularization in tissue constructs as well as *in vivo* transplantations. MSC tissue-constructs cultured at 2% oxygen demonstrated a switch in metabolic pathways and exhibited increased proliferation potential compared to those cultured at normal oxygen tensions.[116] Changes in total protein levels and ECM expression suggest that hypoxia altered the MSC tissue development processes. Furthermore, hypoxic conditions are able to better maintain the stemness of undifferentiated MSCs, preserving their multi-lineage differentiation ability. These findings indicate that oxygen tension may be an important culture parameter in developing *in vitro* tissues using MSCs.

Nevertheless, while considerable work with hypoxia has been done in the field of tissue engineering, there is no convincing evidence that a preculture of cells under hypoxic conditions alone will be sufficient to sustain tissue-engineered constructs larger than a few millimeters after implantation long term. Therefore, a combination of vascularization techniques may be required to complete vascularization *in vivo*.

3.2.2 Physical blood flow

While paracrine and endocrine signals play a large role in controlling MSC behavior, mechanical forces and stimuli may also have an important impact on vascularization. Specifically, shear stress, a mechanical force generated by fluid flow, has been shown to induce MSC differentiation and activation of vasculogenic pathways.[117–119] In the body, shear stress is generated by blood flow through the endothelium, which applies physical tension to cells. In order to mimic this type of mechanical stress *in vitro,* a flow chamber can supply steady fluid shear stress

6

ranging from 5-30 dyn/cm^2. Results after dynamic culturing have indicated an increase in genetic vascular markers and a decrease in MSC characteristics, demonstrating endothelial differentiation of MSCs for potential use in tissue engineering applications[120].

More specifically, molecular blood vessel formation pathways can be triggered by shear stress. It was observed that in some cells, levels of transforming growth factor (TGF β) and monocyte chemoattractant protein-1 (MCP-1) greatly increased in response to shear stress, while VEGF expression remained unaffected. Similarly, studies have identified shear stress receptors on the surface of MSCs that may be involved with molecular events related to vascularization. For example, CD31 receptors activated by shear stress have been shown to increase the recruitment of neutrophils and expression of TNF-α, both indicators of early vascularization[121]. Several other studies have shown that ion channels, specifically Ca^{2+} channels, are sensitive to shear stress and can induce angiogenesis via VEGF-receptor-2 (VEGFR-2) activation and resulting phosphorylation of p38 and increased expression of VEGF[122]. The applied force of fluid flow has also lead to remodeling of the actin cytoskeleton, which regulates important intracellular processes and protein expressions, indicating the important role that mechanotransduction induced by of shear stress plays MSCs' vascularization pathways[123].

Different flow patterns also have an effect on MSCs differentiation. Laminar flow has shown increased VEGF production by MSCs but no change in cell morphology,[124] while dynamic rotational seeding resulted in vascular tube formation of MSCs[125]. The use of shear flow has also become especially popular in

tissue-engineered vascular grafts. Using pulsatile flow on a 3D graft, MSCs were successfully differentiated into endothelial cells (ECs) as seen through an increase in endothelial markers such as platelet-endothelial cell adhesion molecule-1 (PECAM-1) and VE-cadherin. In order withstand a range of shear stress to induce endothelial differentiation of MSCs *in vivo*, tissue engineered scaffolds have been modified with a variety of different bioactive molecules to improve cell adhesion and ensure immobilization in flow environments[126].

Several different factors have been combined in order to promote endothelial differentiation for the purpose of vascularization. For example, cultured MSCs under shear flow conditions as well as hypoxia have shown increased production of angiogenic factors and formation of microvasculature[119]. Such applications validate the complex *in* vivo culturing environment experienced by MSCs. Therefore, the use of flow stimulation may be a crucial step in advancing the field of vascularization in tissue engineering because it is able to imitate the dynamic *in vivo* environment most closely.

3.2.4 Interactions with endothelial cells

MSCs are known to adopt a supporting role when mixed with cells derived from tissues such as muscle, skin, endothelial, and renal epithelial layers[127]. It has been demonstrated that MSCs can promote tumor growth by increasing the secretion of pro-angiogenic factors, which enhance blood vessel formation in the surrounding areas[128]. With a higher blood and oxygen supply, tumor cells are able to proliferate much faster and result in increased tumor size.

The interaction between MSCs and ECs has shown to be highly regulated and requires precise spatial and temporal control. For example, formation of microvasculature is most successful after a delayed addition of MSCs to ECs encapsulated in collagen scaffolds and cocultured in an *in vitro* environment[129]. This setup emulates the *in vivo* environment most accurately because MSCs are recruited to the site of vascularization after the ECs have begun the initial formation of nascent microstructures[129,130].

The interaction between ECs and MSCs has been most pronounced in the application of wound healing. MSCs near the location of the wound secrete paracrine factors, such as VEGF, to recruit macrophages and endothelial cells, accelerating the wound healing process. This process requires a complex series of molecular events including cell migration, ECM deposition, angiogenesis and remodeling.[131] At the same time, damaged endothelial cells are able to recruit MSCs for the same purpose of tissue repair via chemokine receptors found on the surface of MSCs. These MSCs were then able to aid in the wound healing process through growth factor release as well as differentiation into endothelial cells[132].

Direct cell-to-cell contact between ECs and MSCs has been investigated to understand their signaling pathway and complex interaction. Utilizing a parallel plate flow chamber to mimic blood flow conditions, MSCs and human umbilical vein ECs (HUVECs) were cocultured with the objective to study the initial steps of contact[133]. Results showed rapid extension of the podia, followed by rolling and firm adhesion of MSCs to ECs. These results were enhanced when tumor necrosis factor-α (TNF-α) was added to the culture, or suppressed when treated with anti-P-

selectin or anti-vascular cell adhesion protein 1 (VCAM-1), indicating that binding is both selectin and integrin dependent. Additionally, combining any of those parameters would vary the degree of adhesion of MSCs to EPCs. These collaborative pathways indicate that MSCs and ECs are capable of coordinating their rolling and adhesion behaviors[132].

While ECs and MSCs may interact closely *in vivo*, their coculture has been less successful *in vitro*, with many microvessels turning out to be leaky and unstable once implanted[23]. An improved coculturing system with a higher ratio of supporting MSCs, for example, may accelerate the maturation of blood vessels. Additionally, a mixed population of vascular cells types will also closer represent the native populations necessary for vascularization.

Interactions with EPCs

Endothelial progenitor cells (EPCs) circulate the bloodstream and promote neovascularization in places of injury, ischemia, hypoxia, and tumorigenesis[134,135]. Beneficial interactions between MSCs and EPCs promote the development of tubular structures and vascular networks[136,137]. Such vascularization and vascular structure formation has been observed *in vitro* and *in vivo*, lending insight into the mechanisms underlying this process[3,137–139]. MSCs interact with EPCs both directly through gap junctions and indirectly through paracrine signaling, with major pathways highlighted in Figure 3.1[3]. Direct contact between MSCs and EPCs may lead to induced endothelial phenotypes, without the addition of exogenous growth factors, in both cell types [3,140]. These cell-cell interactions elicit dynamic, temporal changes in co-cultured EPCs and MSCs.

Initially, adhesion protein, growth factors and signaling cytokines are upregulated [3]. Proteins, such as CDh-5 and PECAM-1, present in vascular cell junctions and regulators of vessel permeability are upregulated [3,141]. VEGF, IGF1, and angiopoietin1 (ANG-1), responsible for vessel formation, pericyte recruitment, and EC differentiation, also experience early, increased expression [3,142,143]. In addition to these changes in RNA expression, MSCs have been observed to participate with EPCs in forming tube-like structures,[3] further supporting the synergistic relationship between MSCs and EPCs in neovascularization.

In EPC and MSC interactions, bone morphogenetic protein 2 (BMP-2) appears to have an important influence on EPCs through chemotactic effects [144]. Such effects are bolstered by the elution of angiogenic growth factors from MSCs. Secretion of these growth factors from MSCs was found to be dependent on MSC exposure to BMP-2 [144]. These secreted factors include placental growth factor (PIGF), which is a cytokine associated with the recruitment of EPCs [145]. Importantly, paracrine signaling between MSCs and EPCs are strongly dependent on the interplay between VEGF and BMP-2. BMP-2 plays an integral role in the osteogenic differentiation and function of MSCs. However, BMPs have also been shown to stimulate VEGF production. As VEGF stimulation drives angiogenesis, BMP-stimulated VEGF promotes angiogenesis [146]. Particularly, BMP-2 has been shown to stimulate angiogenesis in fracture-healing models [147,148].

These interactive pathways have been explored in functional assessments of EPC and MSC interactions. EPC and MSC synergistic interactions have been studied in critical bone defect repair in rats [137]. The bone defects were repaired with one of

the following treatments: autologous bone, β-tricalcium phosphate (β-TCP) as a scaffold, MSCs seeded on β-TCP, EPCs seeded on β-TCP, and a coculture of MSCs and EPCs seeded on β-TCP. The coculture of MSCs and EPCs produced the highest amount of vascularization, demonstrating the synergistic effects of MSCs and EPCs in bone repair. Co-transplantation of EPCs and MSCs shows good bone regeneration and vascularization potential [138]. In addition to the enhanced vascularization demonstrated with the co-implantation of EPCs and MSCs, it is thought that co-implantation leads to MSCs acting as perivascular mural cells [149]. When cocultured with EPCs, MSCs have also shown a committed differentiation toward smooth-muscle cell and pericyte phenotypes [150]. Differentiation appeared to occur due to direct cell to cell contact and extracellular signal-regulated kinase (ERK) signaling, demonstrating the various pathways influencing the reciprocal interactions between EPCs and MSCs.

3.2.5 Pericytes, MSCs, and vascularization

Pericytes are embedded within capillaries, wrapping around ECs within the basement membrane [99,151]. While it has been shown that some pericytes, also known as mural cells, represent a subpopulation of MSCs, pericytic behavior is not characteristic of all cells classified as MSCs [152]. Still, this particular subpopulation of MSCs appears to interact with ECs much like bone marrow-derived MSCs, utilizing paracrine and direct-contact signaling, and has been extensively reviewed [153]. Pericytes utilize a variety of signaling mechanisms that act on ECs, influencing vascularization and vessel maturation. Like ECs, pericytes are capable of TGF β signaling. TGF β has been directly implicated in pericyte proliferation and

differentiation, as well as in the regulation of EC differentiation and proliferation. In pericytes, TGF β acts on two receptors: Alk-1 and Alk-5. Alk-1 appears to induce cell proliferation and migration, while Alk-5 leads to vessel maturation through differentiation and ECM formation [99]. Similar to TGF β signaling, angiopoietin secreted by mural cells act on tie receptors receptors expressed by ECs [153]. Angiopoietins, acting on Tie receptors expressed by ECs, are secreted by pericytes and are crucial to vascular development and remodeling.[142,153] These signaling loops have been implicated in vascular remodeling, vascular development, and the adhesion of the ECs, MSCs, and ECM [154,155].

Several pathways appear to influence perivascular cell recruitment to ECs, as illustrated by Figure 3.1. On the surface of pericytes, platelet-derived growth factor receptor-beta (PDGFRβ) is expressed, which binds soluble PDGF-BB produced by ECs. This particular signaling pathway plays a significant role in pericyte recruitment to ECs and has been regarded as the major pathway of pericyte recruitment in physiological angiogenesis. In undifferentiated mesenchymal cells, PDGF-BB induces mural cell fate [156,157]. By regulating PDGFRβ expression, Notch signaling has been suggested to possess a role in mural cell recruitment [158,159]. Notch signaling is also crucial for angiogenic sprouting and plays a role in endothelial-pericyte interactions [158,160,161].

Demonstrating the possibility of other pathways associated with pericyte recruitment, stromal-derived factor 1-a (SDF-1α) it has been recently implicated in pericyte recruitment, along with its role in endothelial tube formation and maturation [151,162]. Still, pericyte recruitment associated with SDF-1α may be due to cross-

13

talk between SDF-1 α and PDGF-BB pathways [162]. Another pathway involved in

pericyte recruitment is through heparin-binding epidermal growth factor (HB-

EGF).[163] HB-EGF, implicated in cardiovascular development, has also been found

to have protective effect on pericytes by supporting pericyte proliferation and

minimizing the effects anoxia-induced apoptosis [164]. Several studies have

demonstrated that HB-EGF pathways may experience crosstalk with PDGF pathways

[151,165]. Because of the varied pathways affecting pericyte recruitment and

function, opportunities to affect change in MSC function as pericytes are numerous.
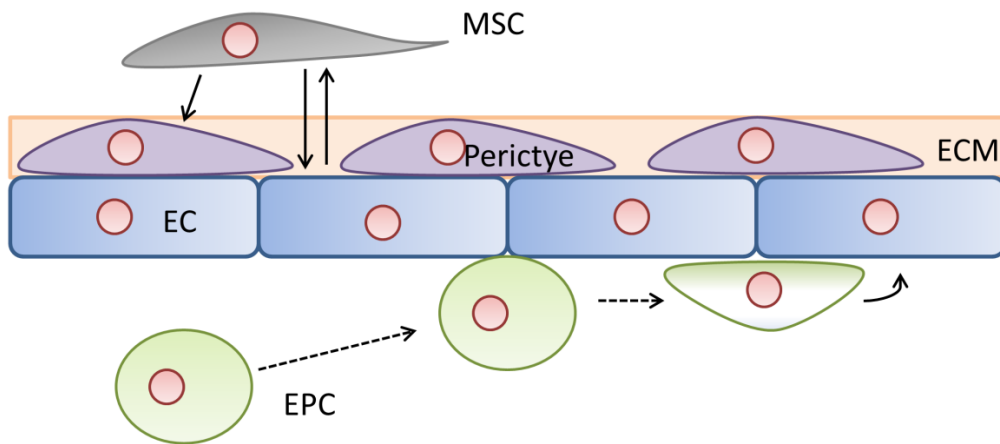
Figure 3.1 Several cell types are involved in angiogenesis and vascularization.
Signaling pathways between these cell types direct vascularization and
differentiation. Differentiation is shown through bold, solid arrows. Dashed lines
show EPCs' method of rolling and attachment to ECs.

3.2.6 Direct endothelial-like differentiation

While much of the MSC's influence on vascularization is primarily through paracrine and endocrine effects on other cells, MSCs may also have a direct role in vascularization through direct endothelial differentiation. Through endothelial differentiation, MSCs have been used in a variety of models, *in vitro* and *in vivo* to enhance vascularization [166–169]. *In vitro,* MSCs exhibited endothelial-specific markers such as VEGFR-1,VEGFR-2, and vWF after incubation with 2% fetal calf serum and 50 ng/ml VEGF [170]. While VEGF may be crucial to inducing arterial fate, VEGF alone has also been shown to be ineffective at enhancing or accelerating the endothelial differentiation of MSCs [171]. Still, further angiogenesis tests demonstrated the functional behavior of conduits formed by the MSCs [166]. Conversely, ECs have been found to differentiate into MSCs [172,173]. EC-derived MSCs have displayed the capability to differentiate into adipocytes, chondrocytes, and osteoblasts [173]. Such differentiation could be induced by TGFβ2 or BMP4. The relationship between EC and MSC differentiation pathways provide alternative approaches to studying and solving issues of vascularization in tissue engineered constructs.

In addition to utilizing natural growth factor, researchers are investigating synthetic chemicals and drugs to induce endothelial differentiation of stem cells. Chemical small molecules have been used to induce mouse embryonic stem cell (ESC) differentiation into ECs. For example, the compound R-ABO effectively induced ESC differentiation into ECs via upregulation of a molecule acting upstream of fibroblast growth factor 2 (FGF-2).[174] Another study used a DNA

methyltransferase inhibitor to induce endothelial differentiation of ESCs via epigenetic activation more efficiently than tradition VEGF treatment strategies [175]. Extending these strategies to MSCs, one study treated adipose-derived MSCs with an epigenetic drug, BIX-01294 [176]. Treatment resulted in significantly increased expression of several markers and factors associated with endothelial cells and blood vessel formation, including VCAM-1, PECAM-1, vWF, VEGFR-2, PDGF, and ANG-1. Continued research into synthetic chemical induced EC differentiation could improve the efficiency of differentiation and thereby reduce the costs of therapeutic MSC differentiation strategies.

In addition to soluble natural and synthetic chemicals, microenvironmental effects are critical to MSC behavior and fate. Substrate topology and mechanical properties are crucial determinants of cell function and fate [177–179]. For example, MSCs differentiated along neural, myogenic, and osteogenic lineages, dependent on the modulus of two-dimensional substrate gels on which MSCs were cultured [180]. MSCs cultured using either vasculogenic and nonvasculogenic and seeded on three-dimensional (3-D) tubular collagen scaffolds experienced EC and SMC differentiation [181]. Thus, it is apparent that the 3-D microenvironment can effectively induce differentiation even without the influence of soluble growth factors. MSCs have also been seeded on three-dimensional nanofiber matrices with elastic moduli tuned to ranges that corresponded with the intima and media layers of blood vessels [182]. The tuned nanofiber matrix moduli enabled control of MSC differentiation into ECs or SMCs. Controlling MSC differentiation into ECs has also been tuned by modification of fibrinogen with various PEG derivatives to achieve a

range of mechanical and physical properties [183]. Adjusting the properties of these substrates resulted in drastic alterations in cell morphology, gene expression, and overall transdifferentiation of MSCs to an EC-like phenotype. Thus, when inducing differentiation of MSCs to an endothelial phenotype, it is crucial to consider both chemical and physical microenvironmental conditions for therapeutic applications.

In an example of therapeutic benefit, researchers utilized MSCs' ability to differentiate into ECs in an *in vivo* canine chronic ischemia model [169]. Injected MSCs were found to have differentiated into SMCs and transdifferentiated into endothelial cells, as suggested by the luminal location of the MCSs and their expressed factor VIII [169]. Such transdifferentiation may have led to the higher capillary density observed in the MSC-treated canines. Canine MSCs have also been seeded on decellularized arterial matrices and cultured in pulsatile flow bioreactors [184]. These MSCs cultured on the matrices expressed vWF and oriented themselves in the flow direction. Endothelial differentiation of MSCs can be promoted by of growth supplements and shear force [166]. While growth supplement administration and shear force exposure were not sufficient alone to differentiate MSCs, the cells produced an endothelial gene expression profile, including CD31, KDR, and vWF, and exhibited morphology consistent with ECs, when seeded in Matrigel. In addition, these MSCs, after growth supplement and shear force priming, were capable of forming a functional capillary network in 3D culture environments, both *in vitro* and *in vivo*. These results demonstrate the complex environment that leads to MSC to EC differentiation, which may be difficult to replicate in an *in vitro* experiment. Still,

these studies validate the potential capability of MSCs to be used as a cell source for not only supporting vascular cells, but also directly vascularizing tissue constructs.

3.3 Applications

As with most developing tissue engineering obstacles, several challenges remain in translating the fundamental relationship between MSCs and vascularization into clinical applications. There is a need to define and develop optimized culture and 3-D microenvironmental conditions for MSCs and any vascular cells that may be included in order to promote healthy tissue development and vascularization. Utilizing these cells in a clinical environment must involve a careful understanding of the safety issues involved with the biomaterials chosen, source of the cells, and any modification (genetic or otherwise) to the cells. While much work has been performed in applying MSCs and vascularization in *in vivo* experiments, a complete understanding of the signaling pathways and cell types involved has yet to be elucidated. Clarifying these more basic fundamental questions will provide greater insight into the results and advancements made in therapeutic *in vivo* applications. For example, considerable debate still remains regarding the precise identities and subtypes of EPCs and pericytes, and, as such, their functional relationship with MSCs must be more closely examined [96,100]. To complement the growing understanding of these relationships, a variety of strategies have been utilized to take advantage of both MSCs influence on vascularization and vascular cells' influence on MSCs. Many of these concepts directly incorporate one or more signaling pathways, various vascular cell types, and deliberate cellular microenvironment design to reach these ends as summarized in Fig. 2.

3.3.1 MSC 3-D microenvironment

MSCs may be seeded onto scaffolds, injected, or implanted on their own to improve tissue vascularization. To examine the perivascular therapeutic potential of MSCs, MSCs were embedded in alginate beads and implanted the beads in ischemic mice.[185] Beads were implanted in the perivascular space around the femoral artery. The implantation of beads containing MSCs activated proangiogenic signaling pathways leading to the activation of VEGF-A. Through these mechanisms, the perivascular MSCs appeared to support neovascularization, significantly improved blood flow, increased tissue oxygenation and reduced toe necrosis. In another application, bone marrow-derived MSCs were seeded into pullulan-collagen hydrogels and implanted in a murine model simulating an excisional wound [186]. MSCs seeded on the hydrogels best secreted angiogenic factors compared to those grown in standard culture conditions. Once implanted, the seeded MSCs were discovered to have differentiated into fibroblasts, ECs, and pericytes, while also demonstrating significantly increased angiogenesis in wounds treated with the MSC-seeded hydrogels.

To bolster cell-cell communication, the three-dimensional microenvironment must be considered. Such an environment may directly affect cell-cell signaling, survival, proliferation, and differentiation. For example, MSCs aggregated into three-dimensional spheroids produce higher amounts of VEGF and FGF-2 [187]. Because of these effects, three-dimensional MSC spheroids were seeded onto porous polyurethane scaffolds [188]. Compared to non-seeded scaffolds and scaffolds seeded with individual MSCs, MSC spheroid seeded scaffolds demonstrated improved

20

scaffold vascularization and higher microvessel functionality. In the absence of biomaterial scaffolds, simply encouraging 3D organization of MSCs also enhances MSC survival and, subsequently, vascularization. For example, in both *in vitro* and *in vivo* environments, MSCs transplanted in spheroids produced by a hanging-drop method improved the viability of the MSCs [189]. MSC spheroid transplantation, compared to MSCs from monolayer, resulted in increased microvessel formation and reduced limb loss and necrosis in ischemic mice. While the 3D environment may increase paracrine signaling and function in the MSCs, the spheroids may also have allowed for longer MSC residency in the tissues compared to MSCs transplanted from monolayer.

Culturing and implanting MSCs in a 3-D microenvironment appears to improve MSCs' promotion of angiogenesis and neovascularization. These strategies appear to work well on small implant sizes and when used in a more supportive role, like perivascular delivery to ischemic tissues, instead of a direct role, such as osteogenesis in a critical-sized bone defect. For larger structures, culturing unmodified MSCs alone has not been sufficient for promoting tissue vascularization.

3.3.2 Genetic modification of MSCs

To bolster the natural influence of MSCs on vascularization, MSCs have been genetically modified to expedite and improve vascularization and tissue formation. Bmp2 gene-modified MSCs and EPCs were delivered in injectable calcium sulfate/alginate scaffolds, providing drastic increases in osteoblast differentiation and endothelial differentiation, resulting in increased bone and vascular formation [190]. Another genetic modification strategy involved modifying MSCs to express VEGF

[191]. The increased expression of VEGF led to a 3-fold increase of vascular density compared to control MSC-seeded grafts. However, the increased VEGF levels resulted in decreased quantities of bone formation and increased osteoclast populations. Such information demonstrates the importance of carefully weighing the benefits of methods to improve vascularization, while ensuring minimal deleterious effects of MSC contributions to bone formation and homeostasis. Relying on genetic modifications of MSCs introduces additional safety concerns, increasing the barriers to clinical applicability.

3.3.3 Combinatorial cell seeding and scaffold incorporation

Besides utilizing MSCs alone, a variety of strategies have incorporated the implantation of ECs, EPCs, and pericytes to better improve engineered vascularization. One group seeded MSCs and EPCs in macroporous polycaprolactone-tricalcium phosphate scaffolds and subsequently cultured within a biaxial bioreactor [192]. Interestingly, scaffolds cultured within the bioreactor did not demonstrate vessel formation as shown in static controls, despite greater mineralization. Despite these *in vitro* results, dynamically cultured scaffolds displayed both earlier vasculogenesis and increased bone formation *in vivo* compared to statically cultured constructs. Dynamically cultured scaffolds yielded 1.2- and 2.3-fold more capillary formation than static and acellular controls, respectively. Prevascularization of tissue engineered bone constructs through the insertion of a vascular bundle have been found to augment both new bone formation and vessel formation once implanted in β-TCP scaffolds seeded with MSCs [193]. In scaffolds with MSCs and inserted vascular bundles, VEGF levels were markedly increased

over control constructs. Combinatorial cell seeding appears to be a good potential strategy for ensuring adequate vascularization in implanted tissue constructs. Prevascularization of tissue constructs, though, could take considerable time and effort before implanting the scaffold in a clinical application, in addition to the safety concerns associated with autologous cell seeding.

3.3.4 Combining Strategies

Scaffold design and modification, genetic modification, combinatorial cell seeding and other vascularization techniques are often not uniquely applied. For example, the close relationship between MSCs and pericytes was used to design a scaffold-free construct of MSCs, ECs, and perivascular-like cells [194]. The perivascular-like cells were differentiated from MSCs and seeded onto a MSC monolayer, along with ECs. EC and perivascular-like cells self-assembled into colonies *in vitro* and vascularized the osteogenic tissue sheets when implanted *in vivo* when seeded by themselves. Using MSCs for perivascular-like and osteogenic functions proved to stabilize the vascular network formed *in vivo*, demonstrating the importance of cross-talk between all these cells during the vascularization process. Likely, successful tissue engineered constructs to support vascularization will necessarily incorporate multiple strategies discussed here.

3.4 Conclusion

While tremendous strides have been made in understanding the complex interactions between MSCs and vascularization, the need for vascularizing MSC-derived tissue constructs still demands the continued development of current and

23

future strategies to enhance the clinical potential of MSC-based therapies. Such strategies will not only entail incorporating vascular cells to support MSCs; successful strategies will likely utilize MSCs' beneficial paracrine and autocrine effects on vascular cells to further improve and expedite vascularization. Vasculogenic MSC pathways can be bolstered through methods such as careful scaffold design, growth factor immobilization, or genetic modification. The optimal construct will incorporate the synergistic effects of MSCs and vascularization.

Chapter 4: Synergistic effect of sustained release of growth factors and dynamic culture on osteogenic differentiation of mesenchymal stem cell[3]

4.1 Introduction

Critical bone defects affect more than 1.5 million Americans each year [195]. The current gold standard of treatment involves autologous bone transplants, which still suffer from several limitations. Therefore, tissue engineering strategies are being explored and include cell seeded 3-dimensional scaffolds that can be cultured in vitro to promote proliferation and differentiation of stem cells prior to implantation into the injury site. However, in vitro static culture techniques of 3D tissue engineering scaffolds face several obstacles including low oxygen and nutrient concentrations toward the center of the scaffold, leading to cell death [196]. A bioreactor is often used to overcome this limitation of nutrient transfer. A bioreactor can support or expand a population of cells through dynamic culture in a controlled environment. Different bioreactors systems have been proposed in bone tissue engineering, including spinner flasks [26,197,198], rotating wall bioreactors [199], and perfusion systems [200,201]. Perfusion systems effectively provide media (at laminar flow regimes) throughout the scaffold, enhancing nutrient transport, while exposing cells to fluid shear stresses shown to be influential in osteogenic differentiation of stem cells and mineralization of the extracellular matrix [200,202].

Mesenchymal stem cells (MSCs) are a multipotent stem cell population present in bone marrow, cartilage, and adipose tissue. They are easily differentiated into osteoblasts, chondrocytes, or adipocytes [90]. During MSCs differentiation, biological and mechanical cues induce specific pathways dictating whether the cell remains multipotent or differentiates into a specific cell type. Recently, Yeatts et al. demonstrated that the tubular perfusion system (TPS) bioreactor can promote differentiation of human MSCs (hMSCs) into osteoblasts via increased supply of convective oxygen and nutrient transport and mechanical stimuli from the shear flow of the media [203,204]. After in vitro culture, the scaffolds can form an aggregated constructed for in vivo implantation [205].

In addition to dynamic culture, it is well known that hMSCs respond favorably towards several biochemical signals. Particularly, it has been reported that biopolymer scaffolds modified with growth factors (GFs) including fibroblast growth factor-2 (FGF-2), vascular endothelial growth factor (VEGF), or bone morphogenetic protein-2 (BMP-2) [206] could enhance in vivo bone growth. For example, VEGF, an angiogenic growth factor, has been used to enhance vascularization and integration of an implanted bone engineered scaffold seeded with MSCs [207,208]. Similarly, BMP-2 has been widely investigated for its role in enhancing in vivo bone growth and in vitro osteoblastic signaling [209–211], and is considered one of the main factors involved in ectopic bone formation [212].

A locally sustained release of growth factors inside the 3D scaffold may provide an additional level of control. However, the production of reliable biopolymer microparticles for controlled release of GFs remains a challenge.

Recently, pharmacologically active microcarriers (PAMs) were proposed as transient scaffolds (or components of it) capable of controlled delivery of bioactive molecules [213,214]. Among all the biopolymers, Poly(D,L lactic-co-glycolic acid) PLGA received a strong interest for the development of bioactive microcarriers [215]. The use of supercritical fluids has been proposed for the production of biopolymer microspheres with an engineered size and distributions by an innovative technology, known as Supercritical Emulsion Extraction Continuous (SEE-C) layout [216]. Bioactive PLGA micro- and nano- carriers with mean diameters between 1 and 3 μm (±0.5 μm) loaded with active compounds [217], proteins [218], or bacteria [219] were successfully produced by SEE-C with a reliable process operations and are well characterized in terms of encapsulation efficiencies, release profiles of the bioactive compound, and good cell viability.

We hypothesized that the temporally and spatially controlled release of hBMP2 or hVEGF under dynamic culture conditions would enhance osteogenic differentiation of hMSCs compared to no GF delivery in static conditions. To provide proof of concept, bioactive alginate scaffolds were loaded with hMSCs and PLGA - encapsulated growth factor microparticles, specifically hVEGF and hBMP2 or a hVEGF-hBMP2 combination of both and cultured under shear stress in the TPS bioreactor. The system developed in this study could be used to deliver multiple bioactive growth factors and could find broad utility in many tissue engineering applications where sustained release of factors in a local environment is advantageous.

4.2 Materials and Methods

4.2.1 PAM production by SEE-C technology

Unloaded and GF-loaded microparticles were fabricated using previously established methods [220] utilizing a fixed water-oil-water emulsion ratio of 1:19:80. Briefly, GFs were dissolved into a 0.04% w/v human serum albumin (hSA) in poly-vinyl alcohol (PVA) solution and added to the oily phase composed of ethyl acetate (EA) and PLGA at 10% w/w. The primary w1-o emulsion was obtained after 90 seconds sonication with a digital ultrasonic probe at 50% of amplitude (Branson Ultrasonics Corporation, Danbury, CT). It was then immediately poured into a 0.6% w/w EA-saturated aqueous Tween 80 solution, which is used as outer water phase to form the secondary emulsion by a high-speed homogenizer (Silverson Machines Ltd., Waterside, Chesham Bucks, United Kingdom) for 6 min at 10°C in an ice bath with a stirring rate of 2800 rpm. The emulsions were then processed by SEE-C. As previously described, the SEE-C apparatus [220] consists of a packed column where gaseous and liquid phases are contacted counter-currently. Briefly, the separator is located downstream to recover the extracted oily phase solvent. SC-CO$_2$ and emulsion is delivered via high pressure diaphragm pump and high pressure piston pump, respectively. The emulsion is fed at the top and the SC-CO2 from the bottom of the column, which is packed with stainless steel packings (Pro-Pak, Scientific Development Company, State College, PA) and thermally insulated by ceramic cloths. During the processing, the oily droplets in the emulsion are continuously pumped into the high pressure packed tower and dried by carbon dioxide, resulting in solid polymer microspheres, which are recovered at the bottom of the tower. A

28

schematic representation of the SEE apparatus is described in Figure 4.1a). The

operating pressure and temperature conditions in the high-pressure column were 8

MPa and 38°C, respectively, with an SC-CO2 flow of 1.4 kg/h and an L/G ratio of

0.1, as previously described [221]. At these conditions, the droplets in emulsions were

converted into a PLGA microparticles water suspension in less than 5 min of

residence time in the column, preventing any aggregation phenomena between

particles. Each run allowed the recovery of 98% of the loaded biopolymer and

assured an excellent batch-to-batch reproducibility. During the runs, the

microparticles in water suspension are continuously collected at the bottom of the

extraction column, washed with sterilized water by centrifugation, and then

lyophilized. Additionally, they passed through a Pen/Strep (1% w/V) solution

followed by washing in PBS prior to lyophilizing to ensure sterility.
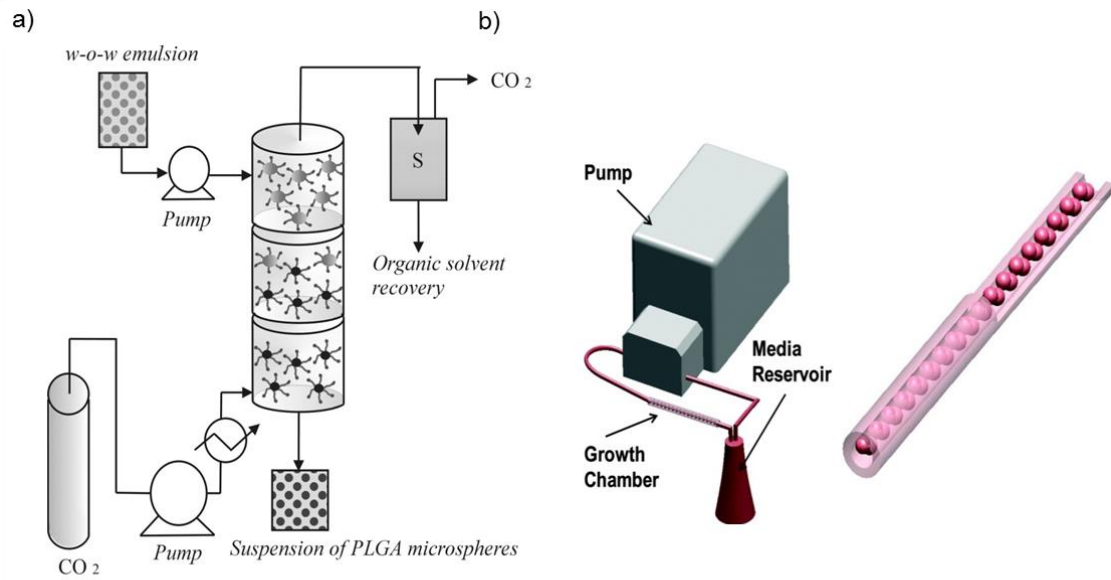
Figure 4.1 Schematic of SEE apparatus (a) and of tubular perfusion system (TPS) bioreactor setup (b). (a) The droplets in the w-o-w emulsion are continuously pumped into the a high pressure packed tower and dried by the carbon dioxide to produce the solid microspheres, which recovered at the bottom of the tower (adapted from Della Porta et al. 2011). (b) TPS bioreactor consists of media reservoir, growth chamber, and pump. Enlargement of growth chamber shows packing of alginate scaffolds.

4.2.2 Droplets and microspheres morphology & size distributions

The droplets formed in the emulsion were observed using an optical microscope (Olympus, Tokyo, Japan) equipped with a phase contrast condenser. The shape and morphology of the microspheres were investigated by field emission-scanning electron microscopy (FE-SEM) (Carl Zeiss, Oberkochen, Germany). Then, the particle size distributions (PSD) were measured using a Mastersizer S apparatus (Malvern Instruments, Worcherstershire, United Kingdom), based on dynamic light scattering (DLS). For each analysis, 50 mg of particles in suspension were loaded into the instrument to monitor their sizes and deviations. Droplets and particle size are expressed as volume MS (mean size, μm) ± SD (standard deviation) of values collected.

4.2.3 hSA and GFs loading and VEGF release study

hSA was used in the microparticle production process as a GF stabilizer in the internal water phase of the double emulsion. The specific amount of hSA loaded into PLGA microparticles was determined by dissolving 10 mg of dried powder in 600 μL of acetonitrile and sonicating it in 1400 μL of water. The remaining undissolved PLGA was separated by centrifugation at 2000 rpm for 2 minutes. The resulting clear supernatant solution was directly analyzed at room temperature by high-performance liquid chromatography (HPLC) (Agilent Technologies Inc.). The amount of hSA in solution was calculated using of a calibration curve and then converting it into the effective loading in terms of amount (mg) of protein loaded into PLGA (g). Similarly, the amount of hVEGF loaded into PLGA microparticles was determined using an ELISA-based assay (PeproTech, Rocky Hill, NJ) and was calculated as the amount

(ug) of protein loaded in PLGA (g). The hBMP2 loading was assumed the same as hVEGF. hVEGF release profiles were monitored in vitro using an ELISA-based assay. 20 mg of microparticles were suspended in 2 mL of Dulbecco's Modified Eagle Medium (DMEM) and placed in an incubator at 35°C and stirred continuously at 50 rpm. At fixed time intervals, the samples were centrifuged at 4000 rpm for 15 minutes and the supernatant was completely removed and replaced with fresh media to maintain sink conditions. Released VEGF concentrations from collected samples were then measured with an ELISA assay (PeproTech, Rocky Hill, NJ). Release experiments were performed in triplicate and the proposed curves are the mean profiles obtained.

4.2.4 hMSC Culture

hMSCs (passage≤5) were purchased from Lonza (Walkersville, MD) and cultured in a growth media containing High Glucose DMEM with L-Glutamine (Gibco, Carlsbad, CA), supplemented with 10% fetal bovine serum (FBS, Invitrogen), 1% v/v penicillin/streptomycin (Gibco), and 0.1 mM nonessential amino acids (Invitrogen) following the manufacture's protocol with a media change every 4 days. Cells were stored at 37°C and 5% of CO_2 and passaged every 6-7 days. The osteogenic media was formulated as previously [222] described by supplementing growth media with 100nM dexamethasone (Sigma, St. Louis, MO), 10mM β-glycerophosphate, and 173 mM ascorbic acid (Sigma).

4.2.5 Ca-Alginate scaffold fabrication and encapsulation of cells and microparticles

A 2% w/w alginate solution (Sigma Aldrich) was prepared by dissolving alginic sodium salt from brown algae (Sigma) in 0.15M NaCl (Sigma) and 0.025M HEPES (Sigma) in deionized water and sterilized via autoclave. hMSCs and GF-loaded PLGA microparticles were resuspended in HEPES buffer solution using sonification in ice water, poured into the sterile alginate solution, and thoroughly mixed. A syringe and 16 1/2G needle were used to create the 3D alginate hydrogel scaffolds by a slow drop wise suspension into a stirred a 0.1M calcium chloride solution (Sigma). Approximately, 72,500 hMSCs and 4.4 mg of PLGA microparticles were incorporated into each crosslinked alginate scaffold. The alginate scaffold mean diameter was of 0.3 ($\pm$ 0.01) cm.

4.2.6 Perfusion Bioreactor for Dynamic Environment

A TPS bioreactor was used as a dynamic fluid conditioner (see Figure 4.1b). It consists of a tubular growth chamber and medium reservoir connected via a tubing circuit, as described in a previous work [222]. The medium's flow was driven by an L/S Multichannel Pump System (Cole Parmer, Vernon Hills, IL) at 2 mL/min. The circuit consists of platinum-cured silicone tubing (Cole Parmer) and connects the growth chamber, which has high gas permeability to allow for easy exchange of carbon dioxide and oxygen. Each chamber's internal volume was of 2.4 mL and loaded with 25 scaffolds (with a volume of 0.014 cm^3) in order to reach a bioreactor packing value of 0.15 ratio (scaffolds/reactor volume). In total, 70 mL of osteogenic media was placed into separate media reservoirs to supply the growth chambers and

was changed every 3 days. The scaffolds were divided into four different groups, based on the GFs loaded microparticles (unloaded, hBMP2, hVEGF, or a combination of hBMP2 and hVEGF), where one growth chamber was utilized per timepoint per group. As a control, scaffolds were also placed into a static culturing environment with 2.13 mL of osteogenic media, to maintain the same media/scaffold ratio.

4.2.7 Immunohistochemistry

At each timepoint (1, 7, 14, and 21 days) alginate scaffolds were recovered from dynamic and static culture conditions. They were fixed in 4% paraformaldehyde (PFA) (Sigma) for 3 hours, followed by an overnight incubation in 0.1M sodium cacodylate/4% PFA (Sigma). The scaffolds were then dehydrated for histological processing in a series of ethanol dilutions (75%, 90%, 100%), embedded in paraffin (Fisher Scientific), and sectioned using a microtome (Lica) into 5-micron-thick sections. The samples were then deparaffinized in Citrisolv (Fisher Scientific) and rehydrated in ethanol.

Osteoblastic differentiation was monitored using immunohistological staining of protein markers, including alkaline phosphatase (ALP), an early differentiation marker, and osteocalcin (OCN), a late differentiation marker. The samples underwent standard immunostaining protocol for antigen retrieval, and endogenous peroxidase and protein blocks. They were incubated for an hour with rabbit monoclonal ALP and mouse monoclonal OCN (Abcam, Cambridge, MA) antibodies, respectively, followed by broadband polyclonal biotinylated secondary antibody (Invitrogen). Antibody binding was visualized using peroxidase-conjugated DAB chromogen,

34

which resulted in a brown stain. For the von Kossa staining, the sections were incubated in 2.5% (w/v) silver nitrate for 20 min under UV light, followed by 5% (w/v) sodium carbonate for 5 min, and 0.1% Nuclear Fast Red (Poly Scientific).

4.2.8 Live/Dead assay

Cell viability was assessed using a Live/Dead assay (Invitrogen) following standard protocols. Scaffolds were placed in 48-well plates and incubated in 2 mM ethidium homodimer and 4 mM calcein AM (Molecular Probes) for 30 min. Dead controls were incubated in 70% methanol (Sigma). Fluorescent images were then taken of the entire bead using a fluorescence microscope (Axiovert 40 CFL with filter set 23; Zeiss, Thornwood, NY) equipped with a digital camera (Diagnostic Instruments 11.2 Color Mosaic, Sterling Heights, MI).

4.2.9 Quantitative Reverse Transcriptase Polymerase Chain Reaction (qRT-PCR)

To isolate mRNA from the cells, the scaffolds were homogenized and total RNA was isolated with Trizol Reagent (Invitrogen, Carlsbad, CA) following the supplier's protocol. Total RNA was quantified using a Nanodrop Spectrometer (Thermo Scientific, Wilmington, DE). Reverse Transcription was performed using TaqMan Reverse Transcription Reagents (Applied Biosystems, Foster City, CA) following the supplier's protocol. qRT-PCR was performed using Taqman PCR Master Mix and Taqman Gene Expression Assays for ALP and OCN (Applied Biosystems). Quantification of target genes was performed relatively to the reference

GADPH gene. The mean minimal cycle threshold values (Ct) were calculated from triplet reactions.

4.2.10 Statistical Analysis

All samples were evaluated in triplicates. Data was analyzed using single-factor analysis of variance followed by Tukey's Multiple Comparison Test assuming normal data distribution with a confidence of 95% ($p<0.05$). Mean values of triplicates and standard deviation error bars are reported on each figure as well as relevant statistical relationships.

4.3 Results and Discussion

4.3.1 PLGA microparticles: size, loading, and in vitro GFs release study

The encapsulation of two different GFs were considered: hBMP2, for its prominent role in the development of bone and cartilage and in inducing osteogenesis [223], and hVEGF, for its dual activity during angiogenesis and osteoblastic differentiation [224,225]. Briefly, double emulsions with a fixed PLGA content in the oily phase of 10% w/w and theoretical loading of 20 ug GF/g PLGA, with hSA as a stabilizer were prepared. Microparticles produced using SEE-C were measured to have MDs of 2.1 µm (± 0.6 µm). Examples of the results obtained are reported in Figure 4.2a), depicting optical microscopy (OM) and FE-SEM images of the emulsions. Three different microparticle batches were produced for the present study: 1) unloaded particles (control), 2) hBMP2-loaded 3) hVEGF-loaded. The PSD curves of the three different microparticles are illustrated in Figure 4.2b). In all cases, the hSA encapsulation efficiency was 80%, leading to the production of PLGA carriers

with a protein content of 2 mg hSA/g PLGA. The encapsulation efficiency value of 80% was also confirmed for the GF loading, and was found to be 16 µg GF/g PLGA. An encapsulation efficiency of 80% exceeds those reported in literature [226,227], especially when ethyl acetate is used as oily phase solvent in a conventional emulsion evaporation technology.

A release study of the encapsulated hVEGF into cell media was performed to evaluate the sustained release of growth factors from SEE-C fabricated microparticles. The release profile of GFs from 2.1µm PLGA microparticles into DMEM was monitored at 35°C and the experimental data are reported in Figure 4.2c). A burst of about 20% of the GF was observed during the first day, followed by a more gradual and linear release over the following 16 days. The entire amount of encapsulated GF was released within 22 days.

The drug release from PLGA can be described in two steps: the first one mainly reflects the diffusion controlled mass transfer of the drug accessible at the solid/media interface and the second step is due to the release of molecule encapsulated in the polymer layers enhanced by its bulk erosion via hydrolysis [228]. Assuming the spherical geometry of the system the diffusion coefficient as constant and the initial molecule concentration fixed, the diffusion controlled mass transfer equation can be written as (see Equation 1), where: M_t represent the amount of the released molecule at given time (t), M_∞ is the maximum amount released, D is the diffusion coefficient of the molecule, and r the radius of the considered system:

$$(1) \quad \frac{M_t}{M_\infty} = 1 - \frac{6}{\pi^2} \cdot \sum_{n=1}^{\infty} \frac{1}{n^2} \cdot \exp\left(-\frac{D \cdot n^2 \cdot \pi^2 \cdot t}{r^2}\right)$$

The hVEGF release data was modeled using Equation 1 to estimate the diffusion coefficient of the encapsulated hVEGF into microparticles considering a hypothetical media droplet with the same diameter as an alginate scaffold. In this case, the diffusion coefficient, D, was found to be 0.11×10^{-7} cm^2/sec, and the resulting curve is reported in Figure 4.2c).

Tanaka et al. [229] reported the diffusion characteristics of several substrates and proteins with different molecular weight, including fibrinogen (MW 34100 Da). The authors also measured the diffusion coefficient value (D) of fibrinogen as 0.33×10^{-7} cm^2/sec from Ca-alginate (2% w/w) scaffolds of 0.33 cm (± 0.02) diameter at 30°, similar to the setup used in this work. The hVEGF used in this work has a MW of 38200 Da, which is similar in size to that of fibrinogen. Therefore the fibrinogen's diffusion coefficient as reported by Tanaka et al. was used in equation (1) to simulate the release profile of free hVEGF from spherical Ca-alginate scaffolds. The resulting curve is seen in Figure 4.2c).

The extrapolated release profiles demonstrate that hVEGF encapsulated into PLGA microparticles result in a more delayed release profile compared to free hVEGF molecules from alginate scaffolds. The sustained release of hVEGF from PLGA microparticles can be considering the predominant step, whereas, the residual diffusion of free hVEGF into alginate can be neglected. Therefore, assuming that the 2% alginate scaffold contains 98% water, we believe that the cells are directly exposed to and are affected by released GFs from PLGA microparticles inside the hydrogel scaffold.
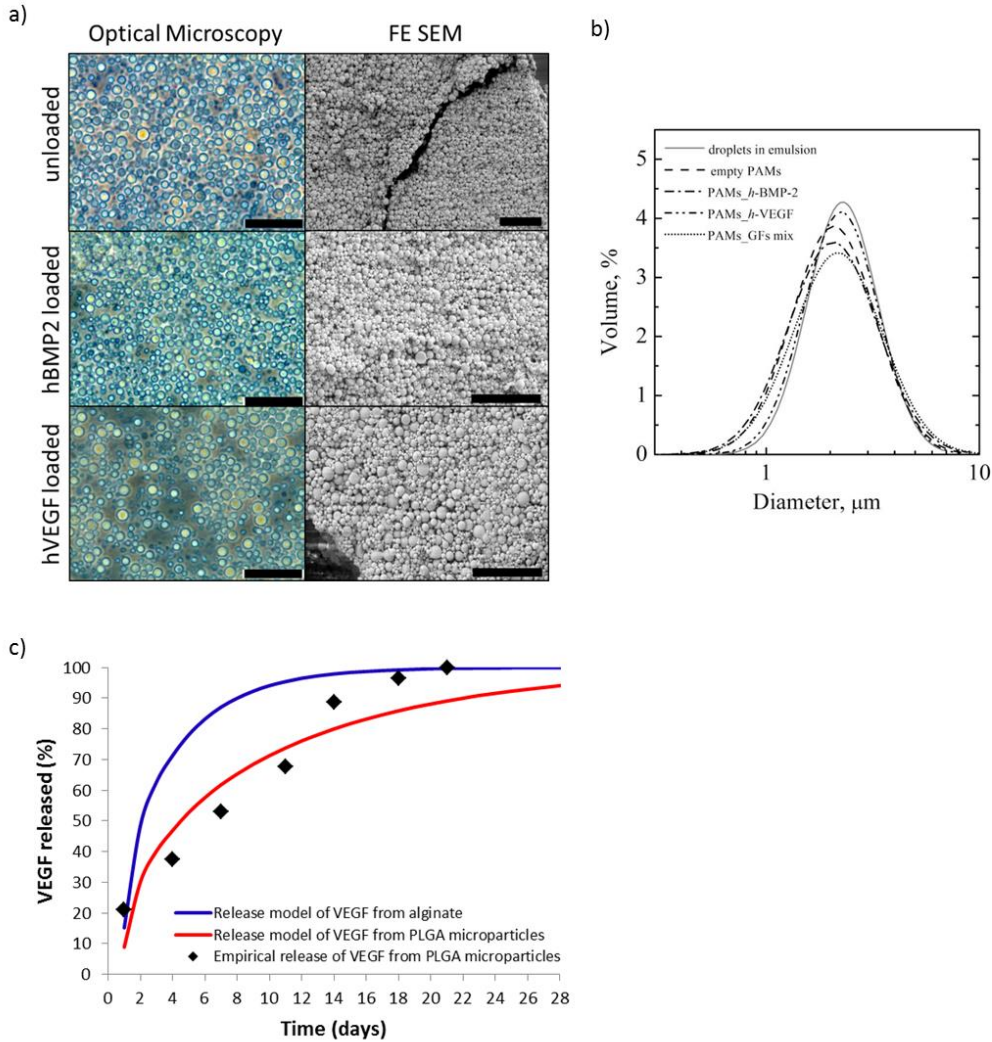
Figure 4.2 Microparticle characterizations. (a) Optical microscopy (left) and FE-SEM (right) images of microparticle emulsion fabricated using SEE-C techniques of unloaded particles, hBMP2 loaded particles, and hVEGF-loaded particles. Each scale bar represents 20 mm. (b) Particle size distribution (PSD) curves of microparticles produced using SEE-C techniques. The size distribution curve of droplets in emulsion is shown as control (solid gray curve). Average size of PLGA microparticles was measured to be 2.3 mm in diameter. The three dashed curves, representing the unloaded, and two GF-loaded particles, are overlapping, confirming the high reproducibility of the SEE-C technology for the production of nanostructured microdevices. (c) hVEGF release curves from microparticles. Mathematically modeled curve of soluble VEGF diffusion out of a 3–mm diameter, 2% (w/w) Ca-alginate scaffold (blue line). Mathematically modeled curve of VEGF release from PLGA microparticle into 3 mm diameter DMEM droplet (red line). Empirically released VEGF from PLGA microparticles into DMEM media (♦). Modeled data results indicate that soluble VEGF exhibits quickest diffusion from 2% alginate scaffold compared to VEGF encapsulated in PLGA microparticles. Collected VEGF release data demonstrates sustained release and correlates closely with modeled VEGF encapsulated PLGA curve.

Engineered bioactive scaffold characterization and TPS bioreactor conditions

Alginate scaffolds with a mean diameter of 0.3 mm were loaded with hVEGF, hBMP-2, and a combination of hBMP2 and hVEGF mix of each per experimental group. 4.4mg of loaded PLGA microparticles were encapsulated in each scaffold, resulting in an average amount of 70 ng of hBMP2 or hVEGF, respectively, while 35 ng of each GF were encapsulated into the scaffold in the hBMP2 with hVEGF experimental group. A schematic representation of the bioactive scaffold is shown in 3a). A fluorescent viability stain was performed on the alginate scaffold at the end of the culture period as seen in Figure 4.3b), where green represents viable cells and red stains dead cells. The image displays high cell viability after encapsulation of the cells and microparticles in scaffolds. The internal structure of a freeze-fractured scaffold was also confirmed using FE-SEM at different magnifications, as seen in Figure 4.3). PLGA microparticles are uniformly distributed in the alginate matrix, allowing for homogenous delivery of GFs to surrounding cells.
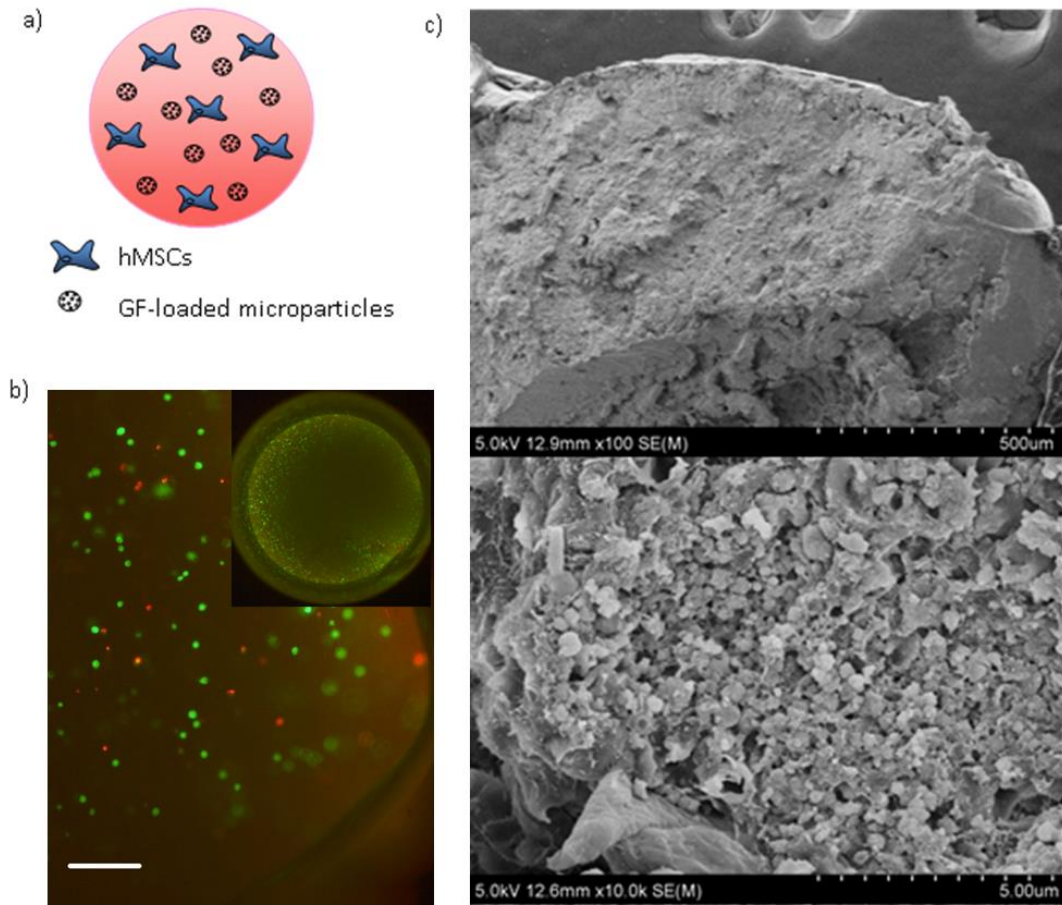
Figure 4.3. Alginate encapsulation of microparticles and cells. (a) Schematic of cells (blue) and GF-loaded microparticles (green) in spherical alginate scaffold (pink). (b) Fluorescence staining of live (green) and dead (red) cells in alginate-microparticle hydrogels on day 1 taken at 103 and2.53 (inset) magnification. The scale bar represents 200 mm. (c) FE-SEM images of hMSC- and microparticle-encapsulated alginate scaffolds at 100x (top) and 1000x (bottom) magnification show homogenous distribution of PLGA microparticles in the alginate scaffold.

4.3.2 Immunoassay for cell differentiation monitoring

Alginate scaffolds were recovered from dynamic and static cultures at all timepoints for immunohistochemical analysis. ALP and OCN proteins were stained to monitor osteogenic differentiation in hMSCs during static and dynamic culture. During osteogenic differentiation, hMSCs will increase their deposition of minerals in the extracellular matrix (ECM). Therefore, von Kossa staining was used to study mineralization and calcification of the ECM, indicative of the stage of osteoblastic differentiation. Figures 4.4 depicts cross-sectional images of alginate scaffolds cultivated until day 14 and stained with von Kossa to observe the calcium deposition by hMSCs within the scaffolds. Mineralization, seen in dark brown/black, was minimal in static culture groups on day 7 (top panel), but increased in intensity by day 14 (bottom panel). While mineralization was more prevalent in all dynamically cultured groups compared to static control, more homogeneous and intense deposition was especially observed in those exposed to sustained release of both hBMP2 and hVEGF on days 7 and 14.
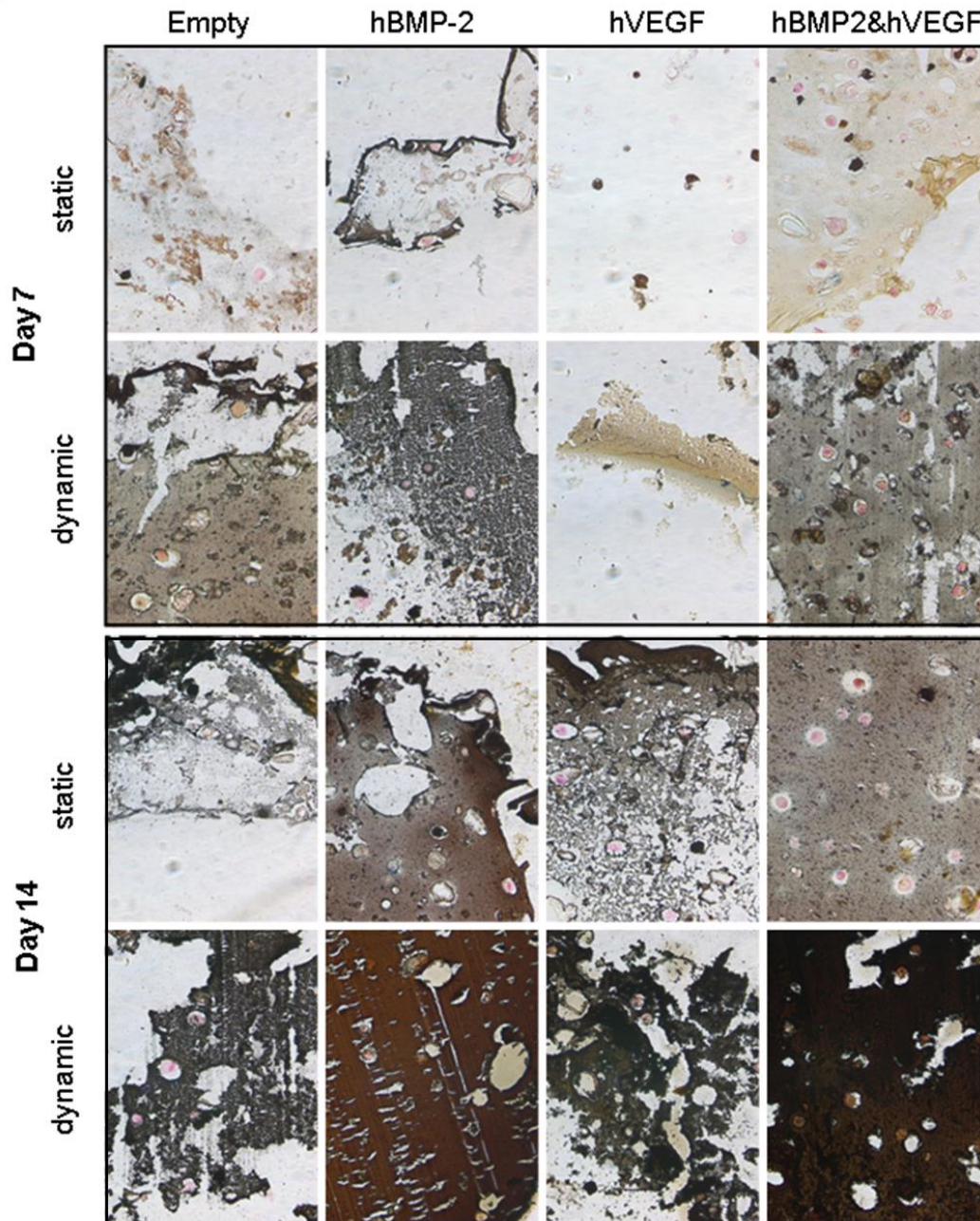
Figure 4.4. Mineralization of alginate scaffolds. Von Kossa histology staining of alginate scaffolds after 7 and 14 days of culture in the TPS bioreactor or static conditions. Calcium deposition is stained in brown/black and cells are stained in light pink. Darkest calcium staining is observed on day 14 for cells exposed to hBMP-2 and a combination of hBMP2 and VEGF compared to empty and VEGF groups in both static and dynamic conditions, indicative of greatest calcium deposition in the extracellular matrix. All images were taken at 40x.

To examine specific osteogenic protein expression, sections were stained for ALP and OCN (Figure 4.5). ALP is considered an early osteogenesis marker and is involved in making inorganic salts available for later calcification of the ECM. Its peak expression occurs between day 6 and 8 of culture [230], after which it decreases back to basal levels. The staining is more intense in the hBMP2, hBMP2 with hVEGF, and control groups but is not visually distinct from their respective static counterparts. Specifically, adding hVEGF seems to have the least beneficial effect on ALP expression, in both the static and dynamic conditions. Based on this ALP staining result, early differentiation protein expression can be affected by adding growth factors, specifically hBMP2, while exposure to hVEGF alone did not have favorable outcomes. Alternatively, OCN is a cellular structural protein in mature osteoblast produced between days 14 and 28 of osteogenic differentiation. The staining does not indicate noticeable differences in differentiation between the experimental groups. However, they have more intense staining than the empty control. Therefore, osteogenic protein production seems to be enhanced by all experimental groups containing growth factors, and further improved by dynamic flow. More evident in the stains, however, is the size of the cells cultured in the GF supplemented dynamic conditions after 21 days, in which they are visibly larger than the cells in the static condition. We believe that this is due to the ability of the cells to expand and deposit more ECM in the degraded scaffolds by day 21 of the osteogenic differentiation culture when supplemented with GFs, resulting in a larger stained area of osteocalcin, a secreted ECM protein.
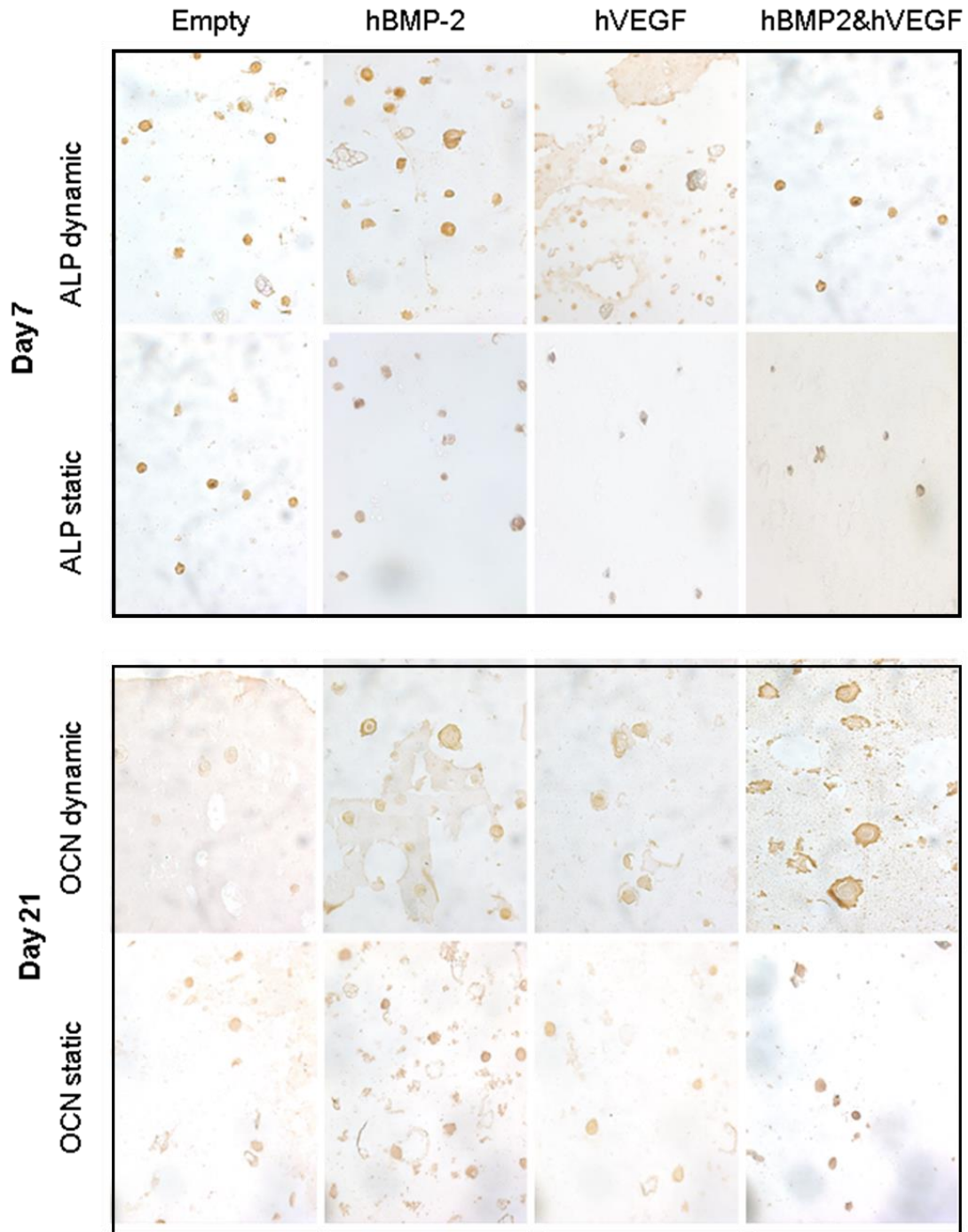
Figure 4.5. Immunohistochemical staining of osteogenic proteins. Immunostaining of ALP on day 7 and OCN on day 14 indicate more intense staining on alginate scaffolds cultured in dynamic conditions compared to the static control. Greater staining was particular evident in cells exposed to hBMP2 and dynamic conditions compared to those exposed to hVEGF or no growth factor control. No qualitative difference was observed between staining of cells exposed to hBMP2 or both hBMP2 and hVEGF.

4.3.3 Osteogenic Gene Expression

mRNA expression of ALP and OCN was also used to monitor osteogenic differentiation as seen in Figure 4.6. When dynamically cultured, ALP mRNA expression increased 10-fold on day 7 in groups supplemented with hBMP2 compared to the remaining groups, which were not statistically different from one another (Figure 4.6a). However when cultured in static conditions, ALP mRNA expression was greatest in groups without growth factors and those exposed to the hBMP2 with hVEGF GFs on day 7 (Figure 4.6b). This could indicate that the burst release of growth factors does not initially affect early osteogenic differentiation, but instead is seen in later stages. For example, on day 21, delayed osteogenic markers OPN and OCN, indicated significantly higher expression in groups exposed to both hBMP2 and hVEGF GFs compared to the other groups (Figure 4.6c). Similarly, OPN mRNA expression was significantly higher in hBMP2 exposed groups, compared to the control or hVEGF group. In static culturing conditions, OCN mRNA expression was highest in groups exposed to hBMP2 and hBMP2 with hVEGF, with a 12.1 and 14.1-fold change, respectively (Figure 4.6d). Therefore, groups exposed to hBMP2 under dynamic culturing conditions performed similarly to when hBMP2 and hVEGF were added together to the TPS bioreactor. This may indicate that shear stress is able to support osteogenic differentiation of hMSCs during its later stages, as has been supported by others [231,232].
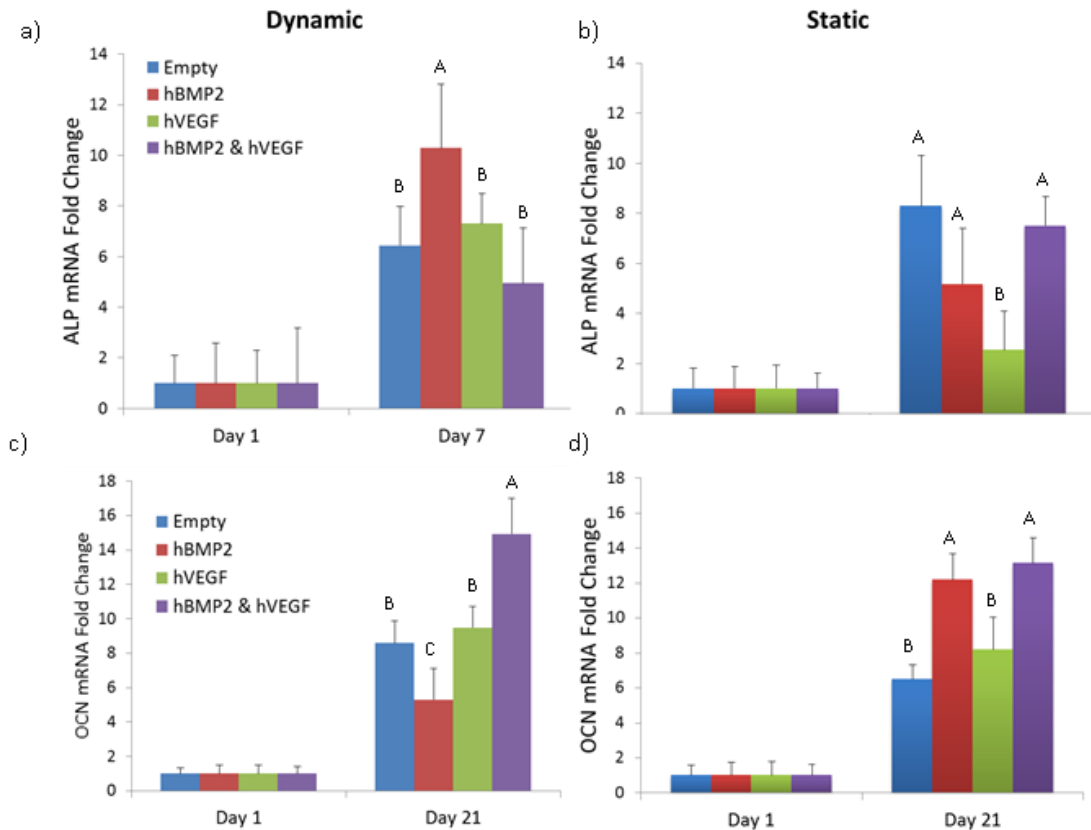
Figure 4.6. Gene expression of osteogenic markers. RT-qPCR for ALP and OCN mRNA expression from both static and dynamic conditions indicated statistically greater expression of ALP in dynamically cultured cells exposed to hBMP2. In static environments, while no statistical difference was observed between cells incubated with empty, hBMP2 loaded, or both GF-loaded microparticles, these groups expressed statistically greater amounts of ALP mRNA than the hVEGF group. OCN mRNA fold changes were also greater in the hBMP2 with hVEGF group when dynamically cultured, and in the hBMP2 and hBMP2 with hVEGF group in the static conditions. Groups with the same letters indicate no statistical difference between groups for that timepoint, with $p < 0.05$.

Overall, hBMP2 and the combination of hBMP2 and hVEGF delivery resulted in greater osteogenic differentiation, compared to control and hVEGF additions alone. ALP mRNA expression was most enhanced when cultured in dynamic conditions and supplemented with hBMP2, resulting in a 10.3 fold increase on day 7 compared to day 1. In static culture, the addition of growth factors did not seem to improve ALP mRNA expression compared to the control, demonstrating that hBMP2 and hVEGF may influence later osteogenic differentiation pathways. On the other hand, dynamic culture largely enhanced differentiation compared to static culture, observed in both early and late osteogenic marker mRNA expressions. Although we hypothesized that the addition of both hBMP2 and hVEGF would individually enhance osteogenesis and therefore amplify the effect when used in tandem, the results indicate that hBMP2 may have a dominant effect on hMSCs over hVEGF, especially when dynamically cultured. The addition of hVEGF had minimal effects on the hMSC culture compared to the non-growth factor supplemented control. Therefore, we believe that the dual application of mechanical stimulation through fluid flow as well as the addition of osteogenic growth factors results in the greatest enhancement of osteogenesis in hMSCs.

The delivery of BMP2 and VEGF for bone tissue engineering has been previously explored in static conditions [59,65,225,233] with many advocating for their synergistic effects on osteogenesis [59,234]. However, several have pointed out the hindering effect of VEGF *in vitro* [235], although it can be beneficial when utilized in vivo. Specifically, high concentrations of VEGF have been found to lead to stem cell differentiation towards the endothelial lineage, decreasing the amount of

cells available to undergo osteogenic differentiation [236]. Others have investigated a variety of different GF ratios, but have had similar results, where BMP2 has a more prominent effect on osteogenic differentiation than VEGF [225]. Lastly, great efforts have been spent on investigating the importance of temporal control of growth factor release. For example, different kinetic rates of GF release have been found to enhance regeneration of critical bone defects [237], where BMP2 enhanced bone formation and a combination of BMP2 and VEGF increased bone bridging and union of defect compared to BMP2 alone. These studies indicate a need to fully understand the interplay between BMP2 and VEGF in bone regenerative applications.

4.4 Conclusion

In this work, PLGA microparticles were utilized as delivery vehicles for hBMP2 and hVEGF to enhance the osteogenic differentiation of hMSCs while dynamically cultured in the TPS bioreactor. The histological staining as well as gene expression assays confirmed that this dual application of biochemical and mechanical stimulation promoted osteoblastic differentiation of hMSCs compared to static conditions. In addition, the sustained release of growth factors to 3D encapsulated cells resulted in improved osteogenic differentiation, therefore indicating that SEE-C technology is a promising tool in the field of tissue engineering and regenerative medicine. These microparticle devices can be included in complex 3D scaffolds with cells onboard for local signal delivery. Further confirming the results, von Kossa staining revealed that hBMP2 and hVEGF mix released in alginate scaffolds has a great influence of the on hMSC differentiation into osteoblasts. Therefore, the combination of hBMP2 and dynamic culture in the TPS bioreactor allows for

enhanced osteogenic differentiation in hMSCs for the repair of bone tissue

engineering defects.

Chapter 5: Tunable Osteogenic Differentiation of hMSCs in Tubular Perfusion System Bioreactor[4]

5.1 Introduction

Mesenchymal stem cells (MSCs) are multipotent cells that have been studied in a variety of bone tissue engineering applications. A combination of specific mechanical and biochemical stimuli commit MSCs to differentiate along an osteogenic lineage into osteoblasts and osteocytes, among the main cell types in bone tissue [238]. In tissue engineering, MSCs are often paired with three-dimensional synthetic or organic scaffolds and cultured for the development of bone tissues. When dynamically cultured, these cell constructs have demonstrated advanced tissue formation [197,239–242].Therefore, these systems have promising applications in treating bone trauma or defects in clinical settings [139,243].

In this work, human MSCs (hMSCs) are encapsulated in alginate scaffolds and studied in vitro under dynamic culture conditions within a bioreactor system. 3D static culture techniques are often inadequate in delivering essential nutrients and oxygen through simple diffusion [196,244]. Various dynamic bioreactor designs have since been conceived to solve these issues by providing increased oxygen and nutrient supply [245]. The tubular perfusion system (TPS) bioreactor, previously developed by Yeatts et. al., utilizes a peristaltic pump to drive media throughout a growth chamber that houses 3D alginate scaffolds [240,246,247]. A media reservoir provides fresh nutrients for the tissue and collects cellular wastes as media perfuses throughout the system. The dynamic culture environment of the TPS bioreactor has several

---

advantages over alternative static methods; engineering three dimensional structures facilitates efficient penetration of nutrients and oxygen into the scaffolds through fluid perfusion. This benefit encourages cell growth and is essential for homogenous construct formation by preventing hypoxia and malnutrition in developing tissues [247].

Further, the TPS bioreactor enhances osteogenic differentiation of hMSCs encapsulated in alginate scaffolds. Fluid shear stress produced by a perfusion bioreactor activates certain biomechanochemical pathways that upregulate key osteogenic differentiation markers such as alkaline phosphatase (ALP), osteocalcin (OCN), and osteopontin (OPN), as well as growth factors, like bone morphogenetic protein-2 (BMP-2) [248–250]. Growth factor concentrations and permutations dominate control of the osteogenic enhancement pathways and are important in paracrine signal regulation in tissue formation [251,252].

Previously, studies have explored the effects of bioreactor flow patterns on osteogenic differentiation of encapsulated stem cells [253]. For example, parallel flow resulted in retained proliferation and hMSC progenicity by reinforcing ECM characteristics, while transverse flow enhanced osteogenic activity after 14 days. These results are attributed to the increased shear stress stimulation during transverse flow compared to parallel flow. Similarly, Du et al. described oscillatory flow that also proceeded to enhance osteogenic differentiation in a uniform manner, compared to unidirectional flow [254].

Several studies have indirectly studied growth factor release in perfusion bioreactors [255–258], yet the effect of flow in an axial growth chamber on paracrine signaling

molecule expression in subpopulations has not been fully described. Understanding a complex dynamic culturing system, where one population may affect another through paracrine signaling, could be greatly useful in coculture setups where a supporting cell population is necessary for the survival and function of a primary cell population [259–262].

Here, we investigate the variances in osteogenic differentiation between encapsulated-hMSCs that lie at the proximal (inlet) end of the axial growth chamber compared to those that lie at the distal end (outlet) of the tubular growth chamber in the TPS bioreactor. We hypothesize that these two regions may experience differences in biochemical (mass transport of growth factors, nutrient and oxygen delivery) factors that govern and enhance osteogenic differentiation. This work promotes greater understanding of axial growth chamber culture, how well-established parameters of osteogenic differentiation can be manipulated for advanced tissue development. Furthermore, this work suggests the ability to control localized microenvironments in a dynamic culturing system such as the TPS bioreactor, which would be advantageous in engineering heterogeneous or co-culture tissue constructs.

5.2 Materials and Methods

5.2.1 Human Mesenchymal Stem Cell Culture

Human mesenchymal stem cells (hMSCs) (passage≤5) were purchased from Lonza (Walkersville, MD) and cultured in a growth media containing High Glucose DMEM with L-Glutamine (Gibco, Carlsbad, CA), supplemented with 10% fetal bovine serum (FBS, Invitrogen), 1% v/v penicillin/streptomycin (Gibco), and 0.1 mM nonessential amino acids (Invitrogen) following the manufacture's protocol with a

media change every 4 days. Cells were stored at 37°C and 5% of CO2 and passaged every 6-7 days. The osteogenic media was formulated as previously described29 by supplementing growth media with 100nM dexamethasone (Sigma, St. Louis, MO), 10mM β-glycerophosphate, and 173 μM ascorbic acid (Sigma).

5.2.2 Cell and Growth Factor Encapsulation

Human recombinant BMP-2 (Sigma) was resuspended in water as described in the manufacturer's protocol. For cell experiments, hMSCs were mixed into 2% w/v alginate (Sigma) solution and used to make alginate scaffolds by adding the mixture dropwise into a suspension of 0.1M calcium chloride (Sigma) (100,000cells/scaffold), Similar, 6mg of BMP-2 was encapsulated in acellular alginate scaffolds, resulting in a BMP-2 concentration of 60ng/scaffold.

5.2.3 TPS Bioreactor Assembly

Alginate scaffolds were divided into experimental (dynamic culture) and control (static culture) groups. The dynamic group was further separated into "A" and "B" groups based on their culture chamber location in the TPS bioreactor. The bioreactor was set-up as described previously (Yeatts et al. 2011). Scaffolds were loaded into tubular growth chambers (10 scaffolds per chamber). Medium flow was driven by an L/S Multichannel Pump System (Cole Parmer, Vernon Hills, IL) at a flow rate of 3 mL/min. Static scaffolds were cultured in six-well plates (10 scaffolds per well). The medium was changed every two days. At each timepoint, hMSCs were isolated from alginate scaffolds by dissolution in ethylenediaminetetraacetic acid (EDTA) for 30

min at 37°C. A cell pellet was formed by centrifugation and used for subsequent analyses.

5.2.3.1 Unidirectional Flow

When unidirectional flow was used in the dynamic culture, 10 hMSC-loaded scaffolds were equally separated into two chambers, A and B (proximal and distal in relation to the source of the flow, respectively) (Figure 5.1b). After 1, 7, and 21 days of culture, all scaffolds were removed from the chamber (first 5 scaffolds categorized as 'inlet' and the latter 5 as 'outlet'), and processed for further analysis.

5.2.3.2 Alternating Flow

To determine the effect of directional flow on osteogenic differentiation of hMSCs, the flow was alternated between clockwise (CW) and counterclockwise (CCW) every 24 hours for 7 days. Culture chambers were categorized as 'A' and 'B', despite the direction of the flow (Figure 5.1c). On day 1 and 7, 5 scaffolds were removed from each chamber for further analysis.

5.2.3.3 Growth Factor-Supplemented Flow

To supplement the culture with control-released growth factor, an additional growth chamber was placed preceding chamber A and B (Figure 5.1d). It contained 20 BMP-2 encapsulated alginate scaffolds. These were fabricated similar to the cell-encapsulation protocol. BMP-2 was mixed into 2% alginate solution, added dropwise into a solution of 0.1 M $CaCl_2$, and stirred for 10 min using a stir bar. Then scaffolds were placed into a growth chamber in the TPS bioreactor, where they would release their contents into the media to travel downstream towards chambers A and B. At each timepoint, 5 scaffolds were removed from chambers And B for further analysis.
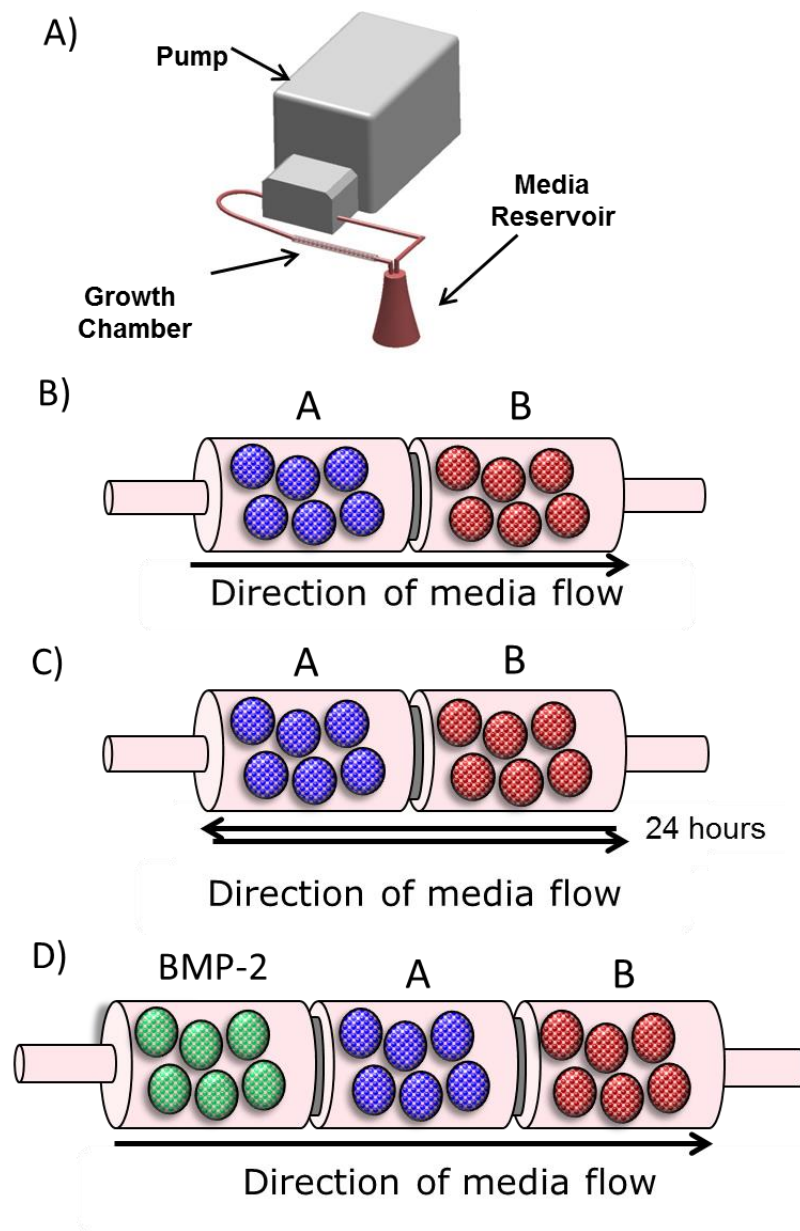
Figure 5.1. TPS Bioreactor Assembly. A) The TPS bioreactor consists of a peristaltic pump, which continuously pumps media through a growth chamber from a media reservoir. B) Two-chamber setup with uni-directional flow. Scaffolds cultured in the proximal and distal chambers are labeled in green and red, respectively. C) Three-chamber setup with uni-directional flow. BMP-2- encapsulated scaffolds (green) release the growth factor towards proximal and distal culture chambers (purple and red).

5.2.4 Computational Fluid Dynamics Modeling of Fluid Shear Stress

SolidWorks (Waltham, MA) was used to create a 3D model of the TPS bioreactor growth chamber. A cylindrical tube 6.35 mm in diameter was fixed in a motion study, and 20 spheres (3.41 mm diameter – based on averaged experimental data, not shown) were dropped in gravity to represent in vitro loading and culturing conditions of alginate bead scaffolds. Contact points were fixed in place, and the model exported to SolidWorks Flow Simulation.   Using an inlet flow rate (3 mL/min), velocity data was generated using the "Point Parameters" function of SolidWorks Flow Simulation and analyzed in MATLAB using numerical approximations of Navier-Stokes Equations and the Cauchy Stress Tensor.

5.2.5 Real-Time Quantitative Polymerase Chain Reaction (RT-qPCR)

5 scaffolds per group were used to isolate total RNA from hMSCs using the RNeasy Plus Mini Kit (Qiagen, Frederick, MD) following standard protocols. Isolated RNA was then reverse transcribed to cDNA using a High Capacity cDNA Archive Kit (Life Technologies). Quantitative RT-PCR was performed by combining the cDNA solution with a Universal Master Mix (Life Technologies), as well as oligonucleotide primers and Taqman probes for ALP and OCN, and the endogenous gene control glyceraldehyde 3 phosphate dehydrogenase (GAPDH) (Life Technologies). The reaction was performed using a 7900HT real-time PCR System (Applied Biosystems) at thermal conditions of 2 min at 50°C, 10 min at 95°C, 40 cycles of 15 s at 95°C, and 1 min at 60°C. The relative gene expression level of each

target gene was then normalized to the mean of day 1 GAPDH expression in each

group. Fold change was calculated using the $\Delta\Delta$CT relative comparative method as

described previously 17. Samples were completed in technical triplicates and standard

deviations are reported (n=3).

5.2.6 Histology

To visualize later stages of osteogenesis via the mineralization of extracellular

matrix (ECM) and deposition of calcium, scaffolds were recovered from static and

dynamic conditions and fixed in 4% paraformaldehyde (PFA) for 3 hours, followed

by an overnight incubation of 0.1M sodium cacodylate/4% PFA (Sigma). Next, the

scaffolds were dehydrated in a series of ethanol dilutions and embedded in paraffin

wax. Samples were sectioned into 5 um slices using a microtome (Lica). For the von

Kossa staining, the sections were incubated in 2.5% (w/v) silver nitrate for 20 min

under UV light, followed by 5% (w/v) sodium carbonate for 5 min, and 0.1% Nuclear

Fast Red (Poly Scientific). Stained samples were visualized under brightfield

microscopy (Zeiss, Germany).

5.2.7 Quantitative ALP Assay

ALP activity in hMSCs is an indicator of early osteoblastic differentiation and

their commitment towards the osteoblastic lineage. Expression of ALP protein was

quantified using media extracts on timepoint days. In the presence of an alkaline

buffer, ALP hydrolyzes phosphate esters, producing organic radicals and inorganic

phosphates. Utilizing the phosphate assay kit (Abcam), media extract was mixed with

a fluorescently tagged phosphate group, which when cleaved results in an intense fluorescent signal.

5.2.8 BMP-2 Release Study

BMP-2 release profiles were monitored in vitro using a BMP-2 specific enzyme-linked immunosorbent assay (ELISA) (Sigma). The growth factor was encapsulated into alginate scaffolds are described above and placed into serum-containing Dulbecco's Modified Eagle Medium (DMEM) and placed in a shaker at 37°C. At fixed time intervals, the media was removed and flash frozen in liquid nitrogen, while the scaffolds were disregarded. The media was evaluated for BMP-2 content and absorbencies read using a plate reader at 450nm. Standard curves were made using human recombinant BMP-2, while serum-containing media was used as a baseline.

5.2.9 Statistical Analysis

Each analysis was performed in triplicate (n=3). Statistical significance was determined by one-way analysis of variance and Tukey's multiple-comparison test. A confidence interval of 95% ($\alpha = 0.05$) was used for all analyses. Mean values of triplicates and standard deviation error bars are reported on each figure as well as relevant statistical relationships.

5.3 Results

5.3.1 Characterization of Axial Position on hMSC Response

First, osteogenic differentiation in cells cultured under unidirectional flow
(Figure 5.1B) was analyzed using gene expression and histological staining. qPCR
analysis showed expression of osteogenic markers such as alkaline phosphatase, an
early differentiation marker, was upregulated on day 7 in cells cultured in chamber B
compared to those cultured chamber A (Figure 5.2A). Similarly, mRNA coding for
osteocalcin, a late osteogenic marker, was also increased 1.5-fold by day 21 in
chamber B, while those in chamber A experienced 0.5-fold decrease compared to day
1 (Figure 5.2B). However, BMP-2 gene expression showed significant increase after
21 days, albeit no statistical difference between groups (Figure 5.2C). The trend in
gene expression was further confirmed through histology staining to visualize
calcification of the extracellular matrix using Von Kossa. The microscopy images
indicate that there is greater mineralization of the ECM (stained in black) by day 7, in
surrounding areas of cells in chamber B compared to those in chamber A (Figure
5.2B). However, calcification is not visibly different by day 21 between the two
groups.

Second, we investigated whether we could mitigate the effects seen in the
unidirectional flow by alternating between CW and CCW every 24 hours.
Specifically, ALP mRNA expression remained similar to day 7 for cells in chambers
A and B (Figure 5.3A). However, we analyzed the concentrations of BMP-2, an
important osteogenic growth factor released during differentiation, and found that
these were not statistically different between media surrounding cells in the chambers

61

A and B (Figure 5.3C). The BMP-2 concentration increased in all groups and was statistically different by day 7 compared to day 1. Increased differentiation was further confirmed with Von Kossa staining for mineralization on day 1 and day 7 (Figure 5.3B). Calcium deposition was visible in both groups by day 7 with no noticeable differences between groups.
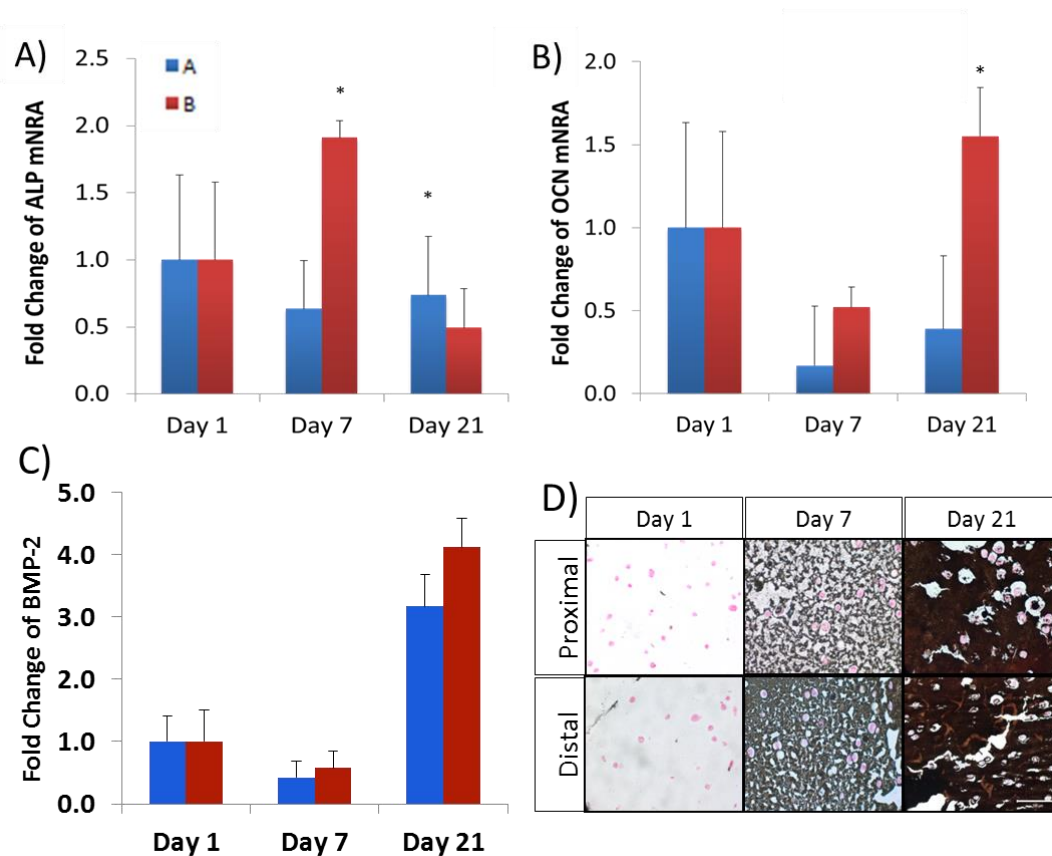
Figure 5.2. Unidirectional Flow Promotes Osteogenic Differentiation in Downstream hMSCs. A) Increased expression of early osteogenic marker ALP was observed in hMSCs cultured in distal scaffolds compared to those in the proximal chamber. B) By day 21, there was significantly greater expression of OCN, a late stage osteogenic marker, in the distal group, compared to the proximal group. C) Von Kossa histology staining shows great calcification (black) in distal cells on Day 7 compared to proximal cells, however no noticeable difference by Day 21. Scale bar represents 100 microns.
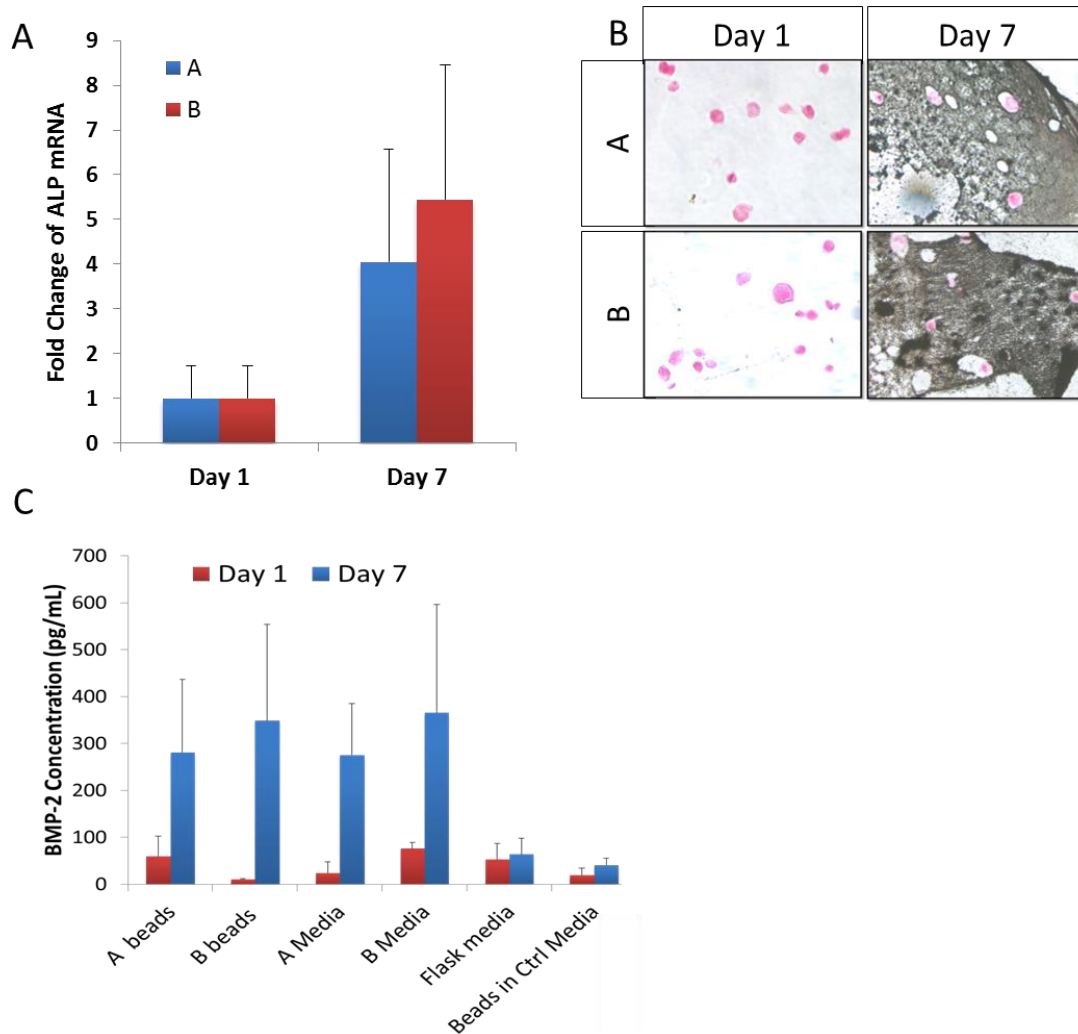
Figure 5.3. Alternating Flow Pattern Mitigates Variances in hMSC Osteogenic Differentiation. A) ELISA detection of BMP-2, a marker of osteogenic differentiation, indicated no statistical differences between hMSCs cultured in the proximal or distal chambers. B) Von Kossa staining on Day 7 indicated no qualitative differences in staining intensity of mineralized ECM (black) between hMSCs (pink) cultured in the distal or proximal chambers. C) mRNA expression of ALP showed significant increase over 7 days of dynamic culture (4 and 5.3-fold), but not significant differences between cells cultured in chamber A or B.

5.3.2 Consideration of Shear Effects

We used computational fluid dynamic (CFD) analysis to confirm that the flow rate in chamber A was not different from that in chamber B during unidirectional flow and therefore was not the leading cause in osteogenic differences seen during unidirectional flow. MATLAB approximation for finite shear stress elements supported the theory that alginate scaffolds in chamber A experienced on average (across all three simulation builds) 15.6 ± 1.8 mPa of fluid shear stress while scaffolds in B experienced 15.1 ± 3.5 mPa, with no statistical difference between groups.

5.3.3 Consideration of Paracrine Signaling Effects

Results from the unidirectional flow experiment indicated the presence of paracrine differences between cells cultured in chamber A and B. Therefore, to demonstrate the signaling behavior between cultured groups, we introduced an additional growth-factor releasing element.

Here, we determined the effect of exogenous growth factor delivery in a unidirectional system on osteogenic differentiation of hMSC. We analyzed gene expression of ALP and BMP-2 in dynamic and static conditions (Figures 5.5A-D). Both ALP and BMP-2 expression fold change were not statistically different between groups in chambers A and B on day 7 when cultured in the TPS bioreactor (Figures 5.5A&C). However, both increased drastically from day 1 values (15-fold and 18-fold, respectively). In addition, BMP-2 supplemented static cultures exhibited statistically different and greater expressions of ALP and BMP-2 mRNA compared to static control (no added growth factor) (Figures 5.5B&D). ALP production was

further quantified using an ALP fluorometric assay (Figure 5.4E). Media taken from all three chambers (BMP-2, A, and B) as well as the media reservoir showed no statistically different ALP protein concentration on day 7. In addition, an ELISA assay was used to model the release of encapsulated BMP-2 from alginate scaffolds (Figure 5.4F). The release profile indicates a relatively slow release of 10% over the initial 40 minutes, followed by a burst release of 40% by 60 minutes. After 2 hours, all BMP-2 has presumably been released from the alginate scaffold.
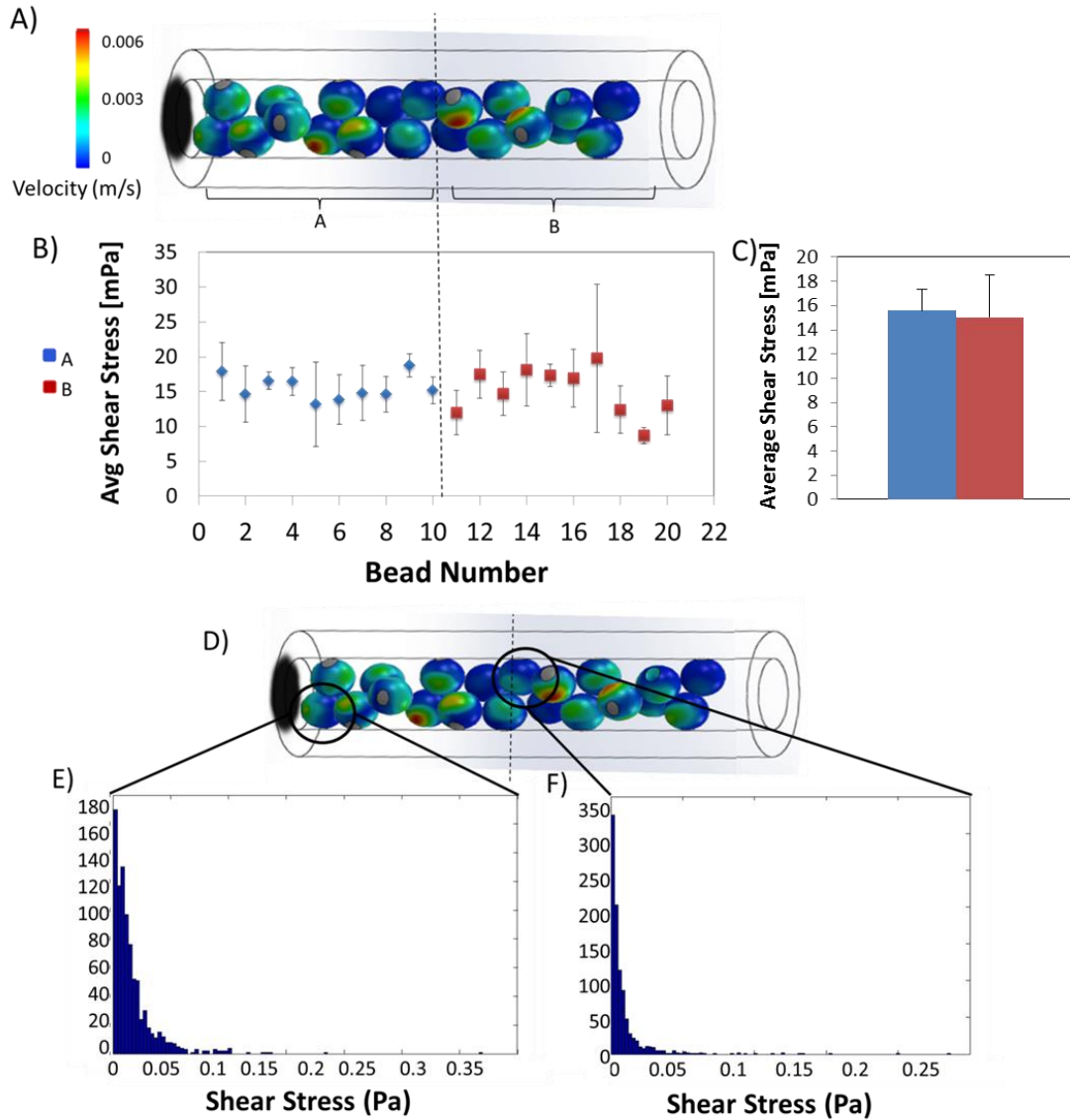
Figure 5.4. Computational Fluid Dynamic Modeling. A) Velocity heat map of unidirectional flow in growth chamber, modeled in SolidWorks. Distribution of velocities are visible on the surface of scaffolds, ranging from 0-0.006 m/s, but no distinguishable difference is visible between scaffolds in part A compared to part B. B) Average shear stress calculated per scaffold, based on average velocity. C) Average shear stress on scaffolds from chamber A and B are not statistically different and display similar variability. D-F) SolidWorks model and histograms of shear stress distribution of individual scaffolds in growth chamber. Both entrance scaffolds and chamber A and B experience shear stresses below 0.05 Pa, with very small pockets of shear stresses greater than 0.5 Pa.
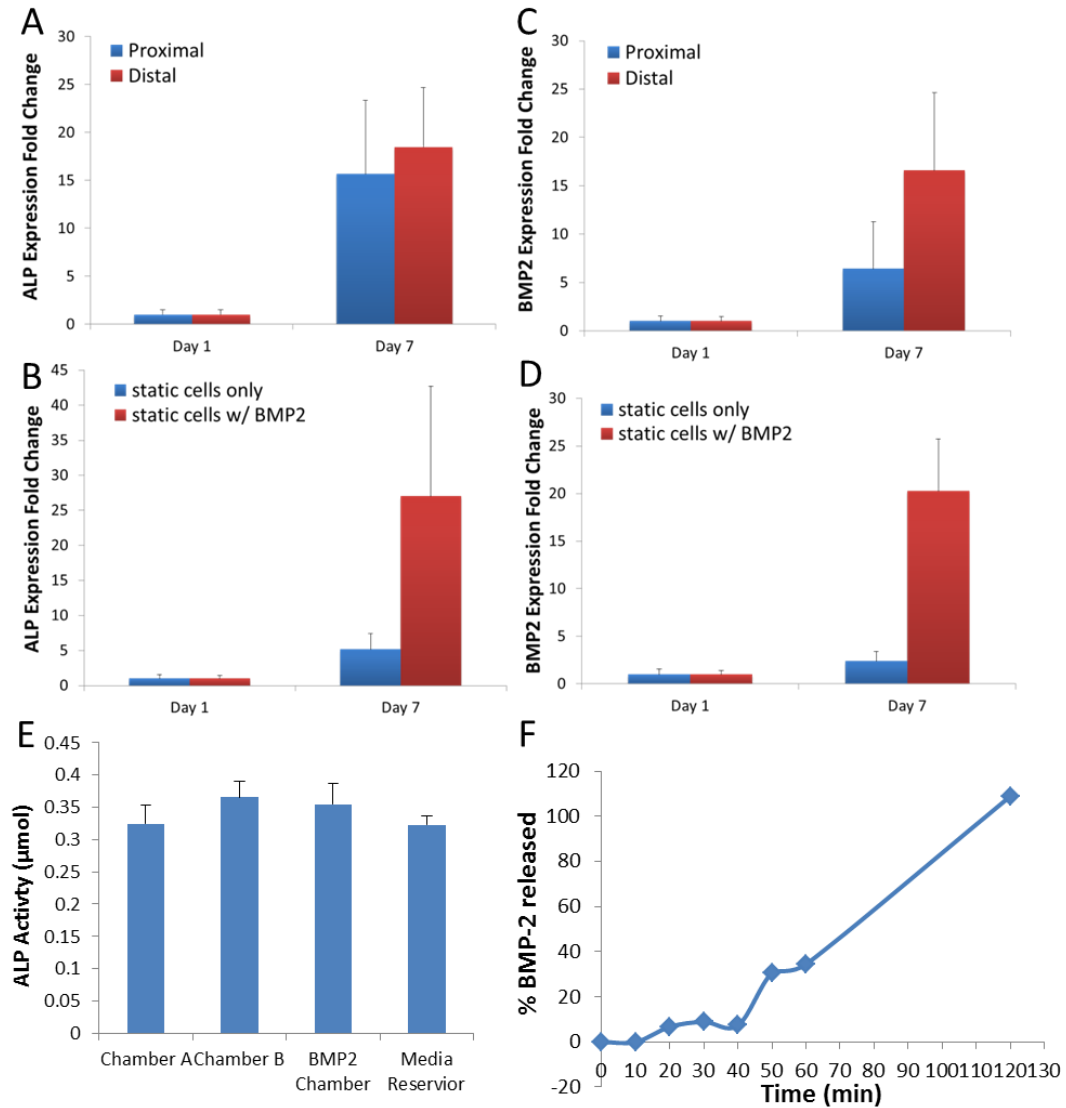
Figure 5.5. Influence of Exogenous BMP-2 Supplemented Flow. A) ALP gene expression fold change in dynamic culture was not statistically different between chambers A and B on day 7, but showed 15-fold increase over 7 days. B) ALP gene expression for cells cultured in static, with or without added BMP-2. The latter expressed significantly higher levels of ALP mRNA. C) BMP-2 expression in dynamically cultured cells. No statistical difference was observed between groups on day 7, but both were significantly increased compared to day 1 levels. D) BMP-2 gene expression in statically cultured cells was significantly enhanced with BMP-2 supplements on Day 7. E) ALP production was quantified using an ALP fluorometric assay. There was no statistical difference in ALP protein detected in media samples on day 7. F) The release profile of BMP-2 encapsulated in 3-mm alginate scaffolds indicates a slow release of 10% over the initial 40 minutes, followed by a burst release of 40% by 60 minutes. After 2 hours, all BMP-2 has presumably been released from the alginate scaffold.

5.4 Discussion

Bioreactors have been widely utilized in tissue engineering applications, especially for bone regeneration due to their ability to provide a dynamic culturing environment, a preferred condition during osteogenic differentiation of hMSCs [49,263–265]. Specifically, the TPS bioreactor increases oxygen and nutrient supply to cells encapsulated in hydrogel scaffolds, but also applies fluid flow forces that lead to molecular changes in cells as surface receptors trigger molecular pathways downstream [240]. Although their overarching effects on hMSCs have been previously investigated, the role of axial position within a perfusion bioreactor, like the TPS, on cell response has not yet been explored. In particular, we hypothesized that these variations in shear stress and/or paracrine signaling affect the genotype of downstream cells. This unique feature allows us to culture distinct populations of differentiating hMSCs for a variety of different tissue engineering applications where a range of differentiating cells are needed.

This series of experiments has investigated the effect of axial position in the TPS bioreactor on the osteogenic differentiation of hMSCs. Empirical experiments using the linear growth chamber demonstrated that differences in differentiation exist between cells cultured along the length of the growth chamber. Specifically, cells cultured downstream (in chamber B) displayed enhanced expression of key osteogenic markers compared to those upstream (in chamber A). We hypothesized that these variations could be attributed to either 1) deviations in shear stress on the surface of dynamically cultured scaffolds, and/or 2) the release of endogenous growth factors and cytokines from one subpopulation of cells to another.

To examine if we could mitigate the osteogenic differences seen during unidirectional flow, we alternated between clockwise and counterclockwise flow every 24 hours. By oscillating the flow between CCW and CW, the osteogenic differentiation occurred at the same pace between cells in chambers A and B, as shown by endogenous BMP-2 production, ALP mRNA expression, and Von Kossa staining for calcium deposition on day 7. This flow pattern further confirmed the importance of directional flow in osteogenesis using any axial perfusion bioreactors [266–268].

We utilized computational fluid dynamic modeling to visualize the shear stress exhibited on alginate scaffolds. This analysis would verify the role of mechanical stimulation in the TPS bioreactor. Growth chamber simulations determined that there were no significant differences in applied fluid shear stress on scaffolds downstream of the inlet flow (Figure 5.1E). Therefore, we investigated paracrine signals as an overarching effect to biochemically induce osteogenic differentiation throughout the alginate scaffold. This theory has also been described by Kim, et al. in which hMSCs' osteogenic differentiation was upregulated using transverse bioreactor flow compared to parallel flow [269]. In this model, they found the shear stress on the surface of the constructs to be 5.5 x 10-4 Pa.

The CFD model confirmed that shear forces are not responsible for the osteogenic differences observed during unidirectional flow. Therefore, we hypothesized that paracrine signaling may be the driving force behind cellular behavioral discrepancies seen previously. We attempt to replicate this phenomenon by delivering exogenous BMP-2, an important growth factor released during

osteogenic differentiation, for an extended period. The sustained release resulted in a

positive feedback mechanism [270,271], in which exogenous BMP-2 triggered

expression of endogenous BMP-2, further enhancing osteogenic differentiation on

day 7. More noticeably, however, was the fold changes of ALP expression on day 7

with and without supplemented BMP-2. Cells cultured in chamber A experienced a

1.9-fold change in ALP expression from day 1 to day 7 (Figure 5.2A). Yet the

expression change was almost 20-fold when supplemented with BMP-2 (Figure

5.4A). This indicates the synergistic role that dynamic culture and exogenous growth

factors play on early osteogenic differentiation of hMSCs.

Furthermore, an analysis of the circulating exogenous growth factor on

cultured cells within the TPS bioreactor provided additional insight into its efficacy.

With an average length of 5 cm each, growth chambers A and B were connected via a

short, meshed connector, which allowed for the flow of media and growth factors, but

prevented alginate scaffolds from leaving their respective growth chambers. The TPS

bioreactor flow was set at 3mL/min, resulting in a media retention time of 31.7

seconds per chamber. Therefore, any soluble growth factors and cytokines released

by the cells, could be carried with the flow towards cells further downstream in

chamber B and exit both growth chambers in about a minute. Such timescale is vital

to consider due to the short half-life of many proteins. For example, the half-life of

BMP-2 in vivo has been found to be 7-16 minutes systemically [272] and an hour in

in vitro culture conditions [273]. At this degradation rate, BMP-2 and other growth

factors should have sufficient time to circulate through the TPS bioreactor system,

while remaining biologically active, to affect cells downstream. Specifically, BMP-2

regulates the proliferation and osteogenic differentiation of precursor cell lines into osteoblasts and osteocytes [147]. Therefore, with the aid of a closed circuit setup of the bioreactor, growth factors are able to continue circulating the system, moving from the media reservoir back into chamber A. In conjunction with the gradual release of exogenous BMP-2 from alginate scaffolds, the encapsulated cells are fully exposed to the growth factor for several hours during the dynamic culture. Despite the burst release of BMP-2, the effect on cells is significant as shown by both mRNA and protein expressions (Figure 5.4).

Finally, these experiments have demonstrated the overarching role of paracrine signaling in axial chamber culture, specifically their role in osteogenic differentiation. It plays a key role in promoting osteogenic differentiation within a subpopulation of cells for a bone tissue engineered construct.

5.5 Conclusion

While perfusion culturing systems like the TPS bioreactor have been shown to improve differentiation of hMSCs into osteoblasts, the ability to control the process has not been investigated. By utilizing the spatial control provided by the TPS bioreactor and the cell's intrinsic expression of growth factors and cytokines, we have been able to show regulation of hMSCs' osteogenic differentiation. Such uniaxial culturing system would be immensely useful in regenerative medicine applications where a coculture of interdependent, yet distinct cell populations is necessary. Such organizational structure is seen in the three defined zonal populations that make up cartilage [274]or in the coupled interaction of smooth muscle cells and endothelial

cells during angiogenesis and vascularization [275], where a coculture system of cells

interact via paracrine signaling is vital.

Chapter 6: Dynamic Bioreactor Culture of High Volume Engineered Bone Tissue[5]

6.1 Introduction

Critically sized bone defects affect an average of 1.5 million Americans per year and command a market of more than 1 billion dollars in repair and regenerative therapies [1]. The current therapies are based on various types of autografts, allografts, or synthetic bone grafts. Unfortunately, current treatments can result in host rejection, improper vascularization, incomplete healing, or life threatening complications from surgery. New efforts have focused on bone grafts generated using tissue engineering techniques. Many groups have utilized bone marrow derived human mesenchymal stem cells (hMSCs) to grow tissue grafts on a variety of natural and synthetic beads [276–278]. hMSCs have the ability to differentiate quickly into osteogenic cells and have been characterized as strong immunomodulators and paracrine activity regulators, which could lead to robust *in vivo* function post implantation [279].

Initially, static conditions were used to culture bone tissue grafts [196,280,281]. However, these fail to deliver adequate nutrient supply and remove waste products, and can lead to poor tissue formation, necrosis, and incorrect cell migration [196,282]. Therefore, the need for a dynamic culture environment is imperative for the *in vitro* formation of functional bone grafts. Bioreactors provide

---

increased control over environmental parameters such as media flow and oxygen distribution. Perfusion bioreactors, by enabling the continuous and circular flow of media and oxygen through the perfusion chamber, have demonstrated improved mass transport inside scaffolds and upregulation of important osteoblastic markers [201,240,241,245,254]. Such bioreactors mimic *in vivo* environments, where human bone tissue is subjected to two mechanical stimuli during development or regeneration: fluid shear strain and physical tissue stress [283].

Notably, our group has shown that the tubular perfusion system (TPS) bioreactor, which comprises a perfusion chamber where the cells and scaffolds are cultured, a medium reservoir, a tubing circuit, and a peristaltic pump, maintains cell viability at the center of grafts and enhances osteogenic differentiation of hMSCs compared to static culture conditions [222,284,285]. Computational modeling of steady-state oxygen concentrations throughout an alginate bead cultured under static and dynamic conditions illustrated that oxygen concentration fell to 0.03 mM and 0.15 mM oxygen, respectively, suggesting that greater oxygen supply to encapsulated cells will maintain their viability and function [284]. Additionally, simplified COMSOL modeling of the fluid flow pattern in the TPS bioreactor growth chamber indicated velocities as high as 3.5 cm/s given a 3mL/min flow rate [284]. This shear stress is applied to the surface of the alginate bead, triggering several mechanotransduction receptors on the cell membrane surface of encapsulated hMSCs, ultimately leading to augmented osteogenic differentiation [231]. Furthermore, we have investigated such mechanical stimulation within the local environment of the alginate bead after 2-3 weeks of dynamic culture and discovered that the effects of

shear stress on the surface, while localized to a volume close to the surface, encourage the release of paracrine factors, that in turn, affect the response of the cells in the core of the bead [250]. Leveraging the dynamic culture of these versatile scaffolds, we aggregated the small alginate beads into a larger construct and demonstrated continued viability and function of the encapsulated cells [205]. More importantly, TPS bioreactor cultured cells were able to induce increased bone formation after implantation into a rat critical sized bone defect [286]. These positive outcomes allow us to further build upon our system, especially in the application of fabricating high volume tissue constructs.

Multiple studies have demonstrated positive effects of dynamic perfusion bioreactor culture on osteogenesis for bone tissue engineered bone grafts [240,287–291]. To date, tissue engineered bone constructs cultured in dynamic conditions using the indirect perfusion bioreactors have been fabricated up to a volume of 10.7 cm^3 [287,288]. However, many systems are currently limited by the size of the culture chamber and inefficient supply of oxygen and nutrients to critical defect sized grafts. The goal of this study is to engineer a scale-up of a 1 inch bone graft to a full-size, superior portion of an adult human femur (200 cm^3). We successfully demonstrate that the TPS bioreactor system can support cell viability and function throughout the entire engineered tissue. This work signifies a major step in tissue engineering by creating high volume bone constructs that could help regenerate entire bones. Further, the scalability of the TPS bioreactor could expedite fabrication of other whole organs and tissues that would otherwise require multiple systems and strategies. To our

knowledge, this is the first time a tissue-engineered bone construct of such size has been fabricated in the laboratory.

6.2 Materials and Methods

6.2.1 Human Mesenchymal Stem Cell Culture

Bone marrow-derived human mesenchymal stem cells (hMSCs) (passage ≤ 5) for use in the 1-inch bone construct were purchased from Lonza (Walkersville, MD) and cultured in a growth media containing High Glucose DMEM with L-Glutamine (Gibco, Carlsbad, CA), supplemented with 10% fetal bovine serum (FBS, Invitrogen), 1% v/v penicillin/streptomycin (Gibco), and 0.1 mM nonessential amino acids (Invitrogen) following the manufacturer's protocol with a media change every 2-3 days, and passaged every 6-7 days. hMSCs (passage 4) for use in the large femur mold study were purchased from RoosterBio (Frederick, MD) and cultured in the accompanying high performance media kit from RoosterBio. To acquire the necessary cell numbers, we cultured the cells in several 2- and 10-stack cell culture flasks from Corning CellSTACK (Sigma). Cells were passaged on day 3 and cultured for an additional 5 days. All cells were cultured at 37°C and 5% of CO_2. The osteogenic media was formulated as previously described [210] by supplementing growth media with 100nM dexamethasone (Sigma, St. Louis, MO), 10mM β-glycerophosphate, and 173 μM ascorbic acid (Sigma). Prior to using hMSCs from the two cell sources, their CD biomarker analysis were compared to ensure positive for known hMSC marker expressions such as CD 105, CD 166, CD 90, and CD70, as well as negative expression of CD 14, CD 34, and CD45. Lastly, osteogenic differentiation of both types of hMSCs was compared over a 21-day differentiation

period to verify that there was no statistical difference in osteogenic gene and protein expressions (data not shown).

6.2.2 Cell Encapsulation

hMSCs were mixed into 2% w/v alginate (Sigma) solution and used to make 3 mm diameter alginate beads by adding the mixture dropwise (flow rate of 1 mL/minute) into a suspension of 0.1M calcium chloride (Sigma) and stirring for 10 minutes (100,000 cells/bead). The 1 inch construct utilized 20 million cells in 200 alginate beads, while the femur shaped construct required 720 million cells in 7200 alginate beads.

6.2.3 Design and 3D Printing of Femur Mold

A human femur render was obtained from the open source online database GrabCAD (Boston, MA). The file was imported into SolidWorks (Waltham, MA) and the superior half of the femur was isolated. An outward extrusion of the composite resulted in a hollow construct with a wall thickness of 2 mm. Cylindrical pores were then placed at an approximate density of 1 hole per 2.83 mm^2 surface area throughout the surface of the mold. Finally, the femur shell mold was split into six pieces for 3D printing. Cuts were made on the transverse and sagittal planes of the femur mold. The construct was printed out of MED610 material using an Objet500 Connexin 3D printer (Stratasys, Eden Prairie, MN) courtesy of the Sheikh Zayed Institute for Pediatric Surgical Innovation at Children's National Health System, Washington, D.C. Post printing, the femur shell was sutured together using medical grade sutures (Ethicon, San Lorenzo, PR), and sterilized in 70% ethanol and under UV light.

6.2.4 TPS Bioreactor Assembly

For the culture of the 1 inch bone construct, the bioreactor was set-up as described previously[247]. Briefly, a 1-inch platinum-cured silicone growth chamber was loaded with 200 hMSC-seeded and 200 acellular alginate beads and connected to the tubing circuit and media reservoir. The flow was driven by an L/S Multichannel Pump System (Cole Parmer, Vernon Hills, IL) at a flow rate of 20 mL/min and media was changed every two days. The cells were cultured for 18 days in the 1 inch construct before cell analysis.

Similarly, to fabricate the human femur bone graft, the 3D printed femur shell mold was filled with 7200 hMSC-loaded alginate beads and placed inside a 10-inch (25.4 cm) long, 4-inch (10.16 cm) diameter culture chamber (MSC Industrial Supply, Melville, NY). The cell-seeded alginate bead filled mold was cultured with the femur head downward and the femur shaft upward in the culture chamber, as seen in Figure 6.2d, right. Acellular alginate beads were placed in the surrounding void space of the culture chamber to ensure uniform media flow throughout the chamber by providing roughly the same resistance to flow as the hMSC-loaded alginate beads inside the femur shell mold. Custom-made reducing connectors were 3D printed and attached to either end of the chamber, and the remainder of the bioreactor was set up as described above. Media flow was driven at a rate of 240 mL/min to maintain velocities and shear stresses previously shown to enhance osteogenic differentiation of hMSCs in the TPS bioreactor [292].

At the end of the 8 day differentiation period, the femur mold was removed from the growth chamber, injected with liquid alginate, and submerged in a solution

of 0.1M CaCl$_2$ in hMSC growth media to aggregate the alginate beads into a single construct. hMSCs were isolated from specific sections of the construct (Figure 2d) and used for subsequent analyses. Three samples from each group were taken (n=3).

6.2.5 Viability Assay

Cell viability was assessed along the length of the femur construct using a fluorescent Live/Dead assay (Invitrogen) following standard protocols. Beads from each designated section were placed in 48-well plates and incubated in 2 mM ethidium homodimer and 4 mM calcein AM (Molecular Probes) for 30 min. Fluorescent images were then taken of the entire bead using a fluorescence microscope (Axiovert 40 CFL, Zeiss, Thornwood, NY) equipped with a digital camera (Diagnostic Instruments 11.2 Color Mosaic, Sterling Heights, MI).

6.2.6 Immunohistochemistry

Antigens were retrieved by exposure to steam composed of Tris base and EDTA buffer (pH = 8) containing TWEEN 20 for 15 minutes. Samples were blocked and then stained with the primary antibodies to detect BMP-2 and ALP (Abcam, Cambridge, MA), respectively. Protein presence was visualized with a 3,3'-diaminobenzidine tetrahydrochloride (DAB) chromogen. Samples were counterstained with hematoxylin, dehydrated and cleared. Negative control slides were stained using the same protocol, omitting the primary antibody.

6.2.7 Real-Time Quantitative Polymerase Chain Reaction (RT-qPCR)

hMSCs from each section (head, trochanter, middle, shaft, and inner and outer shells) were isolated from alginate beads by dissolution in ethylenediaminetetraacetic

acid (EDTA) for 30 min at 37°C and a cell pellet was formed by centrifugation. The RNeasy Plus Mini Kit (Qiagen, Frederick, MD) was used to isolate total RNA from hMSCs encapsulated in alginate beads using following standard protocols. Total RNA was quantified using a Nanodrop Spectrometer (Thermo Scientific, Wilmington, DE). Isolated RNA was then reverse transcribed to cDNA using a High Capacity cDNA Archive Kit (Life Technologies, Frederick, MD). Quantitative RT-PCR was performed by combining the cDNA solution with a Universal Master Mix (Life Technologies), as well as oligonucleotide primers and Taqman probes for ALP and BMP-2, and compared to the endogenous gene control glyceraldehyde 3 phosphate dehydrogenase (GAPDH) (Life Technologies). The reaction was performed using a 7900HT real-time PCR System (Applied Biosystems) at thermal conditions of 2 min at 50°C, 10 min at 95°C, 40 cycles of 15 s at 95°C, and 1 min at 60°C. The relative gene expression level of each target gene was then normalized to the mean of the GAPDH in each group. Fold change was calculated using the $\Delta\Delta CT$ relative comparative method as described previously [293] and represented in comparison to day 0 static control results. Samples were completed in technical triplicates and standard deviations are reported (n=3).

6.2.8 Statistical Analysis

Each analysis was performed in triplicate (n=3). Statistical significance was determined by one-way analysis of variance and Tukey's multiple-comparison test. A confidence interval of 95% ($\alpha = 0.05$) was used for all analyses. Mean values of triplicates and standard deviation error bars are reported on each figure as well as relevant statistical relationships.

6.3 Results

6.3.1 Effect of Location on Osteogenic Differentiation in Dynamically
Cultured 1 Inch Bone Graft

The TPS bioreactor has previously been used to culture hMSC-loaded alginate
beads for the fabrication of bone constructs with a volume of approximately 2.5 cm^3.
However, to demonstrate the ease of use of the off-the-shelf components of the
system, as well as assess location-based osteogenic differentiation of hMSCs, we
expanded the growth chamber dimensions to result in a 12.8 cm^3 construct. After 7
days of dynamic culture in the TPS bioreactor, the alginate beads were aggregated
into a single construct using 2% alginate and then crosslinked in additional $CaCl_2$
(Figure 6.1a). On days 1, 4, and 7, beads from the periphery and interior of the
construct were analyzed for viability (Figure 6.1c) and expression of early osteogenic
marker alkaline phosphatase (ALP) (Figure 6.1d) and late marker osteopontin (OPN)
(Figure 6.1e) gene expression. Fluorescent staining indicated homogenous
distribution of cells throughout the individual beads as well as continuous viability of
cells in both experimental groups throughout the study. The expression of ALP
mRNA increased as expected on day 7 compared to day 1 expression, yet there was
no statistical difference between cells cultured in the peripheral and interior beads
(Figure 6.1d). Similarly, OPN mRNA expression remained consistent between groups
over 7 days of osteogenic differentiation (Figure 6.1e). These results indicated no
significant difference in osteogenic differentiation of hMSCs cultured in the TPS
bioreactor regardless of position in the growth chamber.
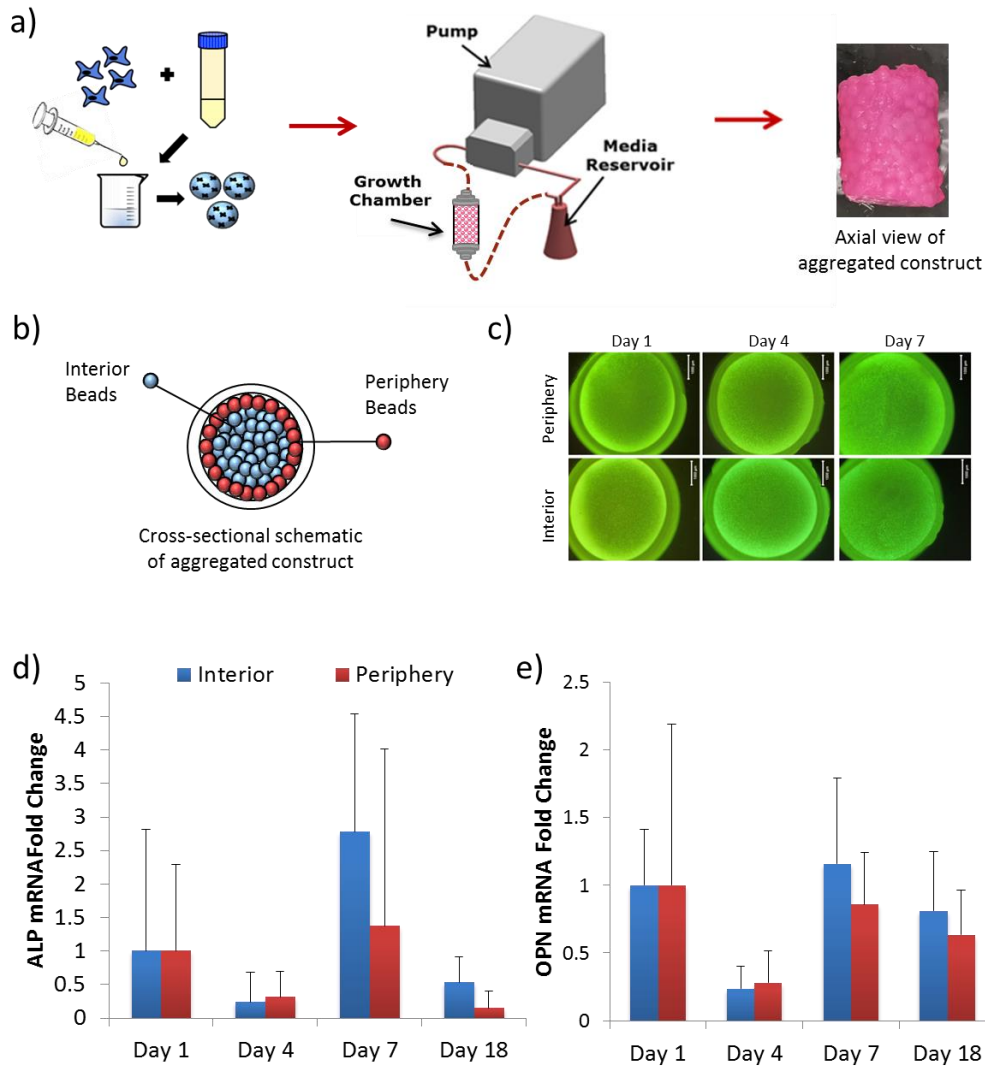
Figure 6.1 Fabrication of 1-inch Bone Graft. a) Encapsulation of hMSCs in 2% alginate solution results in the formation of spherical alginate beads. They were dynamically cultured in the TPS bioreactor setup with adjustable growth chamber, media reservoir, and peristaltic pump. After 7 days of culture, the alginate beads were aggregated into a single construct (1" diameter, 1" height). b) Schematic showing cross-sectional view of alginate beads in 1" construct categorized into either interior beads or peripheral beads for analysis of cell viability and function. c) Fluorescence staining of interior and peripheral alginate beads on days 1, 4, and 7 depicting live (green) and dead (red) cells. Results indicated that cells remained viability throughout the graft with no visible differences between interior and peripheral culture locations. Scale bar represents 1000 μm. d) Gene expression of ALP and OPN mRNA on days 1, 4, and 7. While there was an increasing trend of ALP mRNA expression by day 7, there was no statistical difference between the expression of interior and peripherally cultured cells. Similarly, no difference was observed in OPN mRNA expression on all three timepoints (n=3, p<0.05).

6.3.2 Culture of Human Femur using Osteogenic Differentiated hMSCs

Creating a bone graft of sufficient size has been a major obstacle in the field of bone tissue engineering. Utilizing 3D printing technology, we created a hollow mold of the superior half of a human femur (Figure 6.2a). The printed femur was 22.86 cm in length, 10.16 cm in width at its widest point (femur head to trochanter), and had an internal volume of 200 cm^3. We created 1 mm holes throughout the 3D femur shell, resulting in a 62.5% porosity (with an average density of one hole per 2.81 cm^2) to allow for sufficient media and oxygen flow throughout the interior. The pieces of the femur mold were sutured together and filled with 7200 hMSC-loaded alginate beads (Figure 6.2b). After 8 days of dynamic culture, the femur mold was removed from the growth chamber and the cultured beads were aggregated into a single construct using 2% alginate crosslinked in 100 mM CaCl$_2$ supplemented hMSC growth media (Figure 6.2c). Post aggregation, the bone construct was 20 cm in length, and 8.9 cm in width (femur head to trochanter). We first divided the composite into 4 sections (femur head, trochanter, middle, and femur shaft), followed by an additional inner core and outer shell for each section to analyze the cells' viability and osteogenic differentiation throughout the construct over the culture period.
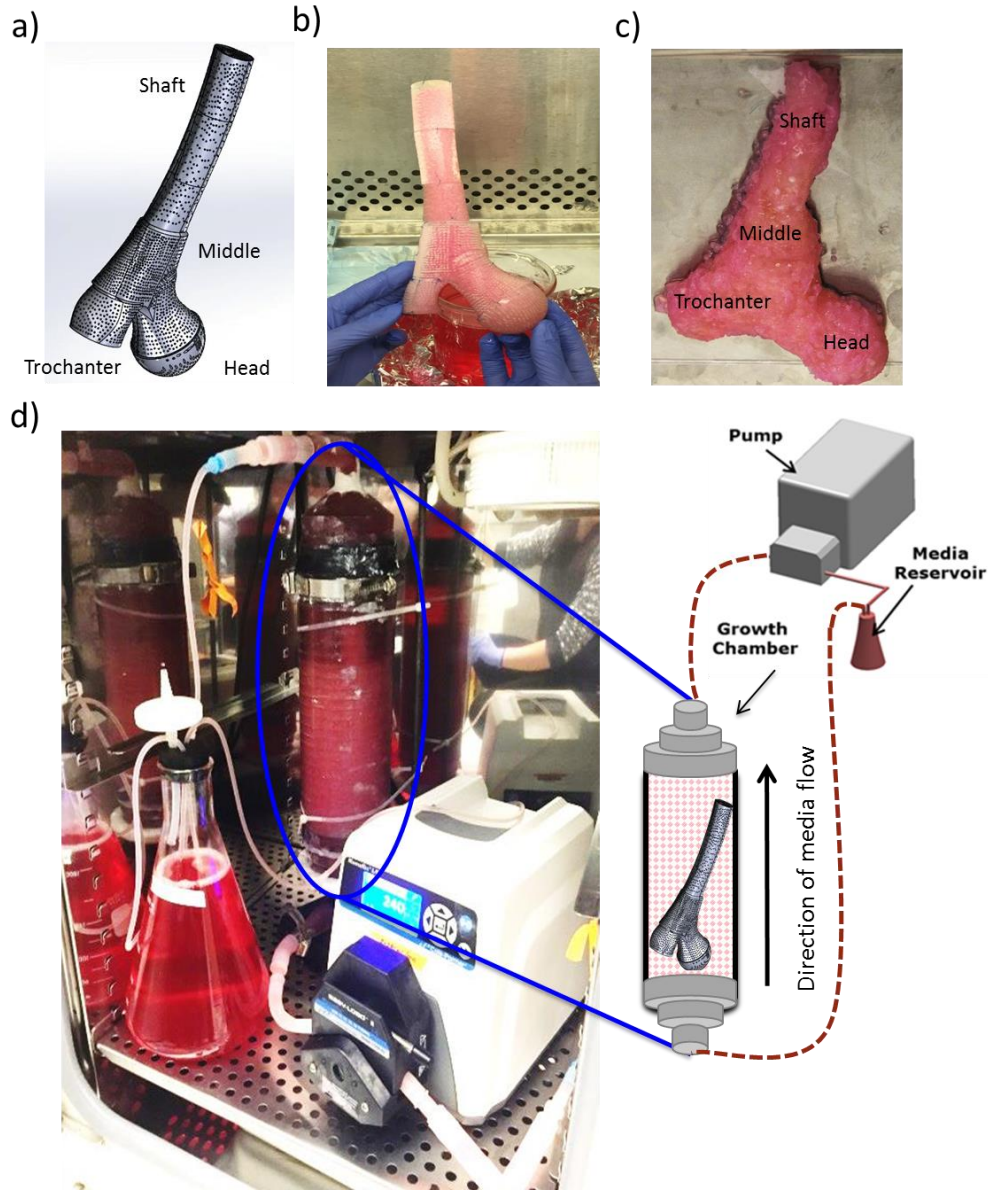
Figure 6.2 Design, Fabrication, and Culture of Human Femur Graft. a) Solidworks CAD rendering of superior half of adult human femur. The mold was 22.86 cm in length, 10.16 cm in width at its widest point (femur head to trochanter), and had an internal volume of 200 cm^3. It was covered 1 mm holes throughout the hollowed mold with an average density of one hole per 2.81 cm^2. b) Image of 3D printed femur mold after it was filled with alginate-encapsulated hMSC beads (light pink color). c) Image of aggregated alginate construct after 8 days of dynamic culture in TPS bioreactor. Its parts were categorized as femur head, trochanter, middle or shaft. d) Image of TPS bioreactor setup in incubator with growth chamber (circled in blue) containing femur mold. Schematic on right depicts TPS assembly with femur mold inside growth chamber and showing the direction of flow from the femur head-trochanter towards the femur shaft.

Fluorescent staining of live (green) and dead (red) cells indicated that the majority of cells remained viable after 8 days of dynamic culture in the TPS bioreactor (Figure 6.3a). There were no qualitative differences visible between cells from the inner core or outer shell of the construct, indicating that sufficient amounts of nutrients and media were supplied throughout the width of the engineered femur. Immunohistochemical staining for ALP and bone morphogenic protein-2 (BMP-2) protein (in brown, cells in blue) on day 8 showed no visible differences between early and late protein markers expressions (Figure 6.3b-c). However, when examining mRNA expression of the same markers on day 8, cells cultured in the inner (dashed line, 25.2-fold) and outer (solid line 39.7-fold) shells of the shaft section in the femur mold expressed a significantly greater amount of ALP and BMP-2 compared to other day 8 sections as well as day 0 static control cells (Figure 6.3d-e). Average values of each femur section (depicted as solid bars) demonstrated that there was no significant difference between ALP mRNA expression of inner and outer shells of the femur head, trochanter, and middle sections of the femur. Similarly, expression of BMP-2 mRNA showed a statistically significant increase in cells cultured in the inner (dotted line) and outer (solid line) shell of the femur shaft as compared to the other sections on day 8 and the day 0 static control. Additionally, the average BMP-2 expression on day 8 in the femur head, trochanter, and middle sections were significantly greater than in the day 0 static control cells. Yet, with the exception of the femur shaft, there were no differences in BMP-2 expression seen between cells cultured in the inner or outer shells of the femur on day 8.

a)

	Head	Trochanter	Middle	Shaft

Viability — Inner

Viability — Outer

b)

	Head	Trochanter	Middle	Shaft

ALP Protein Expression — Inner

ALP Protein Expression — Outer

c)

	Head	Trochanter	Middle	Shaft

BMP-2 Protein Expression — Inner

BMP-2 Protein Expression — Outer
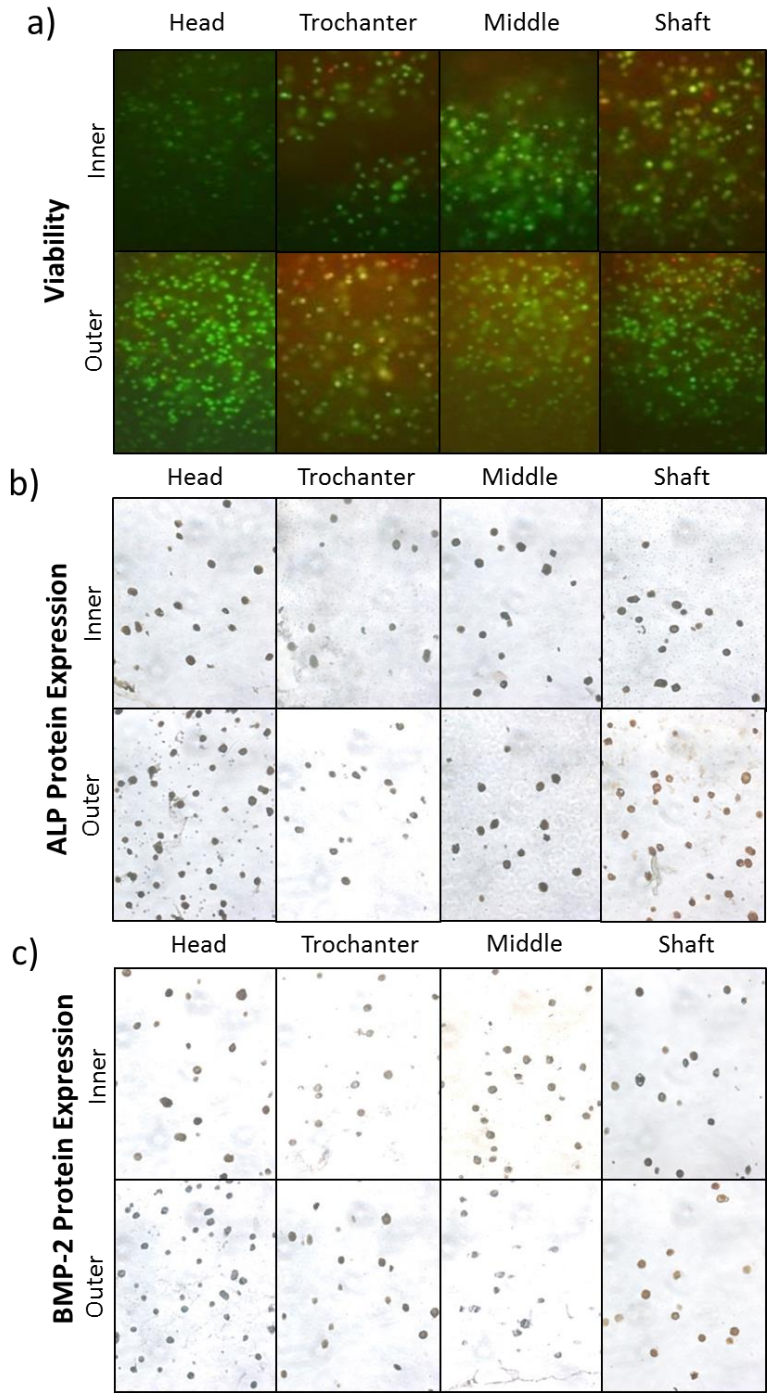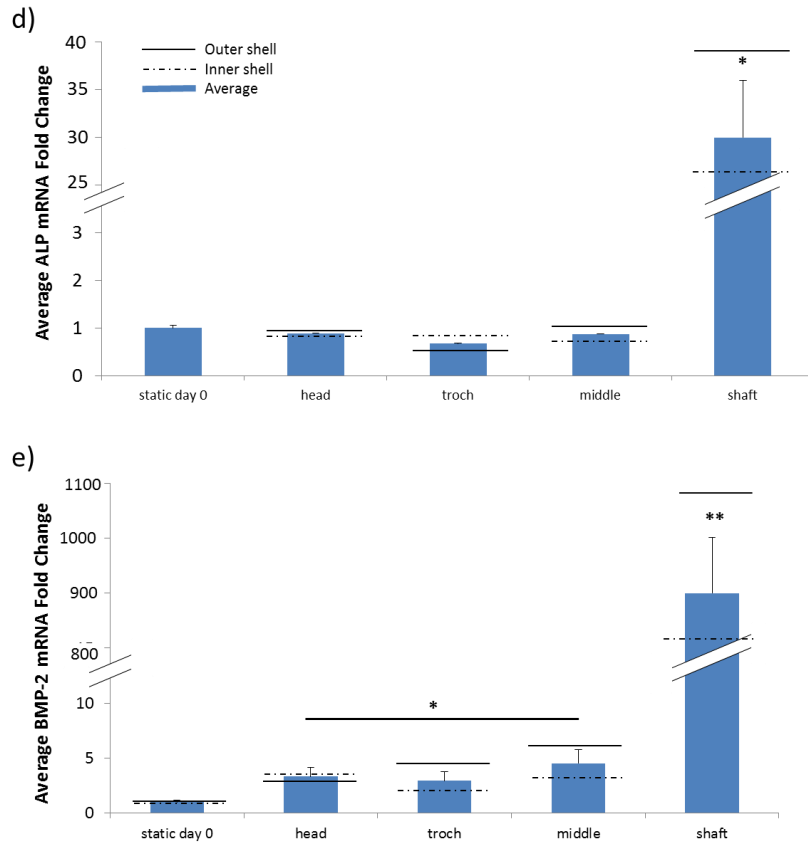
Figure 6.3 Osteogenic Differentiation of hMSCs in Adult Human Femur Mold.
a) Fluorescence staining of hMSCs after 8 days of dynamic culture in the TPS
bioreactor. Live (green) and dead (red) cells are shown in inner and outer shells of the
femur head, trochanter, middle, and shaft sections of the construct. It is visible that
the majority of cells remain viable and that no qualitative differences are observed
between the cultured sections, indicating sufficient oxygen and nutrient supply
throughout the construct. Scale bar represents 200 μm. b-c) Immunohistochemical
staining of ALP and BMP-2 protein expression, respectively, of all experimental
groups. Cells are stained in dark blue and protein in brown. No visible differences are
seen between experimental groups in either inner or outer culture location, indicating
homogenous differentiation of hMSCs over 8 days of dynamic culture. d-e) Average
ALP and BMP-2 mRNA expression on day 8 compared to static day 0 control (blue
bars). Gene expressions of cells cultured in the inner and outer shell are depicted by a
dashed and solid line, respectively. Average ALP expression demonstrated no
statistical difference between cells cultured in the femur head, trochanter, or middle
sections of the femur compared to static day 0. However, an average of 32.4-fold
increase of ALP mRNA was observed in the femur shaft. Gene expression of BMP-2
showed statistically significant increase on day 8 in all experimental groups compared
to the static day 0 control. Additionally, BMP-2 gene expression was approximately
900 times greater in the femur shaft on day 8, which was significantly greater than
expression in all other groups. Markers * and ** indicate statistical significance
compared to control (n=3, p<0.05).

6.4 Discussion

Many bioreactor systems are limited in the size of the tissue that can be fabricated due to lack of oxygen that reaches the center of the graft, leading to cell necrosis. To solve this issue, our system utilizes smaller alginate beads (3 mm in diameter) that can be aggregated into a single construct of any size after dynamic culture in the TPS bioreactor (Figure 6.1a). The TPS bioreactor allows for enhanced osteogenic differentiation of hMSCs by applying fluid shear stress on the surface of the beads[240,247]. The culture and fabrication of the 1 inch bone graft, which is similar in diameter size to the shaft of a human femur, was the next step towards creating critically sized and clinically relevant tissue constructs for the regeneration of bone. Most importantly, this pilot study confirmed continuous viability of cultured cells throughout the culture chamber over 7 days, demonstrating that oxygen and nutrient supply was not different in the periphery or interior of the culture chamber (Figure 6.1b-c). This overcomes a major hurdle in tissue engineering, wherein cells cultured at the center, or core, of the graft experiences necrosis due to the consumption of oxygen by cells at the periphery of the graft. Additionally, osteogenic differentiation of hMSCs, as indicated by increased expression of ALP and OPN mRNA expression, proved to be similar in cells cultured throughout the chamber (Figure 6.1d-e). Therefore, an expansion of the TPS bioreactor growth chamber does not affect viability or osteogenic differentiation of hMSCs. In addition, we were able to demonstrate the ability to create large aggregates of alginate beads after their dynamic culture. The technique of utilizing additional alginate to fabricate a single

construct resulted in a solid hydrogel composite that was easily handled and could be transferred into a defect site.

While the TPS bioreactor enables great flexibility in the size and length of the tubing circuit, the cylindrical shape of the tube defines the resulting architecture of the construct cultured in the growth chamber. In recent years, 3D printing technology has emerged as a leading technological innovation, especially in medical applications. It has allowed for the creation of complex structures with precise architecture and consistency. In this work, 3D printing techniques helped fabricate an accurate model of an adult femur, the largest bone in the human body (Figure 6.2a). This demonstrates not only the potential of the technology, but also its capability to remove size limitations in the tissue engineering field. Additionally, the ability to print patient-specific molds based on magnetic resonance imaging (MRI) or computed tomography (CT) scans leads to more successful patient-specific care and tissue regenerative treatments.

By printing a porous 3D human femur, we were able to ensure fluid flow into and throughout the construct. During the dynamic culture in the TPS bioreactor, the femur mold was cultured with the head and trochanter at the inlet of the growth chamber (Figure 6.2d, right). This portion of the femur held the majority of the cell-loaded beads and therefore needed to receive the most oxygenated media as it circulated via gas permeable tubing from the media reservoir to the inlet at the bottom towards the outlet at the top of the growth chamber. Additionally, to ensure uniform flow throughout the chamber, acellular alginate beads filled the void space surround the femur mold, as depicted by the pink patterned background in schematic 2d. After

90

aggregation of alginate beads into a single construct, it was divided into further segments for viability and gene expression analysis.

On day 8, cell viability remained high in both the inner and outer shell of each section (Figure 6.3a), with no visible differences observed. This is an important and momentous achievement for any large tissue-engineering construct. The advantage of dynamically culturing small alginate beads in the TPS bioreactor prior to aggregation and implantation is most evident with the high cell viability result. Additionally, the immunohistochemical staining of early osteogenic marker ALP and osteogenic growth factor BMP-2 indicated only subtle differences in protein expression between the experimental groups on day 8, with slightly greater staining on femur shaft samples. Therefore, the cells are experiencing similar culture environments that produce homogenous expression of protein throughout the construct.

The average mRNA expression of ALP (Figure 6.3d, blue bars) showed no significant differences between the femur head, trochanter, or middle sections compared to day 0 static control cells. However, a significant increase in expression was observed in cells cultured in the inner and outer femur shaft (26.2- and 39.7-fold change, respectively), compared to the static day 0 control. A similar pattern was seen in the BMP-2 mRNA expression, in which the inner and outer shell of the femur shaft expression was statistically greater than in the other groups on day 8. In addition, the femur head, trochanter, and middle sections expression significantly greater BMP-2 mRNA compared to day 0 static control (3.8-fold, 3.2-fold, and 4.8-fold, respectively). We hypothesize that this substantial increase in ALP and BMP-2 may be attributed to growth factor production and update from cells from the inlet and the

91

outlet of the growth chamber. In particular, we believe that there is a growth factor gradient created during uni-directional flow in the growth chamber, which is generated when growth factors are released from cells cultured at the inlet and taken upstream by the fluid flow to cells cultured at the outlet, where they enhance functions like osteogenic differentiation. We have been able to show diminishing effects of this phenomenon when periodically alternating the direction of the flow inside the growth chamber. Therefore, we believe the direction of the flow can influence the expression of osteogenic markers in differentiating hMSCs. While the expression of osteogenic mRNA was much higher in cells cultured in the femur shaft, we observed trends of increased BMP-2 expression over 8 days of dynamic culture in all sections of the graft. It is also interesting to note that the outer shell of the femur construct expressed greater amounts of osteogenic mRNA in almost all groups on day 8. This could be seen as an advantageous benefit of the culturing system, in which the outer shell experiences relatively accelerated development to form the compact and stiffer cortical bone tissue, leading to structural support for the growth of the interior trabecular bone, which is spongy and weaker in mechanical strength.

6.5 Conclusion

Although this study has demonstrated major strides towards developing a bone graft fit for clinical application, there are still limitations that need to be addressed. This one-time proof of concept provides invaluable information about the ability to create a high volume engineered bone construct, yet additional studies with longer culture periods will generate more data and knowledge on the capabilities of the system. Although bone-marrow derived mesenchymal stem cells have been used

in broad tissue engineering applications, a limitation in their osteogenic differentiation has been found when used in a bone defect composed of cells of neural-crest origin compared to cells of mesoderm origin [294]. Therefore, the stem cell origins as well as final defect destination need to be considered when designing a bone tissue engineering graft. Additionally, the current setup utilizes alginate hydrogels as a cell deliver and culturing environment, due to the natural polymer's known non-cytotoxic and bio-inert properties. However, its lack of mechanical strength makes it non-ideal for future bone tissue engineering applications without further additions or modifications. Therefore, we plan to utilize a scaffold sleeve carrier made from a polymers such as poly(propylene fumarate), which has mechanical properties close to bone [295], that can be utilized to 3D print the femur shell and then be directly implanted into the defect site after aggregation of the alginate beads. Additionally, a drawback of the current scaffold material includes the lack of cell-cell contact between differentiating hMSCs in separate alginate beads during initial dynamic culture. With the aggregation of scaffolds using additional alginate, we hope that cells will be able to migrate within the constructs after *in vivo* implantation. More importantly, in order to bring this technology from bench to bedside, a vascular network will be vital; without it, the encapsulated cells at the core of the construct will not survive after implantation into the patient. Like many organs, bone contains an intricate vasculature that maintains viability throughout the tissue. Therefore, we are developing techniques to incorporate vascular networks within the engineered bone tissue for improved incorporation into the defect and surrounding tissue. With these next steps, we anticipate the fabrication of a fully functional, size

and patient specific tissue engineered bone construct that can be dynamically cultured

in the TPS bioreactor and then directly implanted into a bone defect.

Chapter 7: Dynamic Coculture of Mesenchymal Stem Cells and Endothelial Cells for Bone Tissue Engineering

7.1 Introduction

A major challenge of developing a large bone tissue engineering construct is delivery of nutrients and oxygen to the core once it has been implanted in the patient's defect site. *In vivo,* cells are supplied with vital molecules via nearby blood vessels that carry nutrients and waste to and from the cells. However, without a pre-established vascular network developed *in vitro* prior to implantation, the diffusion of important nutrients is limited to 100-200 μm from the host vasculature, unable to maintain viability of the majority of the construct [2,296]. Therefore, in order to establish a viable system for *in vivo* implantation, the complex interaction between the two main cell types for bone tissue engineering applications, human mesenchymal stem cells (hMSCs) and endothelial cells, need to be better understood. This knowledge will allow for the creation of a prevascularized engineered construct prior to insertion into a patient.

The use of *in vitro* cocultures has been one of the most explored options for this application [20,297–299]. A range of coculture methods investigate the interactions between the endothelial cells and osteogenic differentiated mesenchymal stem cells or osteoblast like cells as they are inherently linked during the osteogenic and angiogenic process [300–302]. The formation of micro-vasculature in some coculture conditions has been demonstrated [43,44,138,225], however, few have been applied for in high-volume tissue engineering constructs, which require an extensive prevascularized network to remain viable *in vivo* [303].

Here we investigate the important role of coculture parameters that influence the osteogenic and angiogenic potential of hMSCs and endothelial cells, respectively. First, we examine the role of scaffolds on cocultures, specifically, the native content of cell-binding sites that exist in natural polymers like collagen but are less abundant in alginate. The sodium alginate polymeric backbone presents no intrinsic cell-binding domains, but can be used to regulate gel mechanical properties. On the other hand, natural collagen fibrils present specific peptide sequences that can be recognized by cell surface receptors, therefore allowing for cell adhesion and spreading that better recreates many *in vivo* contexts [304,305]. The second parameter tested was the influence of shear stress on the coculture system. Dynamic culture conditions can be created in a perfusion bioreactor that mimics *in vivo* conditions. We have previously demonstrated the benefits of the tubular perfusion system (TPS) bioreactor on osteogenic differentiation of hMSCs due to the applied shear flow and the increased oxygen and nutrient supply to the cultured cells [205,240,247,285,306].

To this end, the objective of this study is to determine the importance of specific environmental parameters in HUVEC and hMSCs coculture: 1) cell coculture proximity, and 2) effects of shear stress on hMSC osteogenesis and HUVEC angiogenesis.

7.2 Materials and Methods

7.2.1 Cell culture

Bone marrow derived hMSCs were purchased from RoosterBio, Inc. and cultured in the accompanying high performance media kit from RoosterBio. hMSCs were passaged and given fresh media on Day 5. They were harvested at passage 3 for

96

encapsulation. HUVECs were purchased from Lonza and cultured in endothelial cell growth media (Lonza). HUVECs were given fresh media every 2-3 days and passaged on Day 5. HUVECs were harvested at passage 3 for encapsulation. All cells were cultured at 37°C with 5% CO_2.

7.2.2 Alginate bead scaffold fabrication and hMSC encapsulation

Alginate beads were fabricated using 2% alginate solution (Sigma), homogenously mixed with hMSCs (100,000 hMSCs/bead), and crosslinked in 100mM $CaCl_2$ by dropwise addition of the solution through an 18G needle and syringe. The beads were stirred for 10 minutes to allow for complete crosslinking of the alginate and placed in hMSC growth media until use.

7.2.3 Thin hydrogel fabrication for cell adhesion

2% alginate and 4mg/mL collagen hydrogels were fabricated to test hMSC and HUVEC adhesion to the scaffolds. Cylindrical alginate gels were created using molds (20mm in diameter, 2mm in height) and diffused with 100mM $CaCl_2$ for crosslinking and then transferred to 12 well plates. Collagen hydrogels were made directly in the wells and crosslinked at 37°C for 30 minutes. Hydrogels were stored in PBS until cell seeding.

7.2.4 Cell adhesion assay

hMSCs and HUVECs were lifted using trypsin/0.25% EDTA (Life Technologies) and counted. They were seeded onto the hydrogels in a concentrated solution of 100,000 cells/100uL for 1 hour at 37°C. Additional media was added after 1 hour and cells were allowed to adhere for 3 more hours. Cells were seeded on TCPS

as a positive control for cell attachment. After 4 total hours of incubation, hydrogels were gently washed 3 times with PBS. To visualize and quantify cell adhesion, a live-dead assay (Invitrogen) was performed following standard protocol. Gels were imaged using a fluorescent microscope (Axiovert 40 CFL with filter set 23; Zeiss) equipped with a digital camera (Diagnostic Instruments 11.2 Color Mosaic). Adhesion was also quantified using a plate reader and

7.2.5 Collagen hydrogel formation/encapsulation

All cells were encapsulated in 4mg/mL rat tail derived type I collagen (Corning) and prepared following manufacturer's instructions. The desired collagen concentration was kept on ice while cells were harvested and centrifuged at 500g for 5 minutes. Collagen was added to the cell pellets and mixed and kept on ice. Small gels were created by pipetting 3.33μL of the collagen/cell mixture onto UV-sterilized parafilm and crosslinking for 7 minutes at 37°C. The beads were washed off the parafilm and collected. We created 6 experimental groups: hMSCs in collagen in static conditions, hMSCs in collagen in dynamic condition, HUVECs in collagen in static conditions, HUVECs in collagen in dynamic conditions, a coculture of hMSCs and HUVECs in collagen in static conditions, and a coculture of hMSCs and HUVECs in collagen in dynamic conditions.

7.2.6 Static & dynamic culture

Scaffolds in the static groups were cultured in 6 well plates. Dynamic groups were placed in a TPS bioreactor as previously described. Each group was loaded into a ¼" by 5" growth chamber and connected to the tubing circuit and media reservoir.

The flow was driven by an L/S Multichannel Pump System (Cole Parmer) at a flow rate of 3 mL/min and media was changed every 3 days. All groups were cultured at 37°C with 5% CO_2. All coculture groups were cultured in mixture of 1:1 ratio of osteogenic media to endothelial cell growth media. Osteogenic media was prepared by supplementing growth media containing High Glucose Dulbecco's modified Eagle's medium with l-Glutamine (Gibco), supplemented with 10% fetal bovine serum (Invitrogen), 1% v/v penicillin/streptomycin (Gibco), and 0.1 mM nonessential amino acids (Invitrogen) with 100 nM dexamethasone (Sigma), 10 mM b-glycerophosphate, and 173 mM ascorbic acid (Sigma).

7.2.7 RNA extraction

Cell samples from each group were isolated from collagen gels by dissolution in 1mg/mL collagenase (Sigma) for 60 min at 37°C and a cell pellet was formed by centrifugation and washed with PBS three times. The RNeasy Plus Mini Kit (Qiagen) was used to isolate total RNA following standard protocols. Total RNA was quantified using a Nanodrop Spectrometer (Thermo Scientific).

7.2.8 Real-time quantitative polymerase chain reaction (RT-qPCR)

Isolated RNA was then reverse transcribed to cDNA using a High Capacity cDNA Archive Kit (Life Technologies). RT-qPCR was performed by combining the cDNA solution with a Universal Master Mix (Life Technologies), along with oligonucleotide primers and Taqman probes for ALP, BMP-2, and OCN (hMSCs and coculture samples) and VEGF and PECAM (HUVEC and coculture samples), and compared to the endogenous gene control glyceraldehyde 3 phosphate dehydrogenase

(GAPDH; Life Technologies). The reaction was performed using a 7900HT real-time PCR System (Applied Biosystems) at thermal conditions of 2 min at 50°C, 10 min at 95°C, 40 cycles of 15 s at 95°C, and 1 min at 60°C. The relative gene expression level of each target gene was then normalized to the mean of the GAPDH in each group. Samples were completed in technical triplicates and standard deviations are reported (n = 3).

7.2.9 Immunohistochemistry

At each timepoint, collagen gels were fixed in 4% paraformaldehyde for 2 hours at RT, dehydrated and embedded, and sectioned into 10μm slices. Antigens were retrieved by exposure to steam composed of Tris base and EDTA buffer (pH = 8) containing TWEEN 20 for 15 minutes. Samples were blocked and then stained with the primary antibodies to detect BMP-2 and ALP (Abcam, Cambridge, MA) in hMSCs, PECAM and VEGF in HUVECs, and BMP-2 and PECAM in the coculture. FITC and Cy-5 tagged secondary antibodies were used to visualize the protein, while DAPI stained the nucleus. Samples were imaged using a LSM700 confocal microscope (Zeiss).

7.2.10 Cell Viability Assay

Cell viability was assessed using a fluorescent Live/Dead assay (Invitrogen) following standard protocols. Gels were placed in 1.5mL microcentrifuge tubes (Fisher Scientific) and incubated in 1 mM ethidium homodimer and 2 mM calcein AM (Molecular Probes) for 30 min. Fluorescent images were then taken of the entire

bead using a fluorescence microscope (Axiovert 40 CFL; Zeiss) equipped with a digital camera (11.2 Color Mosaic; Diagnostic Instruments).

7.3 Results

7.3.1 Coculture of hMSCs in alginate and HUVECs in collagen scaffolds

We first examined coculture parameters between hMSCs and HUVECs by culturing them in alginate and collagen, respectively, under either static or dynamic conditions (Figure 7.1a). BMP-2 immunostaining of hMSCs showed increased presence of protein (brown) after 14 days of coculture, especially in the dynamically cultured group (Figure 7.1b). The morphological change seen by day 14 in dynamic conditions indicated cell spreading of the hMSCs. Gene expression of mRNA also showed enhanced expression in both cells cultured in the TPS bioreactor. BMP-2 gene expression in dynamically cultured hMSCs increased 3-fold after 7 days and fell to 2-fold after 14 days, compared to day 0 values (Figure 7.1c, gray). In contrast, static BMP-2 values remained fairly constant over the 14 day period (Figure 7.1b, black). The impact of dynamic culture was also visible in HUVEC gene expression of VEGF, which linearly increased over 14 days to 3.5-fold change compared to day 0 values (Figure 7.1d, gray). Statically cultured cells reached only a 1.8-fold increase on day 7 before decreasing back down to basal levels (Figure 7.1d, black).
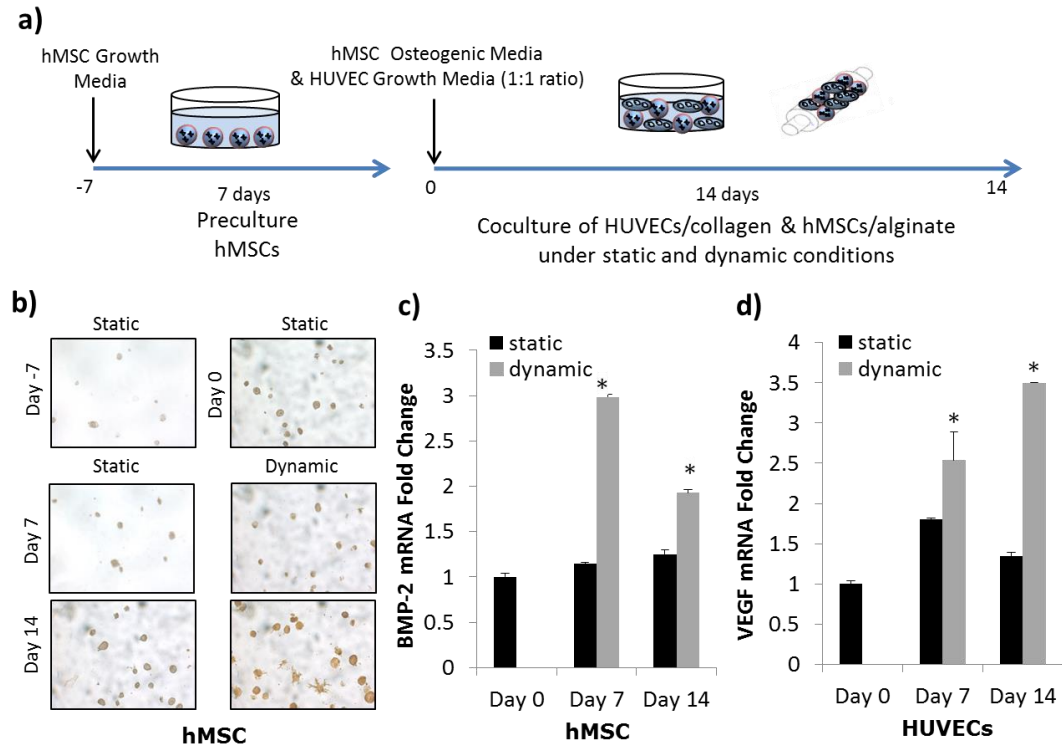
Figure 7.1 Coculture in Alginate and Collagen Scaffolds. A) Experimental setup depicts a 7 day static preculture of hMSCs encapsulated in alginate scaffolds, followed by a 14 day dynamic or static coculture with HUVECs encapsulated in collagen scaffolds. B) BMP-2 immunostaining demonstrates increase in BMP-2 production (brown) in hMSCs (dark blue nucleus). C) BMP-2 mRNA expressions in hMSCs significantly increases over 14 days in dynamic culture but stays constant static culture. D) VEGF mRNA expressions in HUVECs significantly increases over 14 days in dynamic culture and shows an increase on day 7 in static before decreasing back close to basal levels. The symbol '*' indicates statistical significance within groups at a timepoint ($p < 0.05$).

7.3.2 Cell adhesion on collagen and alginate

We examined the importance of binding sites in natural polymers like alginate and collagen on hMSC and HUVEC adhesion and spreading (Figure 7.2a). When seeded on top of alginate hydrogels, hMSCs remained rounded in morphology and very few attached after the 4 hour incubation (Figure 7.2c, top row). HUVECs showed slightly higher attachment ability in comparison, however, little spreading was observed during this period (Figure 7.2c, bottom row). On the other hand, greater number of cells remained attached on collagen hydrogels, for both hMSCs and HUVECs, with a distinctly greater number of elongated HUVECs. Cells seeded on TCPS as positive control adhered on the well surface, with clear spreading and elongated morphology visible. It is important to note that HUVECs, while fully spreading out, most adhered around the edge of the well, due to the small and concentrated media volume at seeding. These cell adhesion results were conferred using a microplate reader to determine total fluorescence (in RFU) (Figure 7.2d). Based on the detected fluorescence, significantly greater number of hMSCs and HUVECs adhered to collagen compared to alginate hydrogel surfaces. In the case of HUVEC, greater fluorescence was detected on collagen compared to TCPS, which can be contributed to the bare well center and a confluent cell ring at the border.
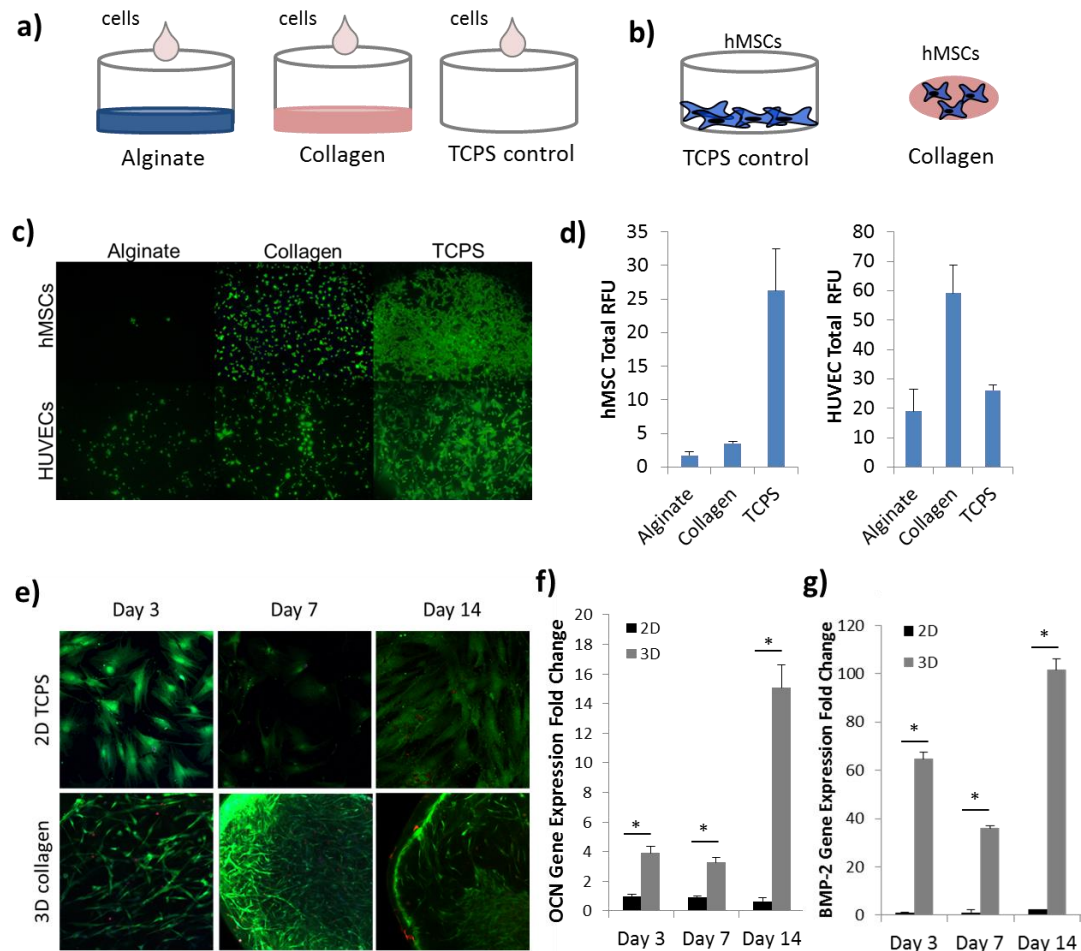
Figure 7.2 Cell Adhesion and Osteogenic Differentiation in Collagen Scaffolds.
A) Experimental setup for cell adhesion study on alginate and collagen substrates,
and TCPS as positive control. B) Experimental setup to investigate the effect of
collagen encapsulation on osteogenic differentiation compared to TCPS as a control.
C) Fluorescence images of hMSCs or HUVECs seeded on alginate, collagen, or
TCPS substrates, taken at 2.5x magnification. D) Quantification of fluorescence
signal read via a spectrophotometer at excitation of 494nm and emission of 517nm
for both hMSCs and HUVECs. Units are listed as RFU (relative fluorescence units).
E) Fluorescence images of hMSCs labeled with live (green) and dead (red) stain on
TCPS or encapsulated in 3D collagen scaffolds. F) Gene expression of osteocalcin
(OCN) mRNA in hMSCs over 14 days. Production was statistically greater in
collagen scaffolds compared to the TCPS control. G) Gene expression of BMP-2
mRNA in hMSCs shows significantly increased expression in 3D collagen compared
to TCPS. The symbol '*' indicates statistical significance within groups at a
timepoint ($p < 0.05$).

104

7.3.3 Osteogenic differentiation of hMSCs in collagen scaffolds

The ability of hMSCs to successfully differentiate in osteoblasts while encapsulated in collagen scaffolds was observed through morphological changes and determined through gene expression of late differentiation marker osteocalcin (OCN) and general osteoblast marker bone morphogenic protein-2 (BMP-2). Results were compared to hMSCs seeded in 2D on TCPS. As visible in the fluorescence live-dead staining, hMSCs greatly elongated when encapsulated in collagen compared to 2D TCPS, resulting in greater cell length but smaller cell width (Figure 7.2e). Additionally, hMSCs expressed significantly greater amounts of OCN and BMP-2 at every timepoint over the 14 day differentiation study (Figure 7.2f-g).

7.3.4 Effects of dynamic culture on hMSC and HUVEC coculture in collagen scaffolds

HUVECs and hMSCs were encapsulated in collagen scaffolds and cultured for 14 days in static or dynamic conditions to determine effects on osteogenic and angiogenic potential of the cells (Figure 3a). Fluorescence microscopy of the cell-encapsulated hydrogel indicated high viability of all three groups (hMSCs, HUVECs, and hMSCs+HUVECs), with great elongation of hMSCs visible while HUVECs remained more rounded in morphology (Figure 3b). Interestingly, cells formed aggregates when cocultured in collagen, more visibly in dynamic culture compared to static coculture (white arrows).

We examined gene expression of common osteogenic markers (ALP and BMP-2) in hMSCs and angiogenic markers (PECAM and VEGF) in HUVECs during mono- and cocultures (Figures 3c-e). As seen in Figure 3c), ALP mRNA expression

increased moderately over 7 days in hMSCs cultured alone in collagen. Expression in dynamic cells was statistically greater on days 1 and 7 compared to static cells (purple and orange striped bars vs. purple and orange solid bars). Similarly BMP-2 mRNA expression in hMSC monoculture significantly increased over 7 days, with dynamically cultured cells leading the way until day 7, when statically cultured cells expressed similar levels, 9.5 and 10.2 fold, respectively. Angiogenic marker expressions in monocultured HUVECs followed a similar trend, where when cultured in the TPS bioreactor produced significantly greater amounts of PECAM and VEGF compared to the control HUVECs in static culture (Figure 3d).

More interestingly, coculture of hMSCs and HUVECs in collagen scaffolds increased expression of all four markers, independent of their static or dynamic culture environment (Figure 3e). For example, ALP expression, while staying constant over the culture period, reached 4-fold increasing levels on day 1 in dynamic culture and day 3 in static culture, but were not reached until day 7 in hMSC monoculture. During coculture, BMP-2 expression in hMSCs was impressively increased, reaching an 18.2-fold increase in the dynamic group and 12.4-fold increase in the static group by day 7. PECAM and VEGF expressions were also greater in coculture conditions compared to the HUVEC monoculture expressions. Specifically, PECAM expression increased 5.5- and 6.0-fold over day 1 values in static and dynamic conditions, respectively, albeit they were not statistically different from one another. VEGF mRNA expressions also significantly, with day 7 dynamic expression twice as high as day 7 static expression.

These mRNA expression results were confirmed using immunofluorescence staining (Figure 3f). hMSCs in monoculture were stained with BMP-2 antibody and showed visible staining throughout the cell by day 7 (red with blue nucleus), in both static and dynamic culture. HUVEC monoculture stained more positive for CD-31 (green) on day 7 in static culture than in dynamic culture, but vice versa with VEGF (red) staining. hMSCs and HUVECs cocultured in collagen scaffolds were stained for BMP-2 (red) and CD31 (green) with DAPI labeled nuclei (blue). There were visibly greater amounts of BMP-2 compared to monocultured hMSCs, with the greatest amounts seen in cells cultured in the TPS bioreactor. An 80x zoom of the area (highlighted in white box), displays diffused BMP-2 (red) throughout the cellular space, with more spotty detection of CD31 around the membrane of the cells.
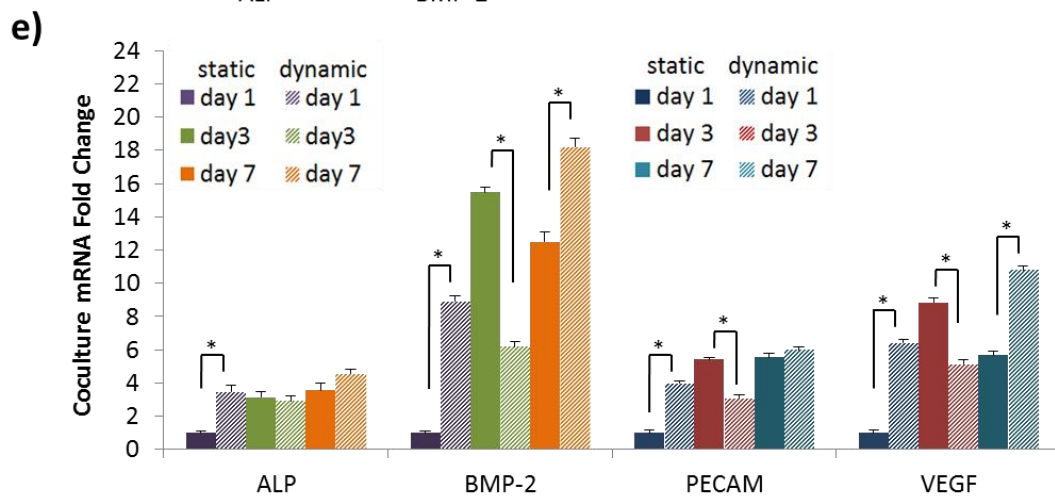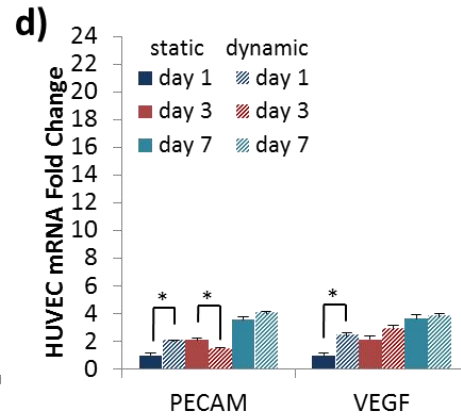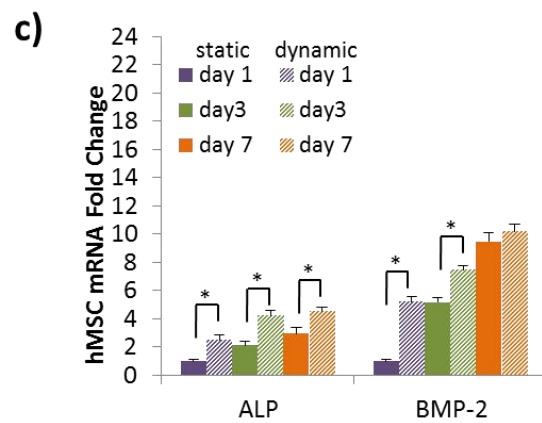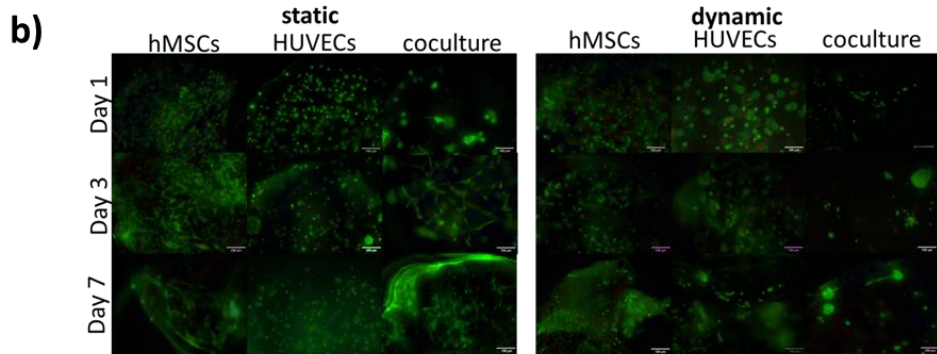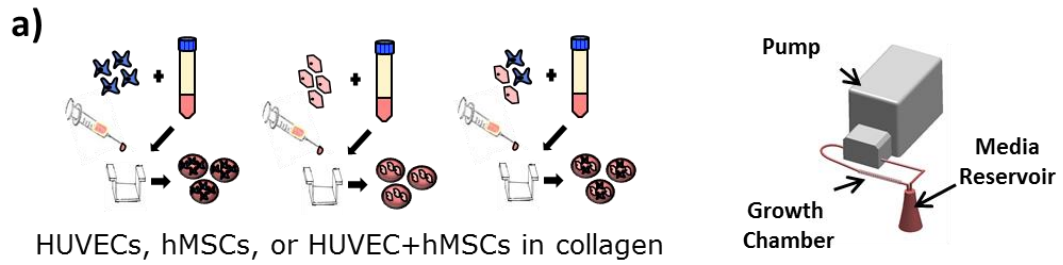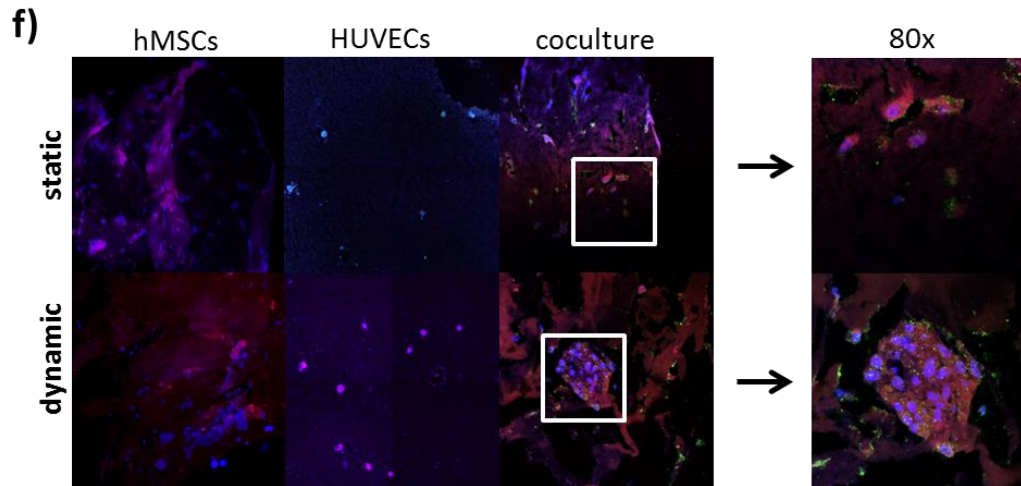
Figure 7.3 Effect of Dynamic Culture on hMSCs and HUVEC coculture. A) Experimental setup of cell encapsulation groups: hMSCs in collagen, HUVECs in collagen, or hMSCs and HUVECs in collagen. Cell-seeded scaffolds were cultured in static well plates or in the TPS bioreactor under dynamic flow conditions. B) E) Fluorescence viability images of hMSCs labeled with live (green) and dead (red) stain on 3D collagen scaffolds after 1, 3, or 7 days of static or dynamic culture. Scale bar represents 100 μm. C) Gene expression of ALP and BMP-2 in hMSCs monocultured in static (solid bars) or dynamic (striped bars). Overall, dynamic coculture resulted in the highest expression of ALP and BMP-2 expression by day 7. D) Gene expression of PECAM and VEGF in HUVEC monocultured in static (solid bars) or dynamic (striped bars). Overall, dynamic coculture resulted in the highest expression of PECAM and VEGF expression by day 7. E) Gene expression of ALP, BMP-2, PECAM, and VEGF in hMSC and HUVEC cocultured in static (solid bars) or dynamic (striped bars). Overall, the synergistic effect of coculture and dynamic coculture resulted in the highest expression of all four markers by day 7. The symbol '*' indicates statistical significance within groups at a timepoint ($p<0.05$). F) Immunofluorescence staining of hMSCs, HUVECs, and coculture in static and dynamic. hMSCs were stained for BMP-2 (pink/red), counterstained with DAPI (blue). HUVECs were stained for CD31 (green), VEGF (red), and counterstained with DAPI (blue). Cocultured samples were stained for BMP-2 (pink/red), CD31 (green), and counterstained with DAPI (blue). Images were taken at 40x with an additional 2x zoom (right panel).

7.4 Discussion

Alginate and collagen are natural polymers that have been shown to be biodegradable, non-toxic, and maintain viability of encapsulated cells. Although alginate has many favorable properties for tissue engineering applications, it lacks specific interaction with cells. Binding sites like Arg-Gly-Asp (RGD) sequences are preserved in collagen fibrils, allowing cells to interact and adhere to the hydrogel.

Using these alginate scaffolds, we have shown successful differentiation of hMSCs into osteoblasts, in both static and dynamic culture conditions. However, in order to progress towards a prevascularized bone construct, we coculture the two main cell types involved in this process: osteogenic differentiating hMSCs and HUVECs. Type I collagen being the most abundant extracellular protein surrounding endothelial cells, we encapsulated HUVECs in collagen hydrogels. Together with alginate-encapsulated hMSCs, they were cultured in either static or dynamic conditions. The objective behind this coculture system was to provide an environment where cytokines and growth factors could be exchanged between HUVECs and hMSCs, similar to *in vivo* environments, where cells may be in proximity but not in cell-to-cell contact. After 14 days of coculture, both cell types showed little response towards osteogenesis or angiogenesis when cultured in static conditions. However, dynamic coculture resulted in enhanced BMP-2 gene production in hMSCs and increased VEGF gene production in HUVECs. More notably was the morphological change of the hMSCs after 14 days of coculture. Cells started to extend outward, which may exhibit behavior of pericytes that support endothelial cells during angiogenesis. The role of MSCs as pericytes has been widely discussed in the field of

tissue engineering, with evidence showing that MSCs can transform to take on the role of support cells when cultured in proximity of endothelial cells [129,307]. This idea would indicate a cytokine or growth factor communication between the cocultured cells, to which the hMSCs can interpret and migrate to in response.

In order to further investigate this idea of HUVEC and hMSCs migration during coculture, we decided to encapsulate the cells in the same natural polymer hydrogel scaffold. Collagen, being an abundant protein also found in bone, we chose it as a coculture cell carrier. However, first, the effect of natural binding sequences in alginate and collagen hydrogels on HUVEC and hMSC seeding was examined. The natural higher content of RGD-like binding sites on collagen allowed hMSCs and HUVECs to more readily bind to the surface, as observed in the adhesion assay fluorescence images (Figure 1b). Both cell types not only adhered but showed early signs of spreading. Although the cells were more confluent and spread on TCPS, with additional time, we believe the cells on collagen could reach similar confluency and adhesion. The quantitative fluorescence measurement of cell adhesion (Figure 1b) also indicated statistically greater numbers of HUVECs and MSCs on collagen compared to alginate. Greater RFUs were detected in hMSCs seeded on collagen than in TCPS, contradicting the fluorescence images. However, this can be explained by the seeding and attachment of hMSCs on the outer ring of the TCPS well, rather than forming a homogenous monolayer on the entire surface. This adhesion pattern resulted in lower RFUs detected during the microplate spectrophotometry.

We have demonstrated successful hMSC differentiation potential in alginate scaffolds, and wanted to confirm similar outcomes in collagen scaffolds. When 2D

111

differentiation on TCPS was used as a control, hMSCs expressed significantly greater amounts of OCN and BMP-2 throughout the 14-day study (Figure 2g-h). We attribute these significant increases not only do the 3D environment, which mimics the cells' natural environment, but believe the additional biological cues received from collagen are able to enhance the osteogenic differentiation process.

Next, we proceeded to evaluate the effects of coculture on hMSC osteogenic differentiation and HUVEC angiogenic vascular network formation. Cells were either mono- or cocultured in static or dynamic conditions. Under static conditions, cells were placed into 6 well plates and provided similar amounts of media as in the TPS bioreactor for dynamic culture, ensuring similar cytokine and endogenous growth factor concentrations. Fluorescence microscopy images showed elongation and spreading of hMSC morphology, which was not visible in the HUVEC population (Figure 2b). As others have noted, depending on the encapsulated cell type, hydrogels like collagen will greatly contract and shrink as cells inherently pull on the scaffold during adhesion and spreading. This was clearly visible in the hMSC and coculture-encapsulating collagen gels, which were half the size as the HUVEC collagen scaffolds by day 3. Interestingly, the aggregates of cells seen in the coculture group (Figure 3d, white arrows) may indicate preferences for the cells to remain in clusters in order to remodel their surrounding extracellular matrix.

Gene expression results of the study showed clear benefits of coculture in dynamic environments for the purpose of osteogenic differentiation in hMSCs and HUVEC angiogenesis compared to static and/or monocultures. With the exception of ALP expression by day 7, which remained similar compared to hMSC monoculture

ALP expression, all other genes showed multiple fold increases over their monoculture counterparts. For example, we observed an 18.2 versus 10.8-fold change of BMP-2 expression in dynamic culture on day 7 compared to day 1. Angiogenic markers PECAM and VEGF also showed enhanced expression in coculture groups, reaching 6-fold and 10-fold increases, respectively.

7.5 Conclusion

This series of experiments indicated that coculture parameters for hMSCs and HUVECs are extremely important in providing the appropriate environment to push the cells towards osteogenesis and angiogenesis, respectively. The culture distance between the two cell types has proven to be crucial in enhancing these processes. In particular, cell-to-cell contact in the collagen hydrogel scaffold demonstrated the greatest benefit to hMSCs and HUVECs, compared to when they were cocultured in separate scaffolds. Additionally, while we have previously showed enhancement of osteogenesis in hMSCs under dynamic flow, the improvements in HUVEC expression of angiogenic markers in both mono- and coculture environments indicates further benefit of the TPS bioreactor for the application of prevascularized bone.

Chapter 8: Summary and Future Directions

8.1 Summary

The overall goal of this work was to develop a method to prevascularize tissue engineered bone construct for the application of high volume bone defects via the coculture of hMSCs and HUVECs in the TPS bioreactor. This goal was achieved through several steps that allowed for understanding of the cell function, environmental stimuli, cell-cell interactions during osteogenesis and angiogenesis, as well as the impact of dynamic culture on individual or combined cell culture.

The first objective of this work was to capitalize on the benefits of the PS bioreactor and further augment cell function during dynamic culture. We utilized growth factor loaded microparticles as a delivery system to alginate-encapsulated hMSCs. With the aid of collaborators, we fabricated BMP-2 and VEGF loaded PLGA microparticles that provided sustained release of important osteogenic growth factors to our cells while cultured in static and dynamic conditions. We found that there was a synergistic link between growth factor delivery and shear flow on osteogenic differentiation of hMSCs. This unique method of fabricating PLGA microparticles allows for high encapsulation efficiency of growth factors while proving to be non-cytotoxic to cells and delivering sustained and bioactive cytokines.

The second objective was to characterize the TPS bioreactor to better understand the mechanism behind its ability to enhance osteogenic differentiation of hMSCs. While the shear stress applied by the dynamic culture has been previously described by our lab, this study indicated that the local effect it has on cells within the axial growth chamber was not uniform. When dividing the tubular growth chamber

114

into 'inlet' and 'outlet' sections, we discovered through computational modeling that while shear stress on the surface of hMSCs-encapsulated alginate beads was constant, the direction of flow resulted in enhanced osteogenic marker expression in cells cultured at the outlet. This phenomenon was eliminated when the direction of the flow was alternated every day for 7 days. Additionally, we could enhance the differentiation of hMSCs in both experimental groups through the delivery of BMP-2 growth factor to the system. These results suggest that the flow of the TPS bioreactor is responsible for the delivery of growth factors and cytokines from cells at the inlet and carries them downstream to cells at the outlet, where they can be used to improve cell function. We believe that this aspect of control in the TPS bioreactor allows for the culture of interdependent, yet distinct cell populations.

The third objective of this work was to scale-up the TPS bioreactor for the fabrication of a patient-specific, high-volume tissue engineered bone construct to regenerative critical sized defects. Previous work from our lab has demonstrated the capabilities of the TPS bioreactor to improve osteogenic differentiation of cells encapsulated in alginate scaffolds. However, in order to provide a clinically relevant sized construct, the system has to be greatly expanded. In this study, we demonstrated successful scale-up of the TPS bioreactor system for an adult femur sized and shaped construct, ranging from flow rate to growth chamber to cell capacity. The results indicated that cells not only remained viable in this setup, proving sufficient oxygen and nutrient supply, but that osteogenic differentiation occurred over the 8 day culture period through the application of shear stress. We see this as a major step towards creating a patient-specific, tissue engineered bone construct of relevant size that will

fill a void in the regenerative medicine field where large tissue replacements are greatly needed.

The fourth objective focused on developing a coculture method for hMSCs and HUVECs such that they could undergo osteogenesis and angiogenesis, respectively. To investigate this objective, we first looked at the coculture of the two cell types in separate scaffolds, alginate and collagen. We showed that there was little effect when cultured separately, indicating a need for closer proximity of the cells, like cell-cell contact, in order to provide enhanced osteo- and angiogenesis. Next, we tested the effect of dynamic culture on a coculture of hMSCs and HUVECs in collagen scaffolds. Similarly, these results suggested that a coculture can enhance cell functions compared to monoculture, and that dynamic culture augments this process even more. Taken together, we demonstrate the synergistic effects of coculture in a dynamic environment for the application of osteogenesis and angiogenesis in hMSCs and HUVECs, respectively.

In conclusion, these studies have demonstrated the advantages of the TPS bioreactor for bone tissue engineering as well as prevascularization of bone constructs. Specifically, we have further characterized the system, utilized it for a scaled-up setup, as well as combined two distinct cell populations for the application for vascularized bone. Taken together, the knowledge of the relationship between endothelial cells and mesenchymal stem cells with the capabilities of the TPS bioreactor can be leveraged to fabricate a single, high-volume tissue construct that is prevascularized and patient specific.

8.2 Future Directions

In this work, we focused on the characterization and scale-up of the TPS bioreactor for the purpose of fabricating a prevascularized tissue engineered bone construct. Each of the 4 objectives contributes to our understanding of the cells' interaction with other cells, with the scaffold, and with the dynamic culture system as a whole. With this knowledge, we have made major strides towards fabricating high-volume tissue engineering construct. Described below are several steps that may bring this concept closer to a clinical reality.

In chapter 4, we discovered the synergistic effects of growth factors like BMP-2 and VEGF with dynamic culture on osteogenic differentiation of hMSCs. In addition to evaluating the beneficial effects of sustained growth factor release on MSCs, a similar effect may be seen in HUVECs. Therefore, further studies on specific growth factors, such as VEGF or platelet-derived growth factor (PDGF), in dynamic culture and their role in vascularization would greatly advance the efforts in establishing a prevascularized network for a variety of engineered tissues.

Furthermore, the results of objective 1 (Chapter 5) demonstrated the unique growth chamber environment that is created in our uniaxial TPS bioreactor. The varying growth factor and cytokine distribution observed in the TPS bioreactor growth chamber could be further explored through direct measurement of endogenous cytokine expression by hMSCs. Additionally, this bimodal system could be used to coculture hMSCs and HUVECs to better understand their paracrine signaling mechanisms that we see in our current coculture experiments. Lastly, by investigating the intricate mechanisms of the TPS bioreactor, we are able to expand the utility of

our system to other tissue engineering applications like the coculture of the three

zonal chondrocyte types for the regeneration of cartilage.

Our findings for objective 3 (Chapter 6) describe the scalability of the TPS

bioreactor for clinically relevant defects that cannot be healed by the host itself and

require a regenerative therapy alternative. This is the first time a bone tissue

engineering construct of that magnitude and size has been fabricated. The results of

this objective indicated sufficient oxygen supply along the entire construct through

high viability and cell function. Therefore, with the functionality of a perfusion

bioreactor that can culture a wide range of sizes, additional studies on the long-term

effects of high-volume cultures would open up the field to more clinically relevant

therapies. Additionally, the 3D printing technology gives way to patient-specific

constructs that can be custom made and fitted, allowing for specific and highly

detailed grafts.

The last objective (Chapter 7) addresses a major hindrance in the field of

tissue engineering. The lack of vasculature prevents not only bone grafts, but almost

all other large tissue engineered organs from successful patient implantation.

Therefore, it is vital to overcome this barrier to bring the field of tissue engineering

closer to a clinical application. The coculture system described in this work suggests

the importance of cell-to-cell contact and physical stimulation in order to enhance the

paired environment. Further studies to investigate the exact mechanism by which the

cells communicate and function in synchronization will allow for a more cohesive

graft fabrication. Additionally, the efficiency of the graft's integration into the host

through anastomosis site would be best tested with an animal model and critical sized

defect. Such study would demonstrate the importance of a prevascularized system and

establish the feasibility of a high-volume engineered bone construct.

Bibliography

1. Medtech Insight. U.S. Markets for Orthopedic Biologic and Tissue Engineered Products [Internet]. p. 116.

2. Fiedler T, Belova I V, Murch GE, Poologasundarampillai G, Jones JR, Roether JA, Boccaccini AR. A comparative study of oxygen diffusion in tissue engineering scaffolds. J. Mater. Sci. Mater. Med. [Internet]. **25**(11), 2573, 2014;

3. Aguirre a, Planell J a, Engel E. Dynamics of bone marrow-derived endothelial progenitor cell/mesenchymal stem cell interaction in co-culture and its implications in angiogenesis. Biochem. Biophys. Res. Commun. Elsevier Inc.; **400**(2), 284, 2010;

4. Pill K, Hofmann S, Redl H, Holnthoner W. Vascularization mediated by mesenchymal stem cells from bone marrow and adipose tissue: a comparison. Cell Regen. (London, England) [Internet]. BioMed Central Ltd; **4**(1), 8, 2015;

5. Bramfeldt H, Sabra G, Centis V, Vermette P. Scaffold vascularization: a challenge for three-dimensional tissue engineering. Curr. Med. Chem. [Internet]. **17**(33), 3944, 2010;

6. Bose S, Roy M, Bandyopadhyay A. Recent advances in bone tissue engineering scaffolds. Trends Biotechnol. [Internet]. **30**(10), 546, 2012;

7. Nerem RM. Tissue engineering: the hope, the hype, and the future. Tissue Eng. [Internet]. Mary Ann Liebert, Inc. 2 Madison Avenue Larchmont, NY 10538 USA; **12**(5), 1143, 2006;

8. Jaklenec A, Stamp A, Deweerd E, Sherwin A, Langer R. Progress in the tissue engineering and stem cell industry "are we there yet?". Tissue Eng. Part B. Rev. [Internet]. Mary Ann Liebert, Inc. 140 Huguenot Street, 3rd Floor New Rochelle, NY 10801 USA; **18**(3), 155, 2012;

9. Phelps EA, García AJ. Engineering more than a cell: vascularization strategies in tissue engineering. Curr. Opin. Biotechnol. [Internet]. **21**(5), 704, 2010;

10. Jain RK, Au P, Tam J, Duda DG, Fukumura D. Engineering vascularized tissue. Nat. Biotechnol. [Internet]. **23**(7), 821, 2005;

11. Lovett M, Lee K, Edwards A, Kaplan DL. Vascularization strategies for tissue engineering. Tissue Eng. Part B. Rev. [Internet]. Mary Ann Liebert, Inc. 140 Huguenot Street, 3rd Floor New Rochelle, NY 10801 USA; **15**(3), 353, 2009;

12. Nishi M, Matsumoto R, Dong J, Uemura T. Engineered bone tissue associated with vascularization utilizing a rotating wall vessel bioreactor. J. Biomed. Mater. Res. A [Internet]. **101**(2), 421, 2013;

13. Weinand C, Gupta R, Huang AY, Weinberg E, Madisch I, Qudsi RA, Neville CM, Pomerantseva I, Vacanti JP. Comparison of Hydrogels in the In Vivo Formation of Tissue-Engineered Bone Using Mesenchymal Stem Cells and Beta-Tricalcium Phosphate. Mary Ann Liebert, Inc. 140 Huguenot Street, 3rd Floor New Rochelle, NY 10801 USA; 2007;

14. Lanza R, Langer R, Vacanti JP. Principles of Tissue Engineering [Internet]. 3rd ed. Burlington, MA: Elsevier Academic Press; 2007.

15. Goldstein SA. Tissue engineering: functional assessment and clinical outcome. Ann. N. Y. Acad. Sci. [Internet]. **961**, 183, 2002;

16. Liu X, Holzwarth JM, Ma PX. Functionalized synthetic biodegradable polymer scaffolds for tissue engineering. Macromol. Biosci. [Internet]. **12**(7), 911, 2012;

17. Kim B-S, Mooney DJ. Development of biocompatible synthetic extracellular matrices for tissue engineering [Internet]. Trends Biotechnol. p. 224–30, 1998.

18. Abshagen K, Schrodi I, Gerber T, Vollmar B. In vivo analysis of biocompatibility and vascularization of the synthetic bone grafting substitute NanoBone. J. Biomed. Mater. Res. A [Internet]. **91**(2), 557, 2009;

19. Rouwkema J, Rivron NC, van Blitterswijk CA. Vascularization in tissue engineering. Trends Biotechnol. [Internet]. **26**(8), 434, 2008;

20. Correia C, Grayson WL, Park M, Hutton D, Zhou B, Guo XE, Niklason L, Sousa RA, Reis RL, Vunjak-Novakovic G. In vitro model of vascularized bone: synergizing vascular development and osteogenesis. Goncalves R, editor. PLoS One [Internet]. Public Library of Science; **6**(12), e28352, 2011;

21. Steffens L, Wenger A, Stark GB, Finkenzeller G. In vivo engineering of a human vasculature for bone tissue engineering applications. J. Cell. Mol. Med. [Internet]. **13**(9B), 3380, 2009;

22. Hegen A, Blois A, Tiron CE, Hellesøy M, Micklem DR, Nör JE, Akslen LA, Lorens JB. Efficient in vivo vascularization of tissue-engineering scaffolds. J. Tissue Eng. Regen. Med. [Internet]. **5**(4), e52, 2011;

23. Tsigkou O, Pomerantseva I, Spencer JA, Redondo PA, Hart AR, O'Doherty E, Lin Y, Friedrich CC, Daheron L, Lin CP, Sundback CA, Vacanti JP, Neville C.

Engineered vascularized bone grafts. Proc. Natl. Acad. Sci. U. S. A. [Internet]. **107**(8), 3311, 2010;

24. Domev H, Amit M, Laevsky I, Dar A, Itskovitz-Eldor J. Efficient engineering of vascularized ectopic bone from human embryonic stem cell-derived mesenchymal stem cells. Tissue Eng. Part A [Internet]. Mary Ann Liebert, Inc. 140 Huguenot Street, 3rd Floor New Rochelle, NY 10801 USA; **18**(21-22), 2290, 2012;

25. Li Z, Guan J. Hydrogels for cardiac tissue engineering. Polymers (Basel). [Internet]. 2011;

26. Meinel L, Karageorgiou V, Fajardo R, Snyder B, Shinde-Patil V, Zichner L, Kaplan D, Langer R, Vunjak-Novakovic G. Bone Tissue Engineering Using Human Mesenchymal Stem Cells: Effects of Scaffold Material and Medium Flow. Ann. Biomed. Eng. [Internet]. **32**(1), 112, 2004;

27. Marolt D, Campos IM, Bhumiratana S, Koren A, Petridis P, Zhang G, Spitalnik PF, Grayson WL, Vunjak-Novakovic G. Engineering bone tissue from human embryonic stem cells. Proc. Natl. Acad. Sci. U. S. A. [Internet]. **109**(22), 8705, 2012;

28. Laschke MW, Strohe A, Menger MD, Alini M, Eglin D. In vitro and in vivo evaluation of a novel nanosize hydroxyapatite particles/poly(ester-urethane) composite scaffold for bone tissue engineering. Acta Biomater. [Internet]. **6**(6), 2020, 2010;

29. Laschke MW, Strohe A, Scheuer C, Eglin D, Verrier S, Alini M, Pohlemann T, Menger MD. In vivo biocompatibility and vascularization of biodegradable porous polyurethane scaffolds for tissue engineering. Acta Biomater. [Internet]. **5**(6), 1991, 2009;

30. Phelps EA, Landázuri N, Thulé PM, Taylor WR, García AJ. Bioartificial matrices for therapeutic vascularization. Proc. Natl. Acad. Sci. U. S. A. [Internet]. **107**(8), 3323, 2010;

31. Moon JJ, Saik JE, Poché RA, Leslie-Barbick JE, Lee S-H, Smith AA, Dickinson ME, West JL. Biomimetic hydrogels with pro-angiogenic properties. Biomaterials [Internet]. **31**(14), 3840, 2010;

32. Shin M, Yoshimoto H, Vacanti JP. In vivo bone tissue engineering using mesenchymal stem cells on a novel electrospun nanofibrous scaffold. Tissue Eng. [Internet]. Mary Ann Liebert, Inc.; **10**(1-2), 33, 2004;

33. Ghanaati S, Unger RE, Webber MJ, Barbeck M, Orth C, Kirkpatrick JA,

Booms P, Motta A, Migliaresi C, Sader RA, Kirkpatrick CJ. Scaffold vascularization in vivo driven by primary human osteoblasts in concert with host inflammatory cells. Biomaterials [Internet]. **32**(32), 8150, 2011;

34. Hutmacher DW, Sittinger M, Risbud M V. Scaffold-based tissue engineering: rationale for computer-aided design and solid free-form fabrication systems. Trends Biotechnol. [Internet]. **22**(7), 354, 2004;

35. Pittenger MF. Multilineage Potential of Adult Human Mesenchymal Stem Cells. Science (80-.). [Internet]. AMER ASSOC ADVANCEMENT SCIENCE; **284**(5411), 143, 1999;

36. Sittichokechaiwut A, Edwards JH, Scutt AM, Reilly GC. Short Bouts of Mechanical Loading are as Effective as Dexamethasone at Inducing Matrix Production by Human Bone Marrow Mesenchymal Stem Cells. Eur. Cell. Mater. [Internet]. SWISS SOC BIOMATERIALS; **20**, 45, 2010;

37. Zhang Z-Y, Teoh S-H, Chong MSK, Lee ESM, Tan L-G, Mattar CN, Fisk NM, Choolani M, Chan J. Neo-vascularization and bone formation mediated by fetal mesenchymal stem cell tissue-engineered bone grafts in critical-size femoral defects. Biomaterials [Internet]. **31**(4), 608, 2010;

38. Rouwkema J, de Boer J, Van Blitterswijk CA. Endothelial cells assemble into a 3-dimensional prevascular network in a bone tissue engineering construct. Tissue Eng. [Internet]. **12**(9), 2685, 2006;

39. Grellier M, Granja PL, Fricain J-C, Bidarra SJ, Renard M, Bareille R, Bourget C, Amédée J, Barbosa MA. The effect of the co-immobilization of human osteoprogenitors and endothelial cells within alginate microspheres on mineralization in a bone defect. Biomaterials [Internet]. **30**(19), 3271, 2009;

40. De la Riva B, Nowak C, Sánchez E, Hernández A, Schulz-Siegmund M, Pec MK, Delgado A, Evora C. VEGF-controlled release within a bone defect from alginate/chitosan/PLA-H scaffolds. Eur. J. Pharm. Biopharm. [Internet]. **73**(1), 50, 2009;

41. Koyama S, Sato E, Tsukadaira A, Haniuda M, Numanami H, Kurai M, Nagai S, Izumi T. Vascular endothelial growth factor mRNA and protein expression in airway epithelial cell lines in vitro. Eur. Respir. J. Off. J. Eur. Soc. Clin. Respir. Physiol. [Internet]. **20**(6), 1449, 2002;

42. Ribatti D. The crucial role of vascular permeability factor/vascular endothelial growth factor in angiogenesis: a historical review. Br. J. Haematol. [Internet]. **128**(3), 303, 2005;

43. Schechner JS, Nath AK, Zheng L, Kluger MS, Hughes CC, Sierra-Honigmann MR, Lorber MI, Tellides G, Kashgarian M, Bothwell AL, Pober JS. In vivo formation of complex microvessels lined by human endothelial cells in an immunodeficient mouse. Proc. Natl. Acad. Sci. U. S. A. [Internet]. **97**(16), 9191, 2000;

44. Sefcik LS, Petrie Aronin CE, Wieghaus KA, Botchwey EA. Sustained release of sphingosine 1-phosphate for therapeutic arteriogenesis and bone tissue engineering. Biomaterials [Internet]. **29**(19), 2869, 2008;

45. Levenberg S, Golub JS, Amit M, Itskovitz-Eldor J, Langer R. Endothelial cells derived from human embryonic stem cells. Proc. Natl. Acad. Sci. U. S. A. [Internet]. **99**(7), 4391, 2002;

46. Fedorovich NE, Haverslag RT, Dhert WJA, Alblas J. The role of endothelial progenitor cells in prevascularized bone tissue engineering: development of heterogeneous constructs. Tissue Eng. Part A [Internet]. Mary Ann Liebert, Inc. 140 Huguenot Street, 3rd Floor New Rochelle, NY 10801 USA; **16**(7), 2355, 2010;

47. Evensen L, Micklem DR, Blois A, Berge SV, Aarsaether N, Littlewood-Evans A, Wood J, Lorens JB. Mural cell associated VEGF is required for organotypic vessel formation. Cao Y, editor. PLoS One [Internet]. Public Library of Science; **4**(6), e5798, 2009;

48. Dejana E. Endothelial cell-cell junctions: happy together. Nat. Rev. Mol. Cell Biol. [Internet]. **5**(4), 261, 2004;

49. Sikavitsas VI, van den Dolder J, Bancroft GN, Jansen JA, Mikos AG. Influence of the in vitro culture period on the in vivo performance of cell/titanium bone tissue-engineered constructs using a rat cranial critical size defect model. J. Biomed. Mater. Res. A [Internet]. **67**(3), 944, 2003;

50. Chen F, Zhou Y, Barnabas ST, Woodruff MA, Hutmacher DW. Engineering tubular bone constructs. J. Biomech. [Internet]. **40 Suppl 1**(null), S73, 2007;

51. Pirraco RP, Obokata H, Iwata T, Marques AP, Tsuneda S, Yamato M, Reis RL, Okano T. Development of osteogenic cell sheets for bone tissue engineering applications. Tissue Eng. Part A [Internet]. **17**(11-12), 1507, 2011;

52. Wernike E, Montjovent MO, Liu Y. VEGF Incorporated into Calcium Phosphate Ceramics Promotes Vascularisation and Bone Formation In Vivo [Internet]. Eur. Cells Mater. p. 30–40, 2010.

53. Ma J, van den Beucken JJJP, Yang F, Both SK, Cui F-Z, Pan J, Jansen JA.

Coculture of osteoblasts and endothelial cells: optimization of culture medium and cell ratio. Tissue Eng. Part C. Methods [Internet]. Mary Ann Liebert, Inc. 140 Huguenot Street, 3rd Floor New Rochelle, NY 10801 USA; **17**(3), 349, 2011;

54. Kirkpatrick CJ, Fuchs S, Unger RE. Co-culture systems for vascularization--learning from nature. Adv. Drug Deliv. Rev. [Internet]. **63**(4-5), 291, 2011;

55. Yu Y, Mu J, Fan Z, Lei G, Yan M, Wang S, Tang C, Wang Z, Yu J, Zhang G. Insulin-like growth factor 1 enhances the proliferation and osteogenic differentiation of human periodontal ligament stem cells via ERK and JNK MAPK pathways. Histochem. Cell Biol. [Internet]. **137**(4), 513, 2012;

56. Huang Z, Ren P-G, Ma T, Smith RL, Goodman SB. Modulating osteogenesis of mesenchymal stem cells by modifying growth factor availability. Cytokine [Internet]. **51**(3), 305, 2010;

57. Geris L, Vandamme K, Naert I, Vander Sloten J, Van Oosterwyck H, Duyck J. Mechanical loading affects angiogenesis and osteogenesis in an in vivo bone chamber: a modeling study. Tissue Eng. Part A [Internet]. Mary Ann Liebert, Inc. 140 Huguenot Street, 3rd Floor New Rochelle, NY 10801 USA; **16**(11), 3353, 2010;

58. Villars F, Bordenave L, Bareille R, Amédée J. Effect of human endothelial cells on human bone marrow stromal cell phenotype: role of VEGF? J. Cell. Biochem. [Internet]. **79**(4), 672, 2000;

59. Huang Y-C, Kaigler D, Rice KG, Krebsbach PH, Mooney DJ. Combined angiogenic and osteogenic factor delivery enhances bone marrow stromal cell-driven bone regeneration. J. Bone Miner. Res. [Internet]. **20**(5), 848, 2005;

60. Peng H, Usas A, Olshanski A, Ho AM, Gearhart B, Cooper GM, Huard J. VEGF improves, whereas sFlt1 inhibits, BMP2-induced bone formation and bone healing through modulation of angiogenesis. J. Bone Miner. Res. [Internet]. **20**(11), 2017, 2005;

61. Lazarous DF, Shou M, Scheinowitz M, Hodge E, Thirumurti V, Kitsiou AN, Stiber JA, Lobo AD, Hunsberger S, Guetta E, Epstein SE, Unger EF. Comparative Effects of Basic Fibroblast Growth Factor and Vascular Endothelial Growth Factor on Coronary Collateral Development and the Arterial Response to Injury. Circulation [Internet]. **94**(5), 1074, 1996;

62. Yilgor P. Incorporation of sequential BMP-2/BMP-7 delivery system into chitosan-based scaffolds for bone tissue engineering [Internet]. Biomaterials. p.

3551–9, 2009.

63.   Hoeben A, Landuyt B, Highley MS, Wildiers H, Van Oosterom AT, De Bruijn
        EA. Vascular endothelial growth factor and angiogenesis. Pharmacol. Rev.
        [Internet]. **56**(4), 549, 2004;

64.   Ozawa CR, Banfi A, Glazer NL, Thurston G, Springer ML, Kraft PE,
        McDonald DM, Blau HM. Microenvironmental VEGF concentration, not total
        dose, determines a threshold between normal and aberrant angiogenesis. J.
        Clin. Invest. [Internet]. **113**(4), 516, 2004;

65.   Geuze RE, Theyse LFH, Kempen DHR, Hazewinkel HAW, Kraak HYA, Oner
        FC, Dhert WJA, Alblas J. A differential effect of bone morphogenetic protein-
        2 and vascular endothelial growth factor release timing on osteogenesis at
        ectopic and orthotopic sites in a large-animal model. Tissue Eng. Part A
        [Internet]. **18**(19-20), 2052, 2012;

66.   Gibot L, Galbraith T, Huot J, Auger FA. A preexisting microvascular network
        benefits in vivo revascularization of a microvascularized tissue-engineered skin
        substitute. Tissue Eng. Part A [Internet]. Mary Ann Liebert, Inc. 140
        Huguenot Street, 3rd Floor New Rochelle, NY 10801 USA; **16**(10), 3199,
        2010;

67.   Okano T, Yamada N, Sakai H, Sakurai Y. A novel recovery system for
        cultured cells using plasma-treated polystyrene dishes grafted with poly(N-
        isopropylacrylamide). J. Biomed. Mater. Res. [Internet]. JOHN WILEY &
        SONS INC; **27**(10), 1243, 1993;

68.   Chen Y, Zhou N, Huang X. [Cell sheet technology and its application in bone
        tissue engineering]. Zhongguo Xiu Fu Chong Jian Wai Ke Za Zhi [Internet].
        26(9), 1122, 2012;

69.   Shimizu T, Yamato M, Kikuchi A, Okano T. Cell sheet engineering for
        myocardial tissue reconstruction. Biomaterials [Internet]. **24**(13), 2309, 2003;

70.   Nishida K. Corneal Reconstruction with Tissue-Engineered Cell Sheets
        Composed of Autologous Oral Mucosal Epithelium — NEJM [Internet]. N.
        Engl. J. Med. p. 1187–96, 2004.

71.   Kanzaki M, Yamato M, Yang J, Sekine H, Kohno C, Takagi R, Hatakeyama H,
        Isaka T, Okano T, Onuki T. Dynamic sealing of lung air leaks by the
        transplantation of tissue engineered cell sheets. Biomaterials [Internet]. **28**(29),
        4294, 2007;

72.   Ohashi K, Yokoyama T, Yamato M, Kuge H, Kanehiro H, Tsutsumi M,

Amanuma T, Iwata H, Yang J, Okano T, Nakajima Y. Engineering functional two- and three-dimensional liver systems in vivo using hepatic tissue sheets. Nat. Med. [Internet]. Nature Publishing Group; **13**(7), 880, 2007;

73.   Dong Q, Shang H, Wu W, Chen F, Zhang J, Guo J, Mao T. Prefabrication of axial vascularized tissue engineering coral bone by an arteriovenous loop: A better model. Mater. Sci. Eng. C [Internet]. **32**(6), 1536, 2012;

74.   Song SJ, Jeon O, Yang HS, Han DK, Kim B-S. Effects of culture conditions on osteogenic differentiation in human mesenchymal stem cells. J. Microbiol. Biotechnol. [Internet]. **17**(7), 1113, 2007;

75.   Lehr HA, Leunig M, Menger MD, Nolte D, Messmer K. Dorsal skinfold chamber technique for intravital microscopy in nude mice. Am. J. Pathol. [Internet]. **143**(4), 1055, 1993;

76.   Laschke MW, Harder Y, Amon M, Martin I, Farhadi J, Ring A, Torio-Padron N, Schramm R, Rücker M, Junker D, Häufel JM, Carvalho C, Heberer M, Germann G, Vollmar B, Menger MD. Angiogenesis in tissue engineering: breathing life into constructed tissue substitutes. Tissue Eng. [Internet]. **12**(8), 2093, 2006;

77.   Druecke D, Langer S, Lamme E, Pieper J, Ugarkovic M, Steinau HU, Homann HH. Neovascularization of poly(ether ester) block-copolymer scaffolds in vivo: long-term investigations using intravital fluorescent microscopy. J. Biomed. Mater. Res. A [Internet]. **68**(1), 10, 2004;

78.   Kneser U, Polykandriotis E, Ohnolz J, Heidner K, Grabinger L, Euler S, Amann KU, Hess A, Brune K, Greil P, Stürzl M, Horch RE. Engineering of vascularized transplantable bone tissues: induction of axial vascularization in an osteoconductive matrix using an arteriovenous loop. Tissue Eng. [Internet]. Mary Ann Liebert, Inc. 2 Madison Avenue Larchmont, NY 10538 USA; **12**(7), 1721, 2006;

79.   Baiguera S, Macchiarini P, Ribatti D. Chorioallantoic membrane for in vivo investigation of tissue-engineered construct biocompatibility. J. Biomed. Mater. Res. B. Appl. Biomater. [Internet]. **100**(5), 1425, 2012;

80.   Buschmann J, Härter L, Gao S, Hemmi S, Welti M, Hild N, Schneider OD, Stark WJ, Lindenblatt N, Werner CML, Wanner GA, Calcagni M. Tissue engineered bone grafts based on biomimetic nanocomposite PLGA/amorphous calcium phosphate scaffold and human adipose-derived stem cells. Injury [Internet]. **43**(10), 1689, 2012;

81. Ilmer M, Karow M, Geissler C, Jochum M, Neth P. Human osteoblast-derived factors induce early osteogenic markers in human mesenchymal stem cells. Tissue Eng. Part A [Internet]. **15**(9), 2397, 2009;

82. Pusztaszeri MP, Seelentag W, Bosman FT. Immunohistochemical expression of endothelial markers CD31, CD34, von Willebrand factor, and Fli-1 in normal human tissues. J. Histochem. Cytochem. [Internet]. SAGE Publications; **54**(4), 385, 2006;

83. Wallez Y, Huber P. Endothelial adherens and tight junctions in vascular homeostasis, inflammation and angiogenesis. Biochim. Biophys. Acta [Internet]. **1778**(3), 794, 2008;

84. Roche B, David V, Vanden-Bossche A, Peyrin F, Malaval L, Vico L, Lafage-Proust M-H. Structure and quantification of microvascularisation within mouse long bones: what and how should we measure? Bone [Internet]. **50**(1), 390, 2012;

85. Fei J, Jia F, Peyrin F, Françoise P, Malaval L, Vico L, Laurence V, Lafage-Proust M-H, Marie-Hélène L-P. Imaging and quantitative assessment of long bone vascularization in the adult rat using microcomputed tomography. Anat. Rec. (Hoboken). [Internet]. **293**(2), 215, 2010;

86. Tang Y, Tang W, Lin Y, Long J, Wang H, Liu L, Tian W. Combination of bone tissue engineering and BMP-2 gene transfection promotes bone healing in osteoporotic rats. Cell Biol. Int. [Internet]. **32**(9), 1150, 2008;

87. Johnson PC, Mikos AG, Fisher JP, Jansen JA. Strategic directions in tissue engineering. Tissue Eng. **13**(12), 2827, 2007;

88. Ding D-C, Shyu W-C, Lin S-Z. Mesenchymal stem cells. Cell Transplant. [Internet]. **20**(1), 5, 2011;

89. Bianco P, Riminucci M, Gronthos S, Robey PG. Bone marrow stromal stem cells: nature, biology, and potential applications. Stem Cells [Internet]. **19**(3), 180, 2001;

90. Caplan AI. Adult mesenchymal stem cells for tissue engineering versus regenerative medicine. J. Cell. Physiol. [Internet]. **213**(2), 341, 2007;

91. Chamberlain G, Fox J, Ashton B, Middleton J. Concise review: mesenchymal stem cells: their phenotype, differentiation capacity, immunological features, and potential for homing. Stem Cells [Internet]. **25**(11), 2739, 2007;

92. Cines DB, Pollak ES, Buck CA, Loscalzo J, Zimmerman GA, McEver RP,

Pober JS, Wick TM, Konkle BA, Schwartz BS, Barnathan ES, McCrae KR, Hug BA, Schmidt AM, Stern DM. Endothelial cells in physiology and in the pathophysiology of vascular disorders. Blood. Am Soc Hematology; **91**(10), 3527, 1998;

93. Sumpio BE, Riley JT, Dardik A. Cells in focus: endothelial cell. Int. J. Biochem. cell Biol. **34**(12), 1508, 2002;

94. Lamalice L, Le Boeuf F, Huot J. Endothelial cell migration during angiogenesis. Circ. Res. **100**(6), 782, 2007;

95. Hirschi KK, Ingram D a, Yoder MC. Assessing identity, phenotype, and fate of endothelial progenitor cells. Arterioscler. Thromb. Vasc. Biol. **28**(9), 1584, 2008;

96. Pearson JD. Endothelial progenitor cells - hype or hope? J. Thromb. Haemost. Blackwell Publishing; **7**(2), 255, 2009;

97. Yoder MC. Human endothelial progenitor cells. Cold Spring Harb. Perspect. Med. **2**(7), a006692, 2012;

98. Ribatti D, Nico B, Crivellato E. The role of pericytes in angiogenesis. Int. J. Dev. Biol. **55**(3), 261, 2011;

99. Armulik A, Genové G, Betsholtz C. Pericytes: developmental, physiological, and pathological perspectives, problems, and promises. Dev. Cell. **21**(2), 193, 2011;

100. Dar A, Itskovitz-Eldor J. Therapeutic potential of perivascular cells from human pluripotent stem cells. J. Tissue Eng. Regen. Med. 2013.

101. Mohyeldin A, Garzón-Muvdi T, Quiñones-Hinojosa A. Oxygen in stem cell biology: a critical component of the stem cell niche. Cell Stem Cell [Internet]. **7**(2), 150, 2010;

102. Grayson WL, Zhao F, Izadpanah R, Bunnell B, Ma T. Effects of hypoxia on human mesenchymal stem cell expansion and plasticity in 3D constructs. J. Cell. Physiol. [Internet]. **207**(2), 331, 2006;

103. Fehrer C, Brunauer R, Laschober G, Unterluggauer H, Reitinger S, Kloss F, Gülly C, Gassner R, Lepperdinger G. Reduced oxygen tension attenuates differentiation capacity of human mesenchymal stem cells and prolongs their lifespan. Aging Cell. **6**(6), 745, 2007;

104. Hirota K, Semenza GL. Regulation of angiogenesis by hypoxia-inducible factor 1. Crit. Rev. Oncol. Hematol. [Internet]. **59**(1), 15, 2006;

105. Das R, Jahr H, van Osch GJVM, Farrell E. The role of hypoxia in bone marrow-derived mesenchymal stem cells: considerations for regenerative medicine approaches. Tissue Eng. Part B. Rev. [Internet]. Mary Ann Liebert, Inc. 140 Huguenot Street, 3rd Floor New Rochelle, NY 10801 USA; **16**(2), 159, 2010;

106. Carmeliet P, Dor Y, Herbert JM, Fukumura D, Brusselmans K, Dewerchin M, Neeman M, Bono F, Abramovitch R, Maxwell P, Koch CJ, Ratcliffe P, Moons L, Jain RK, Collen D, Keshert E, Keshet E. Role of HIF-1alpha in hypoxia-mediated apoptosis, cell proliferation and tumour angiogenesis. Nature [Internet]. **394**(6692), 485, 1998;

107. Shi S, Gronthos S. Perivascular niche of postnatal mesenchymal stem cells in human bone marrow and dental pulp. J. Bone Miner. Res. [Internet]. **18**(4), 696, 2003;

108. Crisan M, Yap S, Casteilla L, Chen C-W, Corselli M, Park TS, Andriolo G, Sun B, Zheng B, Zhang L, Norotte C, Teng P-N, Traas J, Schugar R, Deasy BM, Badylak S, Buhring H-J, Giacobino J-P, Lazzari L, Huard J, Péault B. A perivascular origin for mesenchymal stem cells in multiple human organs. Cell Stem Cell [Internet]. **3**(3), 301, 2008;

109. Potier E, Ferreira E, Andriamanalijaona R, Pujol J-P, Oudina K, Logeart-Avramoglou D, Petite H. Hypoxia affects mesenchymal stromal cell osteogenic differentiation and angiogenic factor expression. Bone [Internet]. **40**(4), 1078, 2007;

110. Wagegg M, Gaber T, Lohanatha FL, Hahne M, Strehl C, Fangradt M, Tran CL, Schönbeck K, Hoff P, Ode A, Perka C, Duda GN, Buttgereit F. Hypoxia promotes osteogenesis but suppresses adipogenesis of human mesenchymal stromal cells in a hypoxia-inducible factor-1 dependent manner. Covas DT, editor. PLoS One [Internet]. Public Library of Science; **7**(9), e46483, 2012;

111. Zwezdaryk KJ, Coffelt SB, Figueroa YG, Liu J, Phinney DG, LaMarca HL, Florez L, Morris CB, Hoyle GW, Scandurro AB. Erythropoietin, a hypoxia-regulated factor, elicits a pro-angiogenic program in human mesenchymal stem cells. Exp. Hematol. [Internet]. **35**(4), 640, 2007;

112. Rochefort GY, Delorme B, Lopez A, Hérault O, Bonnet P, Charbord P, Eder V, Domenech J. Multipotential mesenchymal stem cells are mobilized into peripheral blood by hypoxia. Stem Cells [Internet]. **24**(10), 2202, 2006;

113. Rosová I, Dao M, Capoccia B, Link D, Nolta JA. Hypoxic preconditioning

results in increased motility and improved therapeutic potential of human mesenchymal stem cells. Stem Cells [Internet]. **26**(8), 2173, 2008;

114. Eliasson P, Jönsson J-I. The hematopoietic stem cell niche: low in oxygen but a nice place to be. J. Cell. Physiol. [Internet]. **222**(1), 17, 2010;

115. Valorani MG, Montelatici E, Germani A, Biddle A, D'Alessandro D, Strollo R, Patrizi MP, Lazzari L, Nye E, Otto WR, Pozzilli P, Alison MR. Pre-culturing human adipose tissue mesenchymal stem cells under hypoxia increases their adipogenic and osteogenic differentiation potentials. Cell Prolif. [Internet]. **45**(3), 225, 2012;

116. Ma T, Grayson WL, Fröhlich M, Vunjak-Novakovic G. Hypoxia and stem cell-based engineering of mesenchymal tissues. Biotechnol. Prog. [Internet]. **25**(1), 32.

117. Yamamoto K, Takahashi T, Asahara T, Ohura N, Sokabe T, Kamiya A, Ando J. Proliferation, differentiation, and tube formation by endothelial progenitor cells in response to shear stress. J. Appl. Physiol. [Internet]. **95**(5), 2081, 2003;

118. Yamamoto K, Sokabe T, Watabe T, Miyazono K, Yamashita JK, Obi S, Ohura N, Matsushita A, Kamiya A, Ando J. Fluid shear stress induces differentiation of Flk-1-positive embryonic stem cells into vascular endothelial cells in vitro. Am. J. Physiol. Heart Circ. Physiol. [Internet]. **288**(4), H1915, 2005;

119. Zhang P, Baxter J, Vinod K, Tulenko TN, Di Muzio PJ. Endothelial differentiation of amniotic fluid-derived stem cells: synergism of biochemical and shear force stimuli. Stem Cells Dev. [Internet]. Mary Ann Liebert, Inc. publishers 140 Huguenot Street, 3rd Floor New Rochelle, NY 10801-5215 USA; **18**(9), 1299, 2009;

120. Huang NF, Li S. Mesenchymal stem cells for vascular regeneration. Regen. Med. [Internet]. **3**(6), 877, 2008;

121. Glen K, Luu NT, Ross E, Buckley CD, Rainger GE, Egginton S, Nash GB. Modulation of functional responses of endothelial cells linked to angiogenesis and inflammation by shear stress: differential effects of the mechanotransducer CD31. J. Cell. Physiol. [Internet]. **227**(6), 2710, 2012;

122. Gee E, Milkiewicz M, Haas TL. p38 MAPK activity is stimulated by vascular endothelial growth factor receptor 2 activation and is essential for shear stress-induced angiogenesis. J. Cell. Physiol. [Internet]. **222**(1), 120, 2010;

123. Titushkin I, Cho M. Modulation of cellular mechanics during osteogenic differentiation of human mesenchymal stem cells. Biophys. J. [Internet].

93(10), 3693, 2007;

124. Zeng L, Xiao Q, Margariti A, Zhang Z, Zampetaki A, Patel S, Capogrossi MC, Hu Y, Xu Q. HDAC3 is crucial in shear- and VEGF-induced stem cell differentiation toward endothelial cells. J. Cell Biol. [Internet]. **174**(7), 1059, 2006;

125. Nasseri BA, Pomerantseva I, Kaazempur-Mofrad MR, Sutherland FWH, Perry T, Ochoa E, Thompson CA, Mayer JE, Oesterle SN, Vacanti JP. Dynamic rotational seeding and cell culture system for vascular tube formation. Tissue Eng. [Internet]. Mary Ann Liebert, Inc.; **9**(2), 291, 2003;

126. Bidarra SJ, Barrias CC, Barbosa MA, Soares R, Granja PL. Immobilization of human mesenchymal stem cells within RGD-grafted alginate microspheres and assessment of their angiogenic potential. Biomacromolecules [Internet]. American Chemical Society; **11**(8), 1956, 2010;

127. Pittenger MF, Mosca JD, McIntosh KR. Human mesenchymal stem cells: progenitor cells for cartilage, bone, fat and stroma. Curr. Top. Microbiol. Immunol. [Internet]. **251**, 3, 2000;

128. Zhang T, Lee YW, Rui YF, Cheng TY, Jiang XH, Li G. Bone marrow-derived mesenchymal stem cells promote growth and angiogenesis of breast and prostate tumors. Stem Cell Res. Ther. [Internet]. **4**(3), 70, 2013;

129. McFadden TM, Duffy GP, Allen AB, Stevens HY, Schwarzmaier SM, Plesnila N, Murphy MJ, Barry FP, Guldberg RE, O'Brien FJ. The delayed addition of human MSCs to pre-formed endothelial cell networks results in functional vascularisation of a collagen-GAG scaffold in vivo. Acta Biomater. [Internet]. **null**(null), 2013;

130. Au P, Tam J, Fukumura D, Jain RK. Bone marrow-derived mesenchymal stem cells facilitate engineering of long-lasting functional vasculature. Blood [Internet]. **111**(9), 4551, 2008;

131. Chen L, Tredget EE, Wu PYG, Wu Y. Paracrine factors of mesenchymal stem cells recruit macrophages and endothelial lineage cells and enhance wound healing. Bozza P, editor. PLoS One [Internet]. Public Library of Science; **3**(4), e1886, 2008;

132. Sasaki M, Abe R, Fujita Y, Ando S, Inokuma D, Shimizu H. Mesenchymal stem cells are recruited into wounded skin and contribute to wound repair by transdifferentiation into multiple skin cell type. J. Immunol. [Internet]. American Association of Immunologists; **180**(4), 2581, 2008;

133. Rüster B, Göttig S, Ludwig RJ, Bistrian R, Müller S, Seifried E, Gille J, Henschler R. Mesenchymal stem cells display coordinated rolling and adhesion behavior on endothelial cells. Blood [Internet]. **108**(12), 3938, 2006;

134. Hill JM, Zalos G, Halcox JPJ, Schenke WH, Waclawiw MA, Quyyumi AA, Finkel T. Circulating endothelial progenitor cells, vascular function, and cardiovascular risk. N. Engl. J. Med. **348**(7), 593, 2003;

135. Balbarini A, Barsotti MC, Stefano R Di, Leone A, Santoni T. Circulating Endothelial Progenitor Cells Characterization, Function and Relationship with Cardiovascular Risk Factors. Curr. Pharm. Desing. **13**, 1699, 2007;

136. Kolbe M, Xiang Z, Dohle E, Sc M, Tonak M, Kirkpatrick CJ, Ph D, Fuchs S. Paracrine Effects Influenced by Cell Culture Medium and Consequences on Microvessel-Like Structures in Cocultures of Mesenchymal Stem Cells and Outgrowth Endothelial Cells. Tissue Eng Part A. **17**(17-18), 2199, 2011;

137. Seebach C, Henrich D, Wilhelm K, Barker JH, Marzi I. Endothelial progenitor cells improve directly and indirectly early vascularization of mesenchymal stem cell-driven bone regeneration in a critical bone defect in rats. Cell Transplant. **21**(8), 1667, 2012;

138. Zigdon-Giladi H, Bick T, Lewinson D, Machtei EE. Co-Transplantation of Endothelial Progenitor Cells and Mesenchymal Stem Cells Promote Neovascularization and Bone Regeneration. Clin. Implant Dent. Relat. Res. 1, 2013;

139. Amini AR, Laurencin CT, Nukavarapu SP. Differential analysis of peripheral blood- and bone marrow-derived endothelial progenitor cells for enhanced vascularization in bone tissue engineering. J. Orthop. Res. **30**(9), 1507, 2012;

140. Rahbarghazi R, Nassiri SM, Khazraiinia P, Kajbafzadeh A-M, Ahmadi SH, Mohammadi E, Molazem M, Zamani-Ahmadmahmudi M. Juxtacrine and paracrine interactions of rat marrow-derived mesenchymal stem cells, muscle-derived satellite cells, and neonatal cardiomyocytes with endothelial cells in angiogenesis dynamics. Stem Cells Dev. **22**(6), 855, 2013;

141. Dejana E, Tournier-Lasserve E, Weinstein BM. The control of vascular integrity by endothelial cell junctions: molecular basis and pathological implications. Dev. Cell. Elsevier Inc.; **16**(2), 209, 2009;

142. Thomas M, Augustin HG. The role of the Angiopoietins in vascular morphogenesis. Angiogenesis. Elsevier Ltd; **12**(2), 125, 2009;

143. Cao Y. Positive and negative modulation of angiogenesis by VEGFR1 ligands.

Sci. Signal. **2**(59), re1, 2009;

144. Raida M, Heymann a C, Günther C, Niederwieser D. Role of bone morphogenetic protein 2 in the crosstalk between endothelial progenitor cells and mesenchymal stem cells. Int. J. Mol. Med. **18**(4), 735, 2006;

145. Iwasaki H, Kawamoto A, Tjwa M, Horii M, Hayashi S, Oyamada A, Matsumoto T, Suehiro S, Carmeliet P, Asahara T. PlGF repairs myocardial ischemia through mechanisms of angiogenesis, cardioprotection and recruitment of myo-angiogenic competent marrow progenitors. PLoS One. **6**(9), e24872, 2011;

146. Deckers MML, Van Bezooijen RL, Van Der Horst G, Hoogendam J, Van Der Bent C, Papapoulos SE, Löwik CWGM. Bone morphogenetic proteins stimulate angiogenesis through osteoblast-derived vascular endothelial growth factor A. Endocrinology. Endocrine Soc; **143**(4), 1545, 2002;

147. Date T, Doiguchi Y, Nobuta M, Shindo H. Bone morphogenetic protein-2 induces differentiation of multipotent C3H10T1/2 cells into osteoblasts, chondrocytes, and adipocytes in vivo and in vitro. J. Orthop. Sci. **9**(5), 503, 2004;

148. Carano RAD, Filvaroff EH. Angiogenesis and bone repair. Drug Discov. Today. **8**(21), 980, 2003;

149. Koob S, Torio-Padron N, Stark GB, Hannig C, Stankovic Z, Finkenzeller G. Bone formation and neovascularization mediated by mesenchymal stem cells and endothelial cells in critical-sized calvarial defects. Tissue Eng. Part A. Mary Ann Liebert, Inc. 140 Huguenot Street, 3rd Floor New Rochelle, NY 10801 USA; **17**(3-4), 311, 2011;

150. Goerke S, Plaha J, Hager S, Strassburg S, Torio-Padron N, Stark B, Finkenzeller G. Human endothelial progenitor cells induce ERK-dependent differentiation of mesenchymal stem cells into smooth-muscle cells upon cocultivation. Tissue Eng. Part A. 2012.

151. Stratman AN, Schwindt AE, Malotte KM, Davis GE. Endothelial-derived PDGF-BB and HB-EGF coordinately regulate pericyte recruitment during vasculogenic tube assembly and stabilization. Blood. **116**(22), 4720, 2010;

152. Blocki A, Wang Y, Koch M. Not All MSCs Can Act as Pericytes: Functional In Vitro Assays to Distinguish Pericytes from Other Mesenchymal Stem Cells in Angiogenesis. Stem cells … [Internet]. **22**(17), 2013;

153. Gaengel K, Genové G, Armulik A, Betsholtz C. Endothelial-mural cell

signaling in vascular development and angiogenesis. Arterioscler. Thromb. Vasc. Biol. **29**(5), 630, 2009;

154. Maisonpierre PC, Suri C, Jones PF, Bartunkova S, Wiegand SJ, Radziejewski C, Compton D, McClain J, Aldrich TH, Papadopoulos N, Daly TJ, Davis S, Sato TN, Yancopoulos GD. Angiopoietin-2, a natural antagonist for Tie2 that disrupts in vivo angiogenesis. Science (80-.). American Association for the Advancement of Science; **277**(5322), 55, 1997;

155. Suri C, Jones PF, Patan S, Bartunkova S, Maisonpierre PC, Davis S, Sato TN, Yancopoulos GD. Requisite role of angiopoietin-1, a ligand for the TIE2 receptor, during embryonic angiogenesis. Cell. Cell; **87**(7), 1171, 1996;

156. Abramsson A, Lindblom P, Betsholtz C. Endothelial and nonendothelial sources of PDGF-B regulate pericyte recruitment and influence vascular pattern formation in tumors. J. Clin. Invest. American Society for Clinical Investigation; **112**(8), 1142, 2003;

157. Hellström M, Gerhardt H, Kalén M, Li X, Eriksson U, Wolburg H, Betsholtz C. Lack of pericytes leads to endothelial hyperplasia and abnormal vascular morphogenesis. J. Cell Biol. The Rockefeller University Press; **153**(3), 543, 2001;

158. Liu H, Zhang W, Kennard S, Caldwell RB, Lilly B. Notch3 is critical for proper angiogenesis and mural cell investment. Circ. Res. **107**(7), 860, 2010;

159. Jin S, Hansson EM, Tikka S, Lanner F, Sahlgren C, Farnebo F, Baumann M, Kalimo H, Lendahl U. Notch signaling regulates platelet-derived growth factor receptor-beta expression in vascular smooth muscle cells. Circ. Res. **102**(12), 1483, 2008;

160. Domenga V, Fardoux P, Lacombe P, Monet M, Maciazek J, Krebs LT, Klonjkowski B, Berrou E, Mericskay M, Li Z, Tournier-Lasserve E, Gridley T, Joutel A. Notch3 is required for arterial identity and maturation of vascular smooth muscle cells. Genes Dev. Cold Spring Harbor Laboratory Press; **18**(22), 2730, 2004;

161. Liu H, Kennard S, Lilly B. NOTCH3 expression is induced in mural cells through an autoregulatory loop that requires endothelial-expressed JAGGED1. Circ. Res. **104**(4), 466, 2009;

162. Song N, Huang Y, Shi H, Yuan S, Ding Y, Song X, Fu Y, Luo Y. Overexpression of platelet-derived growth factor-BB increases tumor pericyte content via stromal-derived factor-1alpha/CXCR4 axis. Cancer Res. **69**(15),

6057, 2009;

163. Krampera M, Pasini A, Rigo A, Scupoli MT, Tecchio C, Malpeli G, Scarpa A, Dazzi F, Pizzolo G, Vinante F. HB-EGF/HER-1 signaling in bone marrow mesenchymal stem cells: inducing cell expansion and reversibly preventing multilineage differentiation. Blood. American Society of Hematology; **106**(1), 59, 2005;

164. Yu X, Radulescu A, Chen C-L, James IO, Besner GE. Heparin-Binding EGF-Like Growth Factor Protects Pericytes from Injury. J. Surg. Res. Elsevier Inc; **12**, 1, 2010;

165. Sahin U, Weskamp G, Kelly K, Zhou H-M, Higashiyama S, Peschon J, Hartmann D, Saftig P, Blobel CP. Distinct roles for ADAM10 and ADAM17 in ectodomain shedding of six EGFR ligands. J. Cell Biol. **164**(5), 769, 2004;

166. Janeczek Portalska K, Leferink A, Groen N, Fernandes H, Moroni L, van Blitterswijk C, de Boer J. Endothelial differentiation of mesenchymal stromal cells. PLoS One. **7**(10), e46842, 2012;

167. Zhang X, Nan Y, Wang H, Chen J, Wang N, Xie J, Ma J, Wang Z. Model microgravity enhances endothelium differentiation of mesenchymal stem cells. Naturwissenschaften. **100**(2), 125, 2013;

168. Warrier S, Haridas N, Bhonde R. Inherent propensity of amnion-derived mesenchymal stem cells towards endothelial lineage: vascularization from an avascular tissue. Placenta. Elsevier Ltd; **33**(10), 850, 2012;

169. Silva G V, Litovsky S, Assad J a R, Sousa ALS, Martin BJ, Vela D, Coulter SC, Lin J, Ober J, Vaughn WK, Branco RVC, Oliveira EM, He R, Geng Y-J, Willerson JT, Perin EC. Mesenchymal stem cells differentiate into an endothelial phenotype, enhance vascular density, and improve heart function in a canine chronic ischemia model. Circulation. **111**(2), 150, 2005;

170. Oswald J, Boxberger S, Jørgensen B, Feldmann S, Ehninger G, Bornhäuser M, Werner C. Mesenchymal stem cells can be differentiated into endothelial cells in vitro. Stem Cells [Internet]. **22**(3), 377, 2004;

171. Galas RJ, Liu JC. Vascular endothelial growth factor does not accelerate endothelial differentiation of human mesenchymal stem cells. J. Cell. Physiol. (June 2013), 2013;

172. Medici D, Kalluri R. Endothelial–mesenchymal transition and its contribution to the emergence of stem cell phenotype. Semin. Cancer Biol. Elsevier Ltd; 1, 2012;

173. Medici D, Shore EM, Lounev VY, Kaplan FS, Kalluri R, Olsen BR. Conversion of vascular endothelial cells into multipotent stem-like cells. Nat. Med. Nature Publishing Group; **17**(4), 1400, 2010;

174. Han L, Shao J, Su L, Gao J, Wang S, Zhang Y, Zhang S, Zhao B-X, Miao J. A chemical small molecule induces mouse embryonic stem cell differentiation into functional vascular endothelial cells via Hmbox1. Stem Cells Dev. 1, 2012;

175. Banerjee S, Bacanamwo M. DNA methyltransferase inhibition induces mouse embryonic stem cell differentiation into endothelial cells. Exp. Cell Res. Elsevier Inc.; **316**(2), 172, 2010;

176. Shi Z, Neoh KG, Kang ET, Poh CK, Wang W. Enhanced endothelial differentiation of adipose-derived stem cells by substrate nanotopography. 2012;

177. Yim EKF, Darling EM, Kulangara K, Guilak F, Leong KW. Nanotopography-induced changes in focal adhesions, cytoskeletal organization, and mechanical properties of human mesenchymal stem cells. Biomaterials. Elsevier Ltd; **31**(6), 1299, 2010;

178. Kulangara K, Leong KW. Substrate topography shapes cell function. Soft Matter. **5**(21), 4072, 2009;

179. Watt FM, Huck WTS. Role of the extracellular matrix in regulating stem cell fate. Nat. Rev. Mol. Cell Biol. Nature Publishing Group; **14**(8), 467, 2013;

180. Engler AJ, Sen S, Sweeney HL, Discher DE. Matrix elasticity directs stem cell lineage specification. Cell. **126**(4), 677, 2006;

181. Valarmathi MT, Davis JM, Yost MJ, Goodwin RL, Potts JD. A three-dimensional model of vasculogenesis. Biomaterials. Elsevier Ltd; **30**(6), 1098, 2009;

182. Wingate K, Bonani W, Tan Y, Bryant SJ, Tan W. Compressive elasticity of three-dimensional nanofiber matrix directs mesenchymal stem cell differentiation to vascular cells with endothelial or smooth muscle cell markers. Acta Biomater. Acta Materialia Inc.; **8**(4), 1440, 2012;

183. Zhang G, Drinnan CT, Geuss LR, Suggs LJ. Vascular differentiation of bone marrow stem cells is directed by a tunable three-dimensional matrix. Acta Biomater. Acta Materialia Inc.; **6**(9), 3395, 2010;

184. Dong J-D, Huang J-H, Gao F, Zhu Z-H, Zhang J. Mesenchymal stem cell-

based tissue engineering of small-diameter blood vessels. Vascular. p. 206–13, 2011.

185. Katare R, Riu F, Rowlinson J, Lewis A, Holden R, Meloni M, Reni C, Wallrapp C, Emanueli C, Madeddu P. Perivascular Delivery of Encapsulated Mesenchymal Stem Cells Improves Postischemic Angiogenesis Via Paracrine Activation of VEGF-A. Arterioscler. Thromb. Vasc. Biol. **33**(8), 1872, 2013;

186. Rustad KC, Wong VW, Sorkin M, Glotzbach JP, Major MR, Rajadas J, Longaker MT, Gurtner GC. Enhancement of mesenchymal stem cell angiogenic capacity and stemness by a biomimetic hydrogel scaffold. Biomaterials. Elsevier Ltd; **33**(1), 80, 2012;

187. Bhang SH, Cho S-W, La W-G, Lee T-J, Yang HS, Sun A-Y, Baek S-H, Rhie J-W, Kim B-S. Angiogenesis in ischemic tissue produced by spheroid grafting of human adipose-derived stromal cells. Biomaterials. Elsevier Ltd; **32**(11), 2734, 2011;

188. Laschke MW, Schank TE, Scheuer C, Kleer S, Schuler S, Metzger W, Eglin D, Alini M, Menger MD. Three-dimensional spheroids of adipose-derived mesenchymal stem cells are potent initiators of blood vessel formation in porous polyurethane scaffolds. Acta Biomater. **9**(6), 6876, 2013;

189. Bhang SH, Lee S, Shin J, Lee T, Kim B. Transplantation of Cord Blood Mesenchymal Stem Cells as Spheroids Enhances Vascularization. Tissue Eng Part A. **18**(19 and 20), 2138, 2012;

190. He X, Dziak R, Yuan X, Mao K, Genco R, Swihart M, Sarkar D, Li C, Wang C, Lu L, Andreadis S, Yang S. BMP2 genetically engineered MSCs and EPCs promote vascularized bone regeneration in rat critical-sized calvarial bone defects. PLoS One. **8**(4), e60473, 2013;

191. Helmrich U, Di Maggio N, Güven S, Groppa E, Melly L, Largo RD, Heberer M, Martin I, Scherberich A, Banfi A. Osteogenic graft vascularization and bone resorption by VEGF-expressing human mesenchymal progenitors. Biomaterials. Elsevier Ltd; **34**(21), 5025, 2013;

192. Yeow C. Contrasting Effects of Vasculogenic Induction Upon Biaxial Bioreactor Stimulation of Mesenchymal Stem Cells and Endothelial Progenitor Cells Cocultures in Three-Dimensional Scaffolds Under In Vitro and In Vivo Paradigms for Vascularized Bone Tissue Engine. **19**, 2013;

193. Wang L, Fan H, Zhang Z-Y, Lou A-J, Pei G-X, Jiang S, Mu T-W, Qin J-J, Chen S-Y, Jin D. Osteogenesis and angiogenesis of tissue-engineered bone

constructed by prevascularized β-tricalcium phosphate scaffold and mesenchymal stem cells. Biomaterials. Elsevier Ltd; **31**(36), 9452, 2010;

194. Mendes LF, Pirraco RP, Szymczyk W, Frias AM, Santos TC, Reis RL, Marques AP. Perivascular-Like Cells Contribute to the Stability of the Vascular Network of Osteogenic Tissue Formed from Cell Sheet-Based Constructs. Asakura A, editor. PLoS One. **7**(7), e41051, 2012;

195. Solomon LB, Callary SA, Boopalan PRJVC, Chakrabarty A, Costi JJ, Howie DW. Impaction bone grafting of segmental bone defects in femoral non-unions. Acta Orthop. Belg. [Internet]. **79**(1), 64, 2013;

196. Volkmer E, Drosse I, Otto S, Stangelmayer A, Stengele M, Kallukalam BC, Mutschler W, Schieker M. Hypoxia in static and dynamic 3D culture systems for tissue engineering of bone. Tissue Eng. Part A [Internet]. **14**(8), 1331, 2008;

197. Stiehler M, Bünger C, Baatrup A, Lind M, Kassem M, Mygind T. Effect of dynamic 3-D culture on proliferation, distribution, and osteogenic differentiation of human mesenchymal stem cells. J. Biomed. Mater. Res. A [Internet]. **89**(1), 96, 2009;

198. Wang T-W, Wu H-C, Wang H-Y, Lin F-H, Sun J-S. Regulation of adult human mesenchymal stem cells into osteogenic and chondrogenic lineages by different bioreactor systems. J. Biomed. Mater. Res. A [Internet]. **88**(4), 935, 2009;

199. Zhang Z-Y, Teoh SH, Chong W-S, Foo T-T, Chng Y-C, Choolani M, Chan J. A biaxial rotating bioreactor for the culture of fetal mesenchymal stem cells for bone tissue engineering. Biomaterials [Internet]. **30**(14), 2694, 2009;

200. Bancroft GN, Sikavitsas VI, Mikos AG. Design of a flow perfusion bioreactor system for bone tissue-engineering applications. Tissue Eng. [Internet]. **9**(3), 549, 2003;

201. Janssen FW, Oostra J, Oorschot A van, van Blitterswijk CA. A perfusion bioreactor system capable of producing clinically relevant volumes of tissue-engineered bone: in vivo bone formation showing proof of concept. Biomaterials [Internet]. **27**(3), 315, 2006;

202. Bilodeau K, Mantovani D. Bioreactors for tissue engineering: focus on mechanical constraints. A comparative review. Tissue Eng. [Internet]. **12**(8), 2367, 2006;

203. Li D, Tang T, Lu J, Dai K. Effects of flow shear stress and mass transport on

the construction of a large-scale tissue-engineered bone in a perfusion bioreactor. Tissue Eng. Part A [Internet]. **15**(10), 2773, 2009;

204.   Holtorf HL, Jansen JA, Mikos AG. Flow perfusion culture induces the osteoblastic differentiation of marrow stroma cell-scaffold constructs in the absence of dexamethasone. J. Biomed. Mater. Res. A [Internet]. **72**(3), 326, 2005;

205.   Yeatts AB, Gordon CN, Fisher JP. Formation of an aggregated alginate construct in a tubular perfusion system. Tissue Eng. Part C. Methods [Internet]. **17**(12), 1171, 2011;

206.   Gomes ME, Bossano CM, Johnston CM, Reis RL, Mikos AG. In vitro localization of bone growth factors in constructs of biodegradable scaffolds seeded with marrow stromal cells and cultured in a flow perfusion bioreactor. Tissue Eng. [Internet]. Mary Ann Liebert, Inc. 2 Madison Avenue Larchmont, NY 10538 USA; **12**(1), 177, 2006;

207.   Kannan RY, Salacinski HJ, Sales K, Butler P, Seifalian AM. The roles of tissue engineering and vascularisation in the development of micro-vascular networks: a review. Biomaterials [Internet]. **26**(14), 1857, 2005;

208.   Geiger F, Lorenz H, Xu W, Szalay K, Kasten P, Claes L, Augat P, Richter W. VEGF producing bone marrow stromal cells (BMSC) enhance vascularization and resorption of a natural coral bone substitute. Bone [Internet]. **41**(4), 516, 2007;

209.   Bessa PC, Casal M, Reis RL. Bone morphogenetic proteins in tissue engineering: the road from the laboratory to the clinic, part I (basic concepts). J. Tissue Eng. Regen. Med. [Internet]. **2**(1), 1, 2008;

210.   Betz MW, Yeatts AB, Richbourg WJ, Caccamese JF, Coletti DP, Falco EE, Fisher JP. Macroporous hydrogels upregulate osteogenic signal expression and promote bone regeneration. Biomacromolecules [Internet]. **11**(5), 1160, 2010;

211.   Bessa PC, Casal M, Reis RL. Bone morphogenetic proteins in tissue engineering: the road from laboratory to clinic, part II (BMP delivery). J. Tissue Eng. Regen. Med. [Internet]. **2**(2-3), 81, 2008;

212.   Wozney JM, Rosen V, Celeste AJ, Mitsock LM, Whitters MJ, Kriz RW, Hewick RM, Wang EA. Novel regulators of bone formation: molecular clones and activities. Science [Internet]. **242**(4885), 1528, 1988;

213.   Tatard VM, Venier-Julienne MC, Saulnier P, Prechter E, Benoit JP, Menei P, Montero-Menei CN. Pharmacologically active microcarriers: a tool for cell

therapy. Biomaterials [Internet]. **26**(17), 3727, 2005;

214. Mercier NR, Costantino HR, Tracy MA, Bonassar LJ. Poly(lactide-co-glycolide) microspheres as a moldable scaffold for cartilage tissue engineering. Biomaterials [Internet]. **26**(14), 1945, 2005;

215. Mundargi RC, Babu VR, Rangaswamy V, Patel P, Aminabhavi TM. Nano/micro technologies for delivering macromolecular therapeutics using poly(D,L-lactide-co-glycolide) and its derivatives. J. Control. Release [Internet]. **125**(3), 193, 2008;

216. Porta G Della, Falco N, Reverchon E. Continuous supercritical emulsions extraction: a new technology for biopolymer microparticles production. Biotechnol. Bioeng. [Internet]. **108**(3), 676, 2011;

217. Porta G Della, Campardelli R, Falco N, Reverchon E. PLGA microdevices for retinoids sustained release produced by supercritical emulsion extraction: Continuous versus batch operation layouts. J. Pharm. Sci. [Internet]. 2011;

218. Falco N, Reverchon E, Della Porta G. Continuous Supercritical Emulsions Extraction: Packed Tower Characterization and Application to Poly(lactic- co - glycolic Acid) + Insulin Microspheres Production. Ind. Eng. Chem. Res. [Internet]. American Chemical Society; **51**(25), 8616, 2012;

219. Della Porta G, Castaldo F, Scognamiglio M, Paciello L, Parascandola P, Reverchon E. Bacteria microencapsulation in PLGA microdevices by supercritical emulsion extraction. J. Supercrit. Fluids [Internet]. **63**(null), 1, 2012;

220. Della Porta G, Falco N, Giordano E, Reverchon E. PLGA microspheres by Supercritical Emulsion Extraction: a study on insulin release in myoblast culture. J. Biomater. Sci. Polym. Ed. [Internet]. **24**(16), 1831, 2013;

221. Porta G Della, Falco N, Reverchon E. Continuous supercritical emulsions extraction: a new technology for biopolymer microparticles production. Biotechnol. Bioeng. [Internet]. **108**(3), 676, 2011;

222. Pisanti P, Yeatts AB, Cardea S, Fisher JP, Reverchon E. Tubular perfusion system culture of human mesenchymal stem cells on poly-L-lactic acid scaffolds produced using a supercritical carbon dioxide-assisted process. J. Biomed. Mater. Res. A [Internet]. **100**(10), 2563, 2012;

223. Kempen DHR, Lu L, Hefferan TE, Creemers LB, Heijink A, Maran A, Dhert WJA, Yaszemski MJ. Enhanced bone morphogenetic protein-2-induced ectopic and orthotopic bone formation by intermittent parathyroid hormone (1-

34) administration. Tissue Eng. Part A [Internet]. **16**(12), 3769, 2010;

224. Santo VE, Gomes ME, Mano JF, Reis RL. Controlled release strategies for bone, cartilage, and osteochondral engineering--Part II: challenges on the evolution from single to multiple bioactive factor delivery. Tissue Eng. Part B. Rev. [Internet]. **19**(4), 327, 2013;

225. Patel ZS, Young S, Tabata Y, Jansen JA, Wong MEK, Mikos AG. Dual delivery of an angiogenic and an osteogenic growth factor for bone regeneration in a critical size defect model. Bone [Internet]. **43**(5), 931, 2008;

226. Yang YY, Chung TS, Ng NP. Morphology, drug distribution, and in vitro release profiles of biodegradable polymeric microspheres containing protein fabricated by double-emulsion solvent extraction/evaporation method. Biomaterials [Internet]. **22**(3), 231, 2001;

227. Li M, Rouaud O, Poncelet D. Microencapsulation by solvent evaporation: state of the art for process engineering approaches. Int. J. Pharm. [Internet]. **363**(1-2), 26, 2008;

228. Corrigan OI, Li X. Quantifying drug release from PLGA nanoparticulates. Eur. J. Pharm. Sci. [Internet]. **37**(3-4), 477, 2009;

229. Tanaka H, Matsumura M, Veliky IA. Diffusion characteristics of substrates in Ca-alginate gel beads. Biotechnol. Bioeng. [Internet]. **26**(1), 53, 1984;

230. Gershovich JG, Dahlin RL, Kasper FK, Mikos AG. Enhanced osteogenesis in cocultures with human mesenchymal stem cells and endothelial cells on polymeric microfiber scaffolds. Tissue Eng. Part A [Internet]. Mary Ann Liebert, Inc. 140 Huguenot Street, 3rd Floor New Rochelle, NY 10801 USA; **19**(23-24), 2565, 2013;

231. Yeatts AB, Choquette DT, Fisher JP. Bioreactors to influence stem cell fate: augmentation of mesenchymal stem cell signaling pathways via dynamic culture systems. Biochim. Biophys. Acta [Internet]. **1830**(2), 2470, 2013;

232. Gomes ME, Sikavitsas VI, Behravesh E, Reis RL, Mikos AG. Effect of flow perfusion on the osteogenic differentiation of bone marrow stromal cells cultured on starch-based three-dimensional scaffolds. J. Biomed. Mater. Res. A [Internet]. **67**(1), 87, 2003;

233. Silva EA, Mooney DJ. Effects of VEGF temporal and spatial presentation on angiogenesis. Biomaterials [Internet]. **31**(6), 1235, 2010;

234. Zhang W, Zhu C, Wu Y, Ye D, Wang S, Zou D, Zhang X, Kaplan DL, Jiang

X. VEGF and BMP-2 promote bone regeneration by facilitating bone marrow stem cell homing and differentiation. Eur. Cell. Mater. [Internet]. **27**, 1, 2014;

235. Lin Z, Wang J-S, Lin L, Zhang J, Liu Y, Shuai M, Li Q. Effects of BMP2 and VEGF165 on the osteogenic differentiation of rat bone marrow-derived mesenchymal stem cells. Exp. Ther. Med. [Internet]. **7**(3), 625, 2014;

236. Young S, Patel ZS, Kretlow JD, Murphy MB, Mountziaris PM, Baggett LS, Ueda H, Tabata Y, Jansen JA, Wong M, Mikos AG. Dose effect of dual delivery of vascular endothelial growth factor and bone morphogenetic protein-2 on bone regeneration in a rat critical-size defect model. Tissue Eng. Part A [Internet]. **15**(9), 2347, 2009;

237. Patel Z, Young S, Tabata Y, Jansen J. Dual delivery of an angiogenic and an osteogenic growth factor for bone regeneration in a critical size defect model. Bone [Internet]. **43**(5), 931, 2008;

238. Kraus KH, Kirker-Head C. Mesenchymal stem cells and bone regeneration. Vet. Surg. **35**(3), 232, 2006;

239. Szpalski C, Wetterau M, Barr J, Warren SM. Bone tissue engineering: current strategies and techniques--part I: Scaffolds. Tissue Eng. Part B. Rev. [Internet]. **18**(4), 246, 2012;

240. Yeatts AB, Fisher JP. Bone tissue engineering bioreactors: dynamic culture and the influence of shear stress. Bone [Internet]. **48**(2), 171, 2011;

241. Papantoniou I, Guyot Y, Sonnaert M, Kerckhofs G, Luyten FP, Geris L, Schrooten J. Spatial optimization in perfusion bioreactors improves bone tissue-engineered construct quality attributes. Biotechnol. Bioeng. [Internet]. **111**(12), 2560, 2014;

242. Dong J, Gu Y, Li C, Wang C, Feng Z, Qiu R, Chen B, Li J, Zhang S, Wang Z, Zhang J. Response of mesenchymal stem cells to shear stress in tissue-engineered vascular grafts. Acta Pharmacol. Sin. [Internet]. CPS and SIMM; **30**(5), 530, 2009;

243. Dimitriou R, Jones E, McGonagle D, Giannoudis P V. Bone regeneration: current concepts and future directions. BMC Med. BioMed Central Ltd; **9**(1), 66, 2011;

244. Boschetti F, Raimondi MT, Migliavacca F, Dubini G. Prediction of the micro-fluid dynamic environment imposed to three-dimensional engineered cell systems in bioreactors. J. Biomech. [Internet]. **39**(3), 418, 2006;

245. Gaspar DA, Gomide V, Monteiro FJ. The role of perfusion bioreactors in bone tissue engineering. Biomatter. **2**(4), 167.

246. Pisanti P, Yeatts AB, Cardea S, Fisher JP, Reverchon E. Tubular perfusion system culture of human mesenchymal stem cells on poly- L- lactic acid scaffolds produced using a supercritical carbon dioxide-assisted process. J. Biomed. Mater. Res. Part A [Internet]. **100A**(10), 2563, 2012;

247. Yeatts AB, Geibel EM, Fears FF, Fisher JP. Human mesenchymal stem cell position within scaffolds influences cell fate during dynamic culture. Biotechnol. Bioeng. [Internet]. **109**(9), 2381, 2012;

248. Yourek G, McCormick SM, Mao JJ, Reilly GC. Shear stress induces osteogenic differentiation of human mesenchymal stem cells. Regen. Med. **5**(5), 713, 2010;

249. McCoy RJ, O'Brien FJ. Influence of shear stress in perfusion bioreactor cultures for the development of three-dimensional bone tissue constructs: a review. Tissue Eng. Part B. Rev. [Internet]. Mary Ann Liebert, Inc. 140 Huguenot Street, 3rd Floor New Rochelle, NY 10801 USA; **16**(6), 587, 2010;

250. Yeatts AB, Geibel EM, Fears FF, Fisher JP. Human mesenchymal stem cell position within scaffolds influences cell fate during dynamic culture. Biotechnol. Bioeng. [Internet]. **109**(9), 2381, 2012;

251. Luong LN, Ramaswamy J, Kohn DH. Effects of osteogenic growth factors on bone marrow stromal cell differentiation in a mineral-based delivery system. Biomaterials. **33**(1), 283, 2012;

252. Gurkan UA, Gargac J, Akkus O. The sequential production profiles of growth factors and their relations to bone volume in ossifying bone marrow explants. Tissue Eng. Part A. **16**(7), 2295, 2010;

253. Hsu C-W, Poché RA, Saik JE, Ali S, Wang S, Yosef N, Calderon GA, Scott L, Vadakkan TJ, Larina I V, West JL, Dickinson ME. Improved Angiogenesis in Response to Localized Delivery of Macrophage-Recruiting Molecules. PLoS One [Internet]. Public Library of Science; **10**(7), e0131643, 2015;

254. Du D, Furukawa KS, Ushida T. 3D culture of osteoblast-like cells by unidirectional or oscillatory flow for bone tissue engineering. Biotechnol. Bioeng. [Internet]. **102**(6), 1670, 2009;

255. Chromiak JA, Shansky J, Perrone C, Vandenburgh HH. Bioreactor perfusion system for the long-term maintenance of tissue-engineered skeletal muscle organoids. In Vitro Cell. Dev. Biol. Anim. [Internet]. **34**(9), 694, 1998;

256. Wen F, Chang S, Toh YC, Arooz T, Zhuo L, Teoh SH, Yu H. Development of dual-compartment perfusion bioreactor for serial coculture of hepatocytes and stellate cells in poly(lactic-co-glycolic acid)-collagen scaffolds. J. Biomed. Mater. Res. B. Appl. Biomater. [Internet]. **87**(1), 154, 2008;

257. Minuth WW, Schumacher K, Strehl R, Kloth S. Physiological and cell biological aspects of perfusion culture technique employed to generate differentiated tissues for long term biomaterial testing and tissue engineering. J. Biomater. Sci. Polym. Ed. [Internet]. **11**(5), 495, 2000;

258. Vance J, Galley S, Liu DF, Donahue SW. Mechanical stimulation of MC3T3 osteoblastic cells in a bone tissue-engineering bioreactor enhances prostaglandin E2 release. Tissue Eng. [Internet]. **11**(11-12), 1832.

259. Muscari C, Giordano E, Bonafè F, Govoni M, Guarnieri C. Strategies affording prevascularized cell-based constructs for myocardial tissue engineering. Stem Cells Int. [Internet]. Hindawi Publishing Corporation; **2014**, 434169, 2014;

260. Baldwin J, Antille M, Bonda U, De-Juan-Pardo EM, Khosrotehrani K, Ivanovski S, Petcu EB, Hutmacher DW. In vitro pre-vascularisation of tissue-engineered constructs A co-culture perspective. Vasc. Cell [Internet]. **6**, 13, 2014;

261. Niu M, Hammond P, Coger RN. The effectiveness of a novel cartridge-based bioreactor design in supporting liver cells. Tissue Eng. Part A [Internet]. **15**(10), 2903, 2009;

262. Usuludin SBM, Cao X, Lim M. Co-culture of stromal and erythroleukemia cells in a perfused hollow fiber bioreactor system as an in vitro bone marrow model for myeloid leukemia. Biotechnol. Bioeng. [Internet]. **109**(5), 1248, 2012;

263. Grayson WL, Marolt D, Bhumiratana S, Fröhlich M, Guo XE, Vunjak-Novakovic G. Optimizing the medium perfusion rate in bone tissue engineering bioreactors. Biotechnol. Bioeng. [Internet]. **108**(5), 1159, 2011;

264. Fan J, Jia X, Huang Y, Fu BM, Fan Y. Greater scaffold permeability promotes growth of osteoblastic cells in a perfused bioreactor. J. Tissue Eng. Regen. Med. [Internet]. 2013;

265. Li J, Ma Y, Teng R, Guan Q, Lang J, Fang J, Long H, Tian G, Wu Q. Transcriptional profiling reveals crosstalk between mesenchymal stem cells and endothelial cells promoting pre-vascularization by reciprocal mechanisms. Stem Cells Dev. [Internet]. 2014;

266. Schulz RM, Bader A. Cartilage tissue engineering and bioreactor systems for the cultivation and stimulation of chondrocytes. Eur. Biophys. J. [Internet]. **36**(4-5), 539, 2007;

267. Zhao F, Chella R, Ma T. Effects of shear stress on 3-D human mesenchymal stem cell construct development in a perfusion bioreactor system: Experiments and hydrodynamic modeling. Biotechnol. Bioeng. [Internet]. **96**(3), 584, 2007;

268. Singh H, Hutmacher DW. Bioreactor studies and computational fluid dynamics. Adv. Biochem. Eng. Biotechnol. [Internet]. **112**, 231, 2009;

269. Kim J, Ma T. Perfusion regulation of hMSC microenvironment and osteogenic differentiation in 3D scaffold. Biotechnol. Bioeng. [Internet]. **109**(1), 252, 2012;

270. Nakamura Y, Wakitani S, Nakayama J, Wakabayashi S, Horiuchi H, Takaoka K. Temporal and Spatial Expression Profiles of BMP Receptors and Noggin During BMP-2-Induced Ectopic Bone Formation. J. Bone Miner. Res. [Internet]. **18**(10), 1854, 2003;

271. Yang K, Cao W, Hao X, Xue X, Zhao J, Liu J, Zhao Y, Meng J, Sun B, Zhang J, Liang X-J. Metallofullerene nanoparticles promote osteogenic differentiation of bone marrow stromal cells through BMP signaling pathway. Nanoscale [Internet]. Royal Society of Chemistry; **5**(3), 1205, 2013;

272. Poynton AR, Lane JM. Safety profile for the clinical use of bone morphogenetic proteins in the spine. Spine (Phila. Pa. 1976). [Internet]. **27**(16 Suppl 1), S40, 2002;

273. Zhao B, Katagiri T, Toyoda H, Takada T, Yanai T, Fukuda T, Chung U, Koike T, Takaoka K, Kamijo R. Heparin potentiates the in vivo ectopic bone formation induced by bone morphogenetic protein-2. J. Biol. Chem. [Internet]. **281**(32), 23246, 2006;

274. Coates EE, Fisher JP. Engineering superficial zone chondrocytes from mesenchymal stem cells. Tissue Eng. Part C. Methods [Internet]. Mary Ann Liebert, Inc. 140 Huguenot Street, 3rd Floor New Rochelle, NY 10801 USA; **20**(8), 630, 2014;

275. Williams C, Wick TM. Endothelial Cell–Smooth Muscle Cell Co-Culture in a Perfusion Bioreactor System. Ann. Biomed. Eng. [Internet]. **33**(7), 920, 2005;

276. Fennema E, Rivron N, Rouwkema J, van Blitterswijk C, de Boer J. Spheroid culture as a tool for creating 3D complex tissues. Trends Biotechnol. [Internet]. **31**(2), 108, 2013;

277. Tseng P-C, Young T-H, Wang T-M, Peng H-W, Hou S-M, Yen M-L. Spontaneous osteogenesis of MSCs cultured on 3D microcarriers through alteration of cytoskeletal tension. Biomaterials [Internet]. **33**(2), 556, 2012;

278. Ng MH, Chowdhury SR, Morshed M, Tan KK, Tan GH, Phang MY, Aminuddin BS, Fauziah O, Ruszymah BHI. Effective Cell Seeding and Three-Dimensional Cell Culture for Bone Tissue Engineering. J. Biomater. Tissue Eng. [Internet]. American Scientific Publishers; **4**(7), 573, 2014;

279. Castro-Manrreza ME, Montesinos JJ. Immunoregulation by Mesenchymal Stem Cells: Biological Aspects and Clinical Applications. J. Immunol. Res. [Internet]. **2015**, 394917, 2015;

280. Du D, Asaoka T, Ushida T, Furukawa KS. Fabrication and perfusion culture of anatomically shaped artificial bone using stereolithography. Biofabrication [Internet]. **6**(4), 045002, 2014;

281. Vunjak-Novakovic G, Martin I, Obradovic B, Treppo S, Grodzinsky AJ, Langer R, Freed LE. Bioreactor cultivation conditions modulate the composition and mechanical properties of tissue-engineered cartilage. J. Orthop. Res. [Internet]. **17**(1), 130, 1999;

282. Nguyen LH, Annabi N, Nikkhah M, Bae H, Binan L, Park S, Kang Y, Yang Y, Khademhosseini A. Vascularized bone tissue engineering: approaches for potential improvement. Tissue Eng. Part B. Rev. [Internet]. Mary Ann Liebert, Inc. 140 Huguenot Street, 3rd Floor New Rochelle, NY 10801 USA; **18**(5), 363, 2012;

283. Klein-Nulend J, Bacabac RG, Mullender MG. Mechanobiology of bone tissue. Pathol. Biol. (Paris). [Internet]. **53**(10), 576, 2005;

284. Yeatts AB, Fisher JP. Tubular perfusion system for the long-term dynamic culture of human mesenchymal stem cells. Tissue Eng. Part C. Methods [Internet]. Mary Ann Liebert, Inc. 140 Huguenot Street, 3rd Floor New Rochelle, NY 10801 USA; **17**(3), 337, 2011;

285. Porta G Della, Nguyen B-NB, Campardelli R, Reverchon E, Fisher JP. Synergistic effect of sustained release of growth factors and dynamic culture on osteoblastic differentiation of mesenchymal stem cells. J. Biomed. Mater. Res. A [Internet]. 2014;

286. B. Y, K. B, YangWanxun, S. A, YangFang, P. F, A. J. In Vivo Bone Regeneration Using Tubular Perfusion System Bioreactor Cultured Nanofibrous Scaffolds. Tissue Eng. Part A [Internet]. Mary Ann Liebert, Inc.

140 Huguenot Street, 3rd Floor New Rochelle, NY 10801 USA; 2013;

287. Sladkova M, de Peppo G. Bioreactor Systems for Human Bone Tissue Engineering. Processes [Internet]. Multidisciplinary Digital Publishing Institute; **2**(2), 494, 2014;

288. Olivier V, Hivart P, Descamps M, Hardouin P. In vitro culture of large bone substitutes in a new bioreactor: importance of the flow direction. Biomed. Mater. [Internet]. **2**(3), 174, 2007;

289. Gardel L, Afonso M, Frias C, Gomes M, Reis R. Assessing the repair of critical size bone defects performed in a goat tibia model using tissue-engineered constructs cultured in a bidirectional flow perfusion bioreactor. J. Biomater. Appl. [Internet]. **29**(2), 172, 2014;

290. Kleinhans C, Mohan RR, Vacun G, Schwarz T, Haller B, Sun Y, Kahlig A, Kluger P, Finne-Wistrand A, Walles H, Hansmann J. A perfusion bioreactor system efficiently generates cell-loaded bone substitute materials for addressing critical size bone defects. Biotechnol. J. [Internet]. 2015;

291. Li D, Li M, Liu P, Zhang Y, Lu J, Li J. Tissue-engineered bone constructed in a bioreactor for repairing critical-sized bone defects in sheep. Int. Orthop. [Internet]. 2014;

292. Yeatts AB, Both SK, Yang W, Alghamdi HS, Yang F, Fisher JP, Jansen JA. In vivo bone regeneration using tubular perfusion system bioreactor cultured nanofibrous scaffolds. Tissue Eng. Part A [Internet]. **20**(1-2), 139, 2014;

293. Yoon DM, Curtiss S, Reddi AH, Fisher JP. Addition of hyaluronic acid to alginate embedded chondrocytes interferes with insulin-like growth factor-1 signaling in vitro and in vivo. Tissue Eng. Part A [Internet]. **15**(11), 3449, 2009;

294. Leucht P, Kim J-B, Amasha R, James AW, Girod S, Helms JA. Embryonic origin and Hox status determine progenitor cell fate during adult bone regeneration. Development [Internet]. **135**(17), 2845, 2008;

295. Wang MO, Vorwald CE, Dreher ML, Mott EJ, Cheng M-H, Cinar A, Mehdizadeh H, Somo S, Dean D, Brey EM, Fisher JP. Evaluating 3D-printed biomaterials as scaffolds for vascularized bone tissue engineering. Adv. Mater. [Internet]. **27**(1), 138, 2015;

296. Lovett M, Lee K, Edwards A, Kaplan DL. Vascularization strategies for tissue engineering. Tissue Eng. Part B. Rev. [Internet]. **15**(3), 353, 2009;

297. Unger RE, Ghanaati S, Orth C, Sartoris A, Barbeck M, Halstenberg S, Motta A, Migliaresi C, Kirkpatrick CJ. The rapid anastomosis between prevascularized networks on silk fibroin scaffolds generated in vitro with cocultures of human microvascular endothelial and osteoblast cells and the host vasculature. Biomaterials [Internet]. **31**(27), 6959, 2010;

298. Ma J, van den Beucken JJJP, Yang F, Both SK, Cui F-Z, Pan J, Jansen JA. Coculture of osteoblasts and endothelial cells: optimization of culture medium and cell ratio. Tissue Eng. Part C. Methods [Internet]. **17**(3), 349, 2011;

299. Dahlin RL, Gershovich JG, Kasper FK, Mikos AG. Flow Perfusion Co-culture of Human Mesenchymal Stem Cells and Endothelial Cells on Biodegradable Polymer Scaffolds. Ann. Biomed. Eng. [Internet]. 2013;

300. Melchiorri AJ, Nguyen B-NB, Fisher JP. Mesenchymal stem cells: roles and relationships in vascularization. Tissue Eng. Part B. Rev. [Internet]. Mary Ann Liebert, Inc. 140 Huguenot Street, 3rd Floor New Rochelle, NY 10801 USA; **20**(3), 218, 2014;

301. Percival CJ, Richtsmeier JT. Angiogenesis and intramembranous osteogenesis. Dev. Dyn. [Internet]. WILEY-BLACKWELL, 111 RIVER ST, HOBOKEN 07030-5774, NJ USA; **242**(8), 909, 2013;

302. Kim K-I, Park S, Im G-I. Osteogenic differentiation and angiogenesis with cocultured adipose-derived stromal cells and bone marrow stromal cells. Biomaterials [Internet]. 2014;

303. Nguyen B-NB, Ko H, Moriarty RA, Etheridge JM, Fisher JP. Dynamic Bioreactor Culture of High Volume Engineered Bone Tissue. Tissue Eng. Part A [Internet]. Mary Ann Liebert, Inc. 140 Huguenot Street, 3rd Floor New Rochelle, NY 10801 USA; **22**(3-4), 263, 2016;

304. Branco da Cunha C, Klumpers DD, Li WA, Koshy ST, Weaver JC, Chaudhuri O, Granja PL, Mooney DJ. Influence of the stiffness of three-dimensional alginate/collagen-I interpenetrating networks on fibroblast biology. Biomaterials [Internet]. **35**(32), 8927, 2014;

305. Lee KY, Mooney DJ. Alginate: properties and biomedical applications. Prog. Polym. Sci. [Internet]. **37**(1), 106, 2012;

306. Nguyen B-NB, Ko H, Fisher JP. Tunable osteogenic differentiation of hMPCs in tubular perfusion system bioreactor. Biotechnol. Bioeng. [Internet]. 2016;

307. Hellstrom M, Gerhardt H, Kalen M, Li X, Eriksson U, Wolburg H, Betsholtz C. Lack of Pericytes Leads to Endothelial Hyperplasia and Abnormal Vascular

Morphogenesis. J. Cell Biol. [Internet]. **153**(3), 543, 2001;